

MEASUREMENT OF THE ELASTIC - PLASTIC BOUNDARY  
AROUND COLDWORKED FASTENER HOLES

Dissertation for the Degree of Ph. D.

MICHIGAN STATE UNIVERSITY

SARAVUT POOLSUK

1977



This is to certify that the  
thesis entitled  
Measurement of the Elastic-Plastic Boundary Around  
Coldworked Fastener Holes

presented by

Saravut Poolsuk

has been accepted towards fulfillment  
of the requirements for

Ph.D. degree in Mechanics

  
Major professor

Date July 15, 1977

## ABSTRACT

### MEASUREMENT OF THE ELASTIC-PLASTIC BOUNDARY AROUND COLDWORKED FASTENER HOLES

By

Saravut Poolsuk

A fastener hole which is pre-expanded with an oversize mandrel is known as a coldworked hole. Coldworking of the hole creates residual compressive stresses around the hole. These compressive stresses reduce the high tensile stresses produced by stress concentration near the hole. This results in the fatigue life enhancement of the structural component under applied cyclic loading. The elastic-plastic boundary around a coldworked hole, caused by the hole expansion with an oversize mandrel, is an important measure of the amount of coldworking.

The existing theories developed for the coldworked hole are discussed, their assumptions and deficiencies pointed out. The elastic-plastic boundary given by the various theories is not the same for the same loading conditions. Knowledge of the elastic-plastic boundary around a coldworked hole is required in both theoretical analysis and design. The purpose of this thesis is to measure the elastic-plastic boundary around coldworked fastener holes and compare with the theoretical predictions.

Two experimental techniques have been developed to evaluate the existing theories. The two techniques used to locate the

elastic-plastic boundary are foil gages and thickness change measurement. Their accuracies have been compared and found to be similar.

To test the validity of the theories, two kinds of aluminum, 7075-T6 and 1100, with two different thicknesses: 6.35 mm. (1/4 in.) and 3.18 mm. (1/8 in.), are used as specimens. Holes in the circular specimens are coldworked with four different sizes of the oversize mandrel. This industrial coldworking process is found to give non-uniform deformation through the specimen thickness.

The final results of the measurements around the coldworked holes obtained by the thickness change method are presented in dimensionless form for hole size, amount of coldwork, and material. The comparison of the experiments with seven theories shows that the Nadai theory is the best one to predict the elastic-plastic boundary around the coldworked 3.18 mm. (1/8 in.) thick plate, while the Sachs and Rich-Impellizzeri theories are suitable for the coldworked 6.35 mm. (1/4 in.) thick plate for smaller amounts of coldwork. None of the theories predicts the elastic-plastic boundary well for the 6.35 mm. (1/4 in.) thick plate for larger amounts of coldwork. Also, none of them agrees with the experiments of the softer 1100 aluminum. In addition, the results show that the plate thickness is an important factor in determining the plane condition during coldworking process. The experimentally determined final diameters of relaxed holes are also presented and compared with four theories.

MEASUREMENT OF THE ELASTIC-PLASTIC BOUNDARY  
AROUND COLDWORKED FASTENER HOLES

By

Saravut Poolasuk

A DISSERTATION

Submitted to  
Michigan State University  
in partial fulfillment of the requirements  
for the degree of

DOCTOR OF PHILOSOPHY

Department of Metallurgy,  
Mechanics and Materials Science

1977

## ACKNOWLEDGMENTS

The author would like to express his heartfelt appreciation to his major professor and chairman of his guidance committee, Professor William N. Sharpe, Jr., who suggested the problem and provided invaluable guidance and encouragement through all phases of this study. Thanks are also extended to the other members of his guidance committee, Dr. Denton D. McGrady, Dr. George E. Mase, and Dr. Carl L. Foiles. Special thanks are due to Dr. McGrady, who spent many hours correcting the author's writing.

The author wishes also to thank Mr. Donald L. Childs and Mr. Robert E. Rose, respectively for their helpful preparation of specimens and electrical equipment. Financial support was granted through his major professor's research by the Air Force Office of Scientific Research, Bolling Air Force Base, Washington, D. C. 20332. This support is gratefully acknowledged.

Special thanks also are due to his dear wife, Rutchaneeporn, and daughter, Ketsanee, for their understanding, help, and encouragement throughout the course of this study.

## TABLE OF CONTENTS

Chapter	Page
LIST OF TABLES . . . . .	v
LIST OF FIGURES . . . . .	vii
1. INTRODUCTION . . . . .	1
1.1. <u>Coldworked Fastener Holes</u> . . . . .	1
1.2. <u>Theoretical Solutions</u> . . . . .	6
1.3. <u>The Elastic-Plastic Boundary</u> . . . . .	7
1.4. <u>Coldworking Procedure</u> . . . . .	9
1.5. <u>Overview of Dissertation</u> . . . . .	10
2. MATERIAL SPECIFICATIONS . . . . .	12
3. HOLE PREPARATION AND COLDWORKING . . . . .	17
3.1. <u>Hole Preparation</u> . . . . .	17
3.2. <u>Coldworking Procedure</u> . . . . .	19
4. THEORIES OF RESIDUAL STRESSES AROUND A COLDWORKED HOLE . . . . .	27
4.1. <u>Introduction</u> . . . . .	27
4.2. <u>Nadai Theory</u> . . . . .	33
4.3. <u>Swainger Theory</u> . . . . .	35
4.4. <u>Taylor Theory</u> . . . . .	36
4.5. <u>Alexander-Ford and Mangasarian Theories</u> . . . . .	37
4.6. <u>Carter-Hanagud Theory</u> . . . . .	38
4.7. <u>Hsu-Forman Theory</u> . . . . .	39
4.8. <u>Adler-Dupree's Finite Element Method</u> . . . . .	42
4.9. <u>Potter-Grandt Theory</u> . . . . .	43
4.10. <u>Thick-Walled Tube Theory</u> . . . . .	46
4.11. <u>Rich-Impellizzeri Theory</u> . . . . .	47
4.12. <u>Discussion</u> . . . . .	49
5. ELASTIC-PLASTIC BOUNDARY MEASUREMENT TECHNIQUES . . . . .	53
5.1. <u>Nature of Deformation around a Coldworked Hole</u> . . . . .	53
5.2. <u>Foil Strain Gage Technique</u> . . . . .	55
5.3. <u>Thickness Change Measurement Technique</u> . . . . .	74
5.4. <u>Photoelastic Coating Technique</u> . . . . .	87

Chapter	Page
6. ELASTIC-PLASTIC BOUNDARY MEASUREMENT . . . . .	92
6.1. <u>Elastic-Plastic Boundary Measurement with Foil</u>	92
<u>Gages</u> . . . . .	
6.1.1. 6.35 mm. (1/4 in.) Thick, 7075-T6 Specimen Data	
6.1.2. 3.18 mm. (1/8 in.) Thick, 7075-T6 Specimen Data	
6.1.3. 3.18 mm. (1/8 in.) Thick, Aluminum Type 1100 Specimen Data	
6.2. <u>Elastic-Plastic Boundary Measurement with</u>	
<u>Thickness Change Measurement</u> . . . . .	98
6.2.1. 6.35 mm. (1/4 in.) Thick, 7075-T6 Specimen Data	
6.2.2. 3.18 mm. (1/8 in.) Thick, 7075-T6 Specimen Data	
6.2.3. 3.28 mm. (1/8 in.) Thick, Aluminum Type 1100 Specimen Data	
6.3. <u>Discussion</u> . . . . .	106
7. COMPARISON OF THEORIES WITH EXPERIMENTS . . . . .	114
8. CONCLUSIONS . . . . .	127
REFERENCES . . . . .	131

## LIST OF TABLES

Table	Page
2.1 Mechanical properties of materials used . . . . .	15
3.1 Original diameters of holes for a typical set of 6.35 mm. (1/4 in.) thick, 7075-T6 specimens . . .	20
3.2 Original diameters of holes for a typical set of 3.18 mm. (1/8 in.) thick, 7075-T6 specimens . . .	21
3.3 Original diameters of holes for a typical set of 3.18 mm. (1/8 in.) thick, type 1100 specimens . .	22
6.1 Measured $r_p/a$ and its uncertainty obtained from foil gage technique when foil gages were applied on one side and on both sides surfaces of the 6.35 mm. (1/4 in.) thick, 7075-T6 aluminum specimens. . . . .	93
6.2 Measured $r_p/a$ and its uncertainty obtained from foil gage technique with foil gages applied to one side and to both sides of the 3.18 mm. (1/8 in.) thick, 7075-T6 aluminum specimen . . . . .	96
6.3 Measured $r_p/a$ obtained from thickness change measurement technique for the 6.35 mm. (1/4 in.) thick, 7075-T6 aluminum specimens . . . . .	99
6.4 Measured $r_p/a$ obtained from thickness change measurement technique for the 3.18 mm. (1/8 in.) thick, 7075-T6 aluminum specimens . . . . .	103
6.5 Measured $r_p/a$ obtained from thickness change measurement technique for the 3.18 mm. (1/8 in.) thick, type 1100 aluminum specimens with $\pm 0.005$ in. scale of Daytronic amplifier . . . . .	107
7.1 Percent differences between the measured $r_p/a$ obtained from thickness change measurement for the 3.18 mm. (1/8 in.) thick, 7075-T6 aluminum and the Nadai and Hsu-Forman theories . . . . .	117
7.2 Percent differences between the measured $r_p/a$ obtained from thickness change measurement for the 6.35 mm. (1/4 in.) thick, aluminum and the Thick-Walled Tube and Rich-Impellizzeri theories . . . . .	118



Table	Page
7.3 Average measured $r_p/a$ obtained from thickness change measurement and predicted $r_p/a$ from four theories for the 3.18 mm. (1/8 in.) thick, type 1100 aluminum . . . . .	119
7.4 Measured final diameters of 6.35 mm. (1/4 in.) thick, 7075-T6 specimens after the mandrel was pulled through the holes . . . . .	122
7.5 Measured final diameters of 3.18 mm. (1/8 in.) thick, 7075-T6 specimens after the mandrel was pulled through the holes . . . . .	123
7.6 Measured final diameters of 3.18 mm. (1/8 in.) thick, type 1100 aluminum specimens after the mandrel was pulled through the holes . . . . .	124
7.7 Comparison of measured final diameters with theories for the 7075-T6 aluminum specimens as four different sizes of the oversize mandrels were pulled through the holes . . . . .	126

## LIST OF FIGURES

Figure		Page
1.1	Stress concentration factor at the edge of a hole of radius "a" in infinite plate due to tensile stress, $\sigma$ . . . . .	2
1.2	Residual stresses predicted by the Nadai and Hsu-Forman theories for a 0.305 mm. (0.012 in.) diametral expansion of a 6.60 mm. (0.26 in.) hole in 7075-T6 aluminum . . . . .	5
1.3	Elastic-plastic boundary predicted by Hsu-Forman's theory (8) located where the predicted loading radial and tangential strains are equal in magnitude and opposite in sign for a 0.305 mm. (0.012 in.) diametral expansion of 6.60 mm. (0.26 in.) hole in 7075-T6 aluminum . . . . .	8
2.1	Stress-strain curves for the two different sheets of 7075-T6 aluminum . . . . .	13
2.2	Stress-strain curves for the 3.18 mm. (1/8 in.) thick, type 1100 aluminum . . . . .	14
2.3	Photomicrographs of the two sheets of 7075-T6 aluminum (100X) and one sheet of 1100 aluminum (500 X) . . . . .	16
3.1	Specimen configuration . . . . .	18
3.2	Photograph of mandrels and sleeves . . . . .	23
3.3	Schematic of the J. O. King coldworking process . . . . .	25
4.1	Geometry and coordinate system used in coldworking hole theories . . . . .	28
4.2	Loading elastic-plastic boundary, $\tilde{p}$ , vs. radial displacement at the hole, $\tilde{u}$ . . . . .	45
4.3	Elastic-plastic boundaries predicted by various theories . . . . .	50
5.1	Photograph of the deformed region around the hole in a 6.35 mm. (1/4 in.) thick specimen (100 X) . . . . .	54

Figure		Page
5.2	Photograph of equipment set up for the foil gage technique . . . . .	57
5.3	Photograph of bonded specimen with radial and tangential foil gages on the upper side . . . . .	58
5.4	Radial and tangential strains measured with foil gages on the upper side of the 6.35 mm. (1/4 in.) thick, 7075-T6 aluminum (P.18) as the mandrel of 0.076 mm. (0.003 in.) radial expansion was pulled through the hold . . . . .	60
5.5	Radial and tangential strains measured with foil gages on the upper side of the 6.35 mm. (1/4 in.) thick, 7075-T6 aluminum (P.18) as the mandrel of 0.102 mm. (0.004 in.) radial expansion was pulled through the hole . . . . .	61
5.6	Radial and tangential strains measured with foil gages on the upper side of the 6.35 mm. (1/4 in.) thick, 7075-T6 aluminum (P.18) as the mandrel of 0.127 mm. (0.005 in.) radial expansion was pulled through the hole . . . . .	62
5.7	Radial and tangential strains measured with foil gages on the upper side of the 6.35 mm. (1/4 in.) thick, 7075-T6 aluminum (P.18) as the mandrel of 0.152 mm. (0.006 in.) radial expansion was pulled through the hole . . . . .	63
5.8	Radial and tangential strains measured with foil gages on the upper side of the 3.18 mm. (1/8 in.) thick, 7075-T6 aluminum (P.20) as the mandrel of 0.076 mm. (0.003 in.) radial expansion was pulled through the hole . . . . .	64
5.9	Radial and tangential strains measured with foil gages on the upper side of the 3.18 mm. (1/8 in.) thick, 7075-T6 aluminum (P.20) as the mandrel of 0.102 mm. (0.004 in.) radial expansion was pulled through the hole . . . . .	65
5.10	Radial and tangential strains measured with foil gages on the upper side of the 3.18 mm. (1/8 in.) thick, 7075-T6 aluminum (P.20) as the mandrel of 0.127 mm. (0.005 in.) radial expansion was pulled through the hole . . . . .	66

Figure	Page
5.11 Radial and tangential strains measured with foil gages on the upper side of the 3.18 mm. (1/8 in.) thick, 7075-T6 aluminum (P.20) as the mandrel of 0.152 mm. (0.006 in.) radial expansion was pulled through the hole . . . . .	67
5.12 Typical method used to locate the elastic-plastic boundary, $r_p$ , of typical 6.35 mm. (1/4 in.) thick, 7075-T6 aluminum (P.18) in which foil gages were applied on one side . . . . .	68
5.13 Typical method used to locate the elastic-plastic boundary, $r_p$ , of typical 3.18 mm. (1/8 in.) thick, 7075-T6 aluminum (P.20) in which foil gages were applied on one side . . . . .	69
5.14 Typical method used to locate the elastic-plastic boundary, $r_p$ , of typical 6.35 mm. (1/4 in.) thick, 7075-T6 aluminum (P.14) . . . . .	71
5.15 Typical method used to locate the elastic-plastic boundary, $r_p$ , of typical 3.18 mm. (1/8 in.) thick, 7075-T6 aluminum (P.28) . . . . .	72
5.16 Calibration curve of the LVDT on $\pm 0.005$ in. scale of Daytronic amplifier model 300C . . . . .	77
5.17 Calibration curve of the LVDT on $\pm 0.001$ in. scale of Daytronic amplifier model 300C . . . . .	78
5.18 Calibration curve of linear potentiometer . . . . .	79
5.19 Photograph of the thickness change measurement setup . . . . .	82
5.20 Photograph of the LVDT and linear potentiometer mounted in holders . . . . .	83
5.21 Typical method used to locate the elastic-plastic boundary, $r_p$ , from the thickness profile of the 6.35 mm. (1/4 in.) thick, 7075-T6 aluminum (P.12) on direction number 2 and $\pm 0.001$ in. scale after four different sizes of oversize mandrel were pulled through the hole . . . . .	84
5.22 Typical method used to locate the elastic-plastic boundary, $r_p$ , from the thickness profile of the 3.18 mm. (1/8 in.) thick, 7075-T6 aluminum (P.28) on direction number 2 and $\pm 0.001$ in. scale after four different sizes of oversize mandrel were pulled through the hole . . . . .	85

Figure	Page
5.23	Typical method used to locate the elastic-plastic boundary, $r_p$ , from the thickness profile of the 3.18 mm. (1/8 in.) thick, type 1100 aluminum (P.36) on direction number 2 and $\pm 0.005$ in. scale after four different sizes of oversize mandrel were pulled through the hole . . . . . 86
5.24	Isochromatic-fringe patterns and elastic-plastic boundaries obtained around the coldworked 6.35 mm. (1/4 in.) thick specimen (P.4) as four different sizes of oversize mandrel were pulled through the hole . . . . . 90
6.1	Comparison of the measured $r_p/a$ obtained from foil gages applied on one side and on both sides of the 6.35 mm. (1/4 in.) thick, 7075-T6 aluminum . . . . . 94
6.2	Comparison of the measured $r_p/a$ obtained from foil gages applied on one side and on both sides of the 3.18 mm. (1/8 in.) thick, 7075-T6 aluminum . . . . . 97
6.3	Comparison of the measured $r_p/a$ obtained from thickness change measurement technique with 1 CW. and 4 CW. on one specimen of the 6.35 mm. (1/4 in.) thick, 7075-T6 aluminum . . . . . 101
6.4	Comparison of the measured $r_p/a$ obtained from thickness change measurement technique with 1 CW. and 4 CW. on one specimen of the 3.18 mm. (1/8 in.) thick, 7075-T6 aluminum . . . . . 105
6.5	Comparison of the measured $r_p/a$ obtained from thickness change measurement technique with 1 CW. and 4 CW. on one specimen of the 3.18 mm. (1/8 in.) thick, type 1100 aluminum with $\pm 0.005$ in. scale of Daytronic amplifier . . . . . 108
6.6	Comparison of the measured $r_p/a$ obtained from thickness change measurement and foil gage (both sides) techniques of the 6.35 mm. (1/4 in.) thick, 7075-T6 aluminum (P.11,12,14) . . . . . 111
6.7	Comparison of the measured $r_p/a$ obtained from thickness change measurement and foil gage (both sides) techniques of the 3.18 mm. (1/8 in.) thick, 7075-T6 aluminum (P.25,28,30) . . . . . 112

Figure		Page
7.1	Comparison of the elastic-plastic boundaries predicted by various theories and experiments for 7075-T6 aluminum . . . . .	115
7.2	Comparison of the measured final relaxed hole diameters with four theories (Nadai, Hsu-Forman, Potter-Grandt, and Adler-Dupree) . . . . .	125

## CHAPTER 1

### INTRODUCTION

It is known that the stress concentration is very high at the edge of a hole in a plate which is subjected to a uniform tensile stress at its ends. Figure 1.1 shows the elastic stress distributions on one side of an open hole in an infinite plate with a uniform tensile stress at infinity (1,2). The tangential stress,  $\sigma_{\theta}$ , at the hole wall is about three times the remote stress,  $\sigma$ , and decreases rapidly away from the hole. These high stresses at the hole edge may locally exceed the material's yield stress. A crack will then initiate and lead to an early failure of the plate (2). When the plate is subjected to cyclic loading, its failure will occur at a stress lower than its yield point, and its service life is much shorter than usual, viz., in the aircraft structures (3,4,5). One common method for increasing the service life is coldworking.

The purpose of this thesis is to experimentally measure the elastic-plastic boundary around coldworked fastener holes and compare with the theoretical predictions.

#### 1.1 Coldworked Fastener Holes

Many investigators (3,4,5,6,7) have indicated that pre-expansion of the hole before loading reduces the fastener hole stress concentration effect by creating beneficial compressive residual



stresses at the hole edge. These compressive residual stresses are created by plastic deformation of the material surrounding the hole, resulting from expansion of the hole and subsequent removal of the radial load. As a circular hole in a flat infinite plate having a

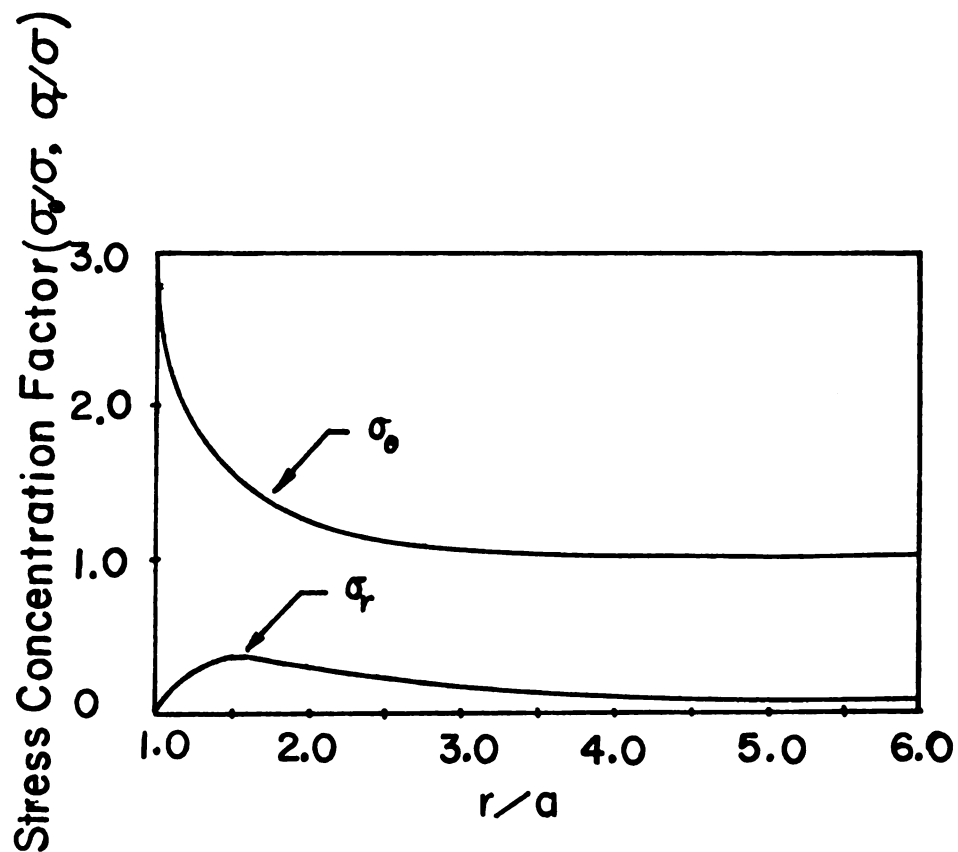


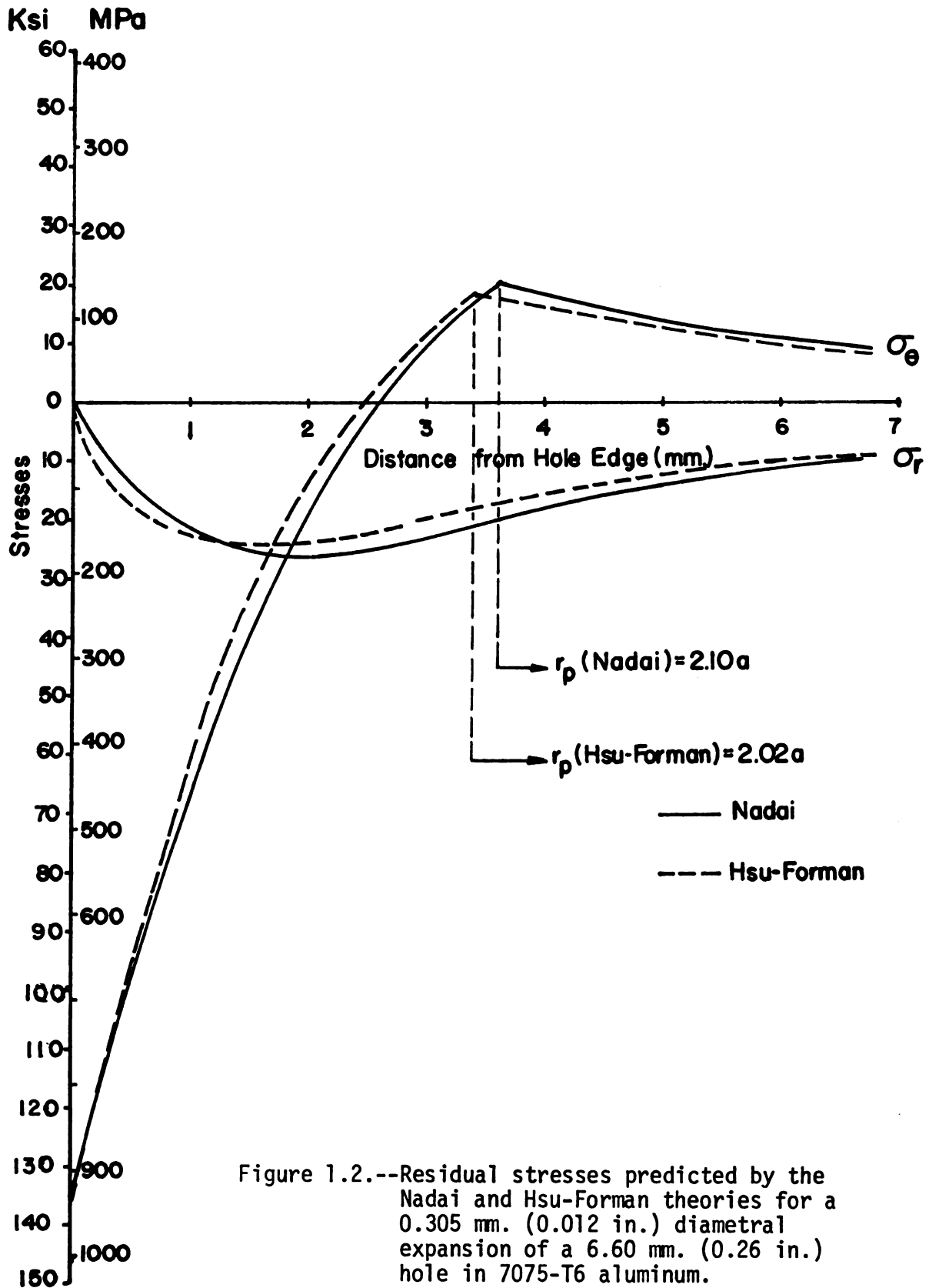
Figure 1.1.--Stress concentration factor at the edge of a hole of radius "a" in infinite plate due to tensile stress,  $\sigma$ .

well-defined yield point is expanded either by uniform pressure or radial displacement, yielding will start along the hole edge. If the pressure is increased further, the plate will yield in a zone,  $a \leq r < r_p$ , but will remain elastic beyond it,  $r \geq r_p$ , (where  $a$  and  $r_p$  represent the hole radius and elastic-plastic boundary around the hole, respectively). After the removal of pressure the compressive residual stresses are created by the "springback" of the elastic material around the plastic zone.

Fastener holes are by far the most common stress concentrations existing in aircraft structures. These stress concentrations affect and are usually the controlling factors in fatigue life of structural components of the aircraft. Gran et al. (4), in 1971, indicated that flaws originating at fastener holes are among the most prevalent sources of fracture in aircraft structures. Allen-Ellis (3) and Grandt-Gallagher (6) suggested that proper interference fitting in the structure of aircraft wings not only prevents possible cracks but also prolongs the fatigue life of the structure. One common technique for enhancing fatigue life of fastener holes is to introduce a controlled residual stress field around the fastener holes by means of an interference-fit fastener (6) or by pre-expansion of the holes with an oversize mandrel (5), which is known as the coldworking process. Coldworking differs mainly from interference-fit applications in allowing the hole to radially unload before inserting the fastener. Tiffany et al. (5), in 1973, concluded from their investigation of fatigue and stress-corrosion tests of fastener holes processed in various ways that coldworking is

advantageous. Fatigue life of the cracked fastener holes has been shown to be substantially increased through the coldworking operation.

Basic understanding of the residual nonlinear stress around prestressed holes will come from theoretical and experimental studies of representative problems. The theories developed have shown that the compressive residual tangential stress at the edge of a coldworked hole is very high and decays rapidly. At a distance approximately equal to the diameter of the hole (depending on the amount of coldworking used), the residual stress becomes tensile and the maximum tension stress occurs at the elastic-plastic boundary,  $r_p$ . The residual stress distributions predicted by the Nadai (7) and the Hsu-Forman (8) theories are shown in Figure 1.2. Discussion of the theories in Chapter 4 and comparison with the measurements in Chapter 7 will show that this earliest theory by Nadai is still very useful. The elastic-plastic boundary,  $r_p$ , predicted by each theory occurs at the tensile peak of the residual tangential stress. The value of residual tangential stress at this boundary is equal to the residual radial stress in magnitude. Figure 1.2 shows a very large compressive residual stress next to the edge of the hole. This stress tends to counteract the tensile stress concentration which would otherwise occur in practice. Analytical, numerical, and finite-element theories have been used to predict the residual stresses and strains around a prestressed hole; but the validation of these theories with experimental results has been extremely limited.



## 1.2 Theoretical Solutions

There are several theoretical solutions to the problem of an expanding hole in a thin sheet of material, discussed in more detail in Chapter 4 of this thesis, all of which assume that the hole is radial loaded (prescribing either pressure or displacement at the hole) until the material near the hole is loaded above its yield stress. All of the theories (except the ones by Sachs and Rich-Impellizzeri) assume that a state of plane stress exists everywhere in the infinitely large sheet. After the loading is removed at the hole edge, most theories assume that the material unloads elastically with no reverse yielding.

The theories may be classified according to their kinds of solution. Analytical solutions, in which expressions for the stresses and strains are given in closed form, are desirable because of their ease of application. Some numerical solutions in which the differential equations, along with their boundary conditions, are solved via a computer are also available. As the results of these numerical solutions are presented in dimensionless form, they are also easy to use. One finite-element solution which employs an elastic-plastic finite-element computer code also exists. Equally as important as the form of the solution is the assumption about the material behavior in the plastic region. The constitutive behavior assumed ranges from perfectly plastic to elastic-perfectly-plastic to a two-parameter power law. A fair amount of research has been done on this residual stress problem in the past few years.

### 1.3 The Elastic-Plastic Boundary

Designers encounter considerable difficulty because no plasticity solution is available for the coldworked hole that makes it possible to evaluate the true stress and strain distributions or the elastic-plastic boundary. The elastic-plastic boundary not only determines the residual stress field around a coldworked hole but also is very important in the design and spacing of hole locations in practice. Only the theory of Potter-Grandt (9) has provided the relation between  $r_p$  and  $u_a$  in dimensionless form. The plot of this relationship is useful to the designer in that he can directly predict the elastic-plastic boundary of his plate geometry and material associated with amount of coldwork. But the value of the elastic-plastic boundary predicted by this theory is relatively small when compared with the others, due to its assumptions as discussed in Chapter 4. Therefore, there still is need for a theory which will accurately predict  $r_p$  for a particular coldworked hole. A simple and precise technique is required to initially evaluate theories, which is the objective of this thesis. The elastic-plastic boundary can be located not only by the residual stress distributions (as described in section 1.1) but also by the strain distributions and the change in thickness of the plate.

All theories indicate that the elastic-plastic boundary around a coldworked hole is exactly at the location where loading or unloading radial and tangential strains are first equal in magnitude. To indicate how to locate the elastic-plastic boundary, loading strains predicted by the Hsu-Forman theory are plotted in Figure 1.3.

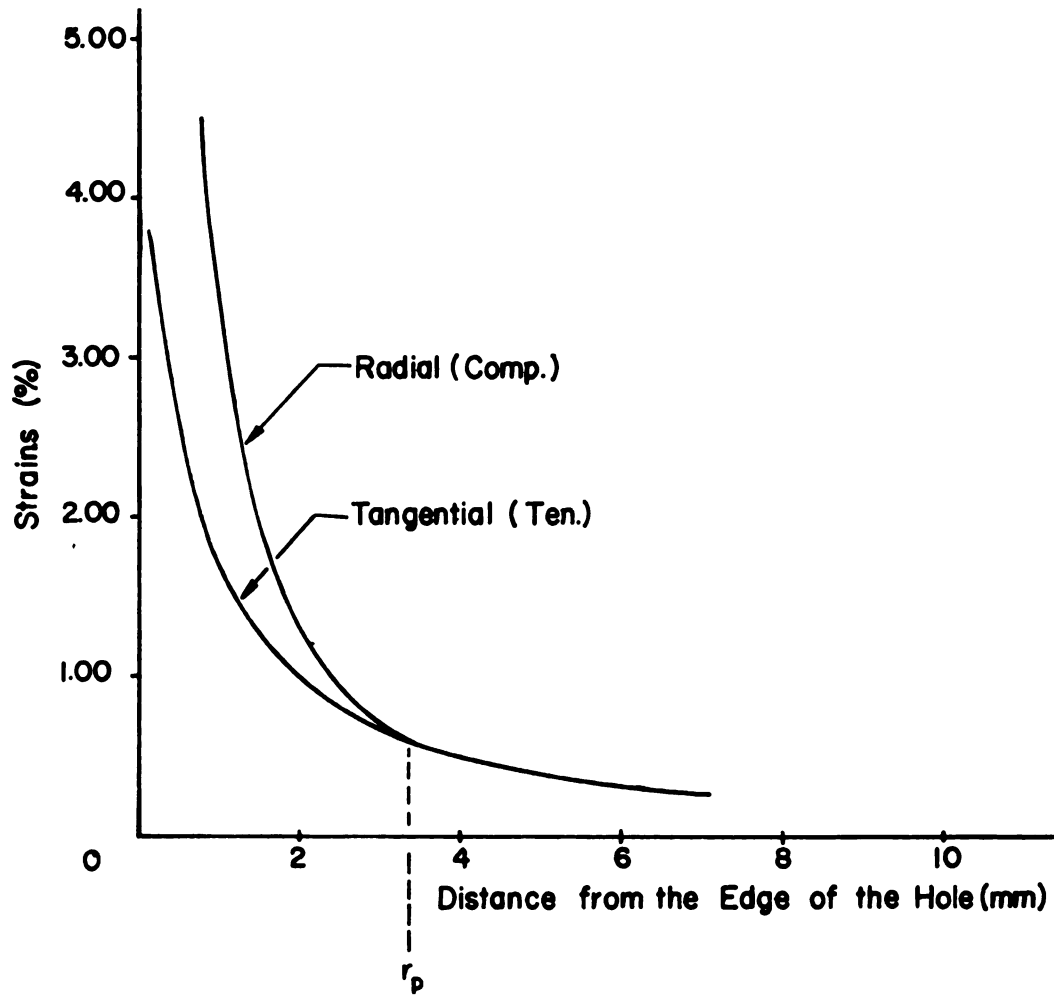


Figure 1.3.--Elastic-plastic boundary predicted by Hsu-Forman (8) located where the predicted loading radial and tangential strains are equal in magnitude and opposite in sign for a 0.305 mm. (0.012 in.) diametral expansion of 6.60 mm. (0.26 in.) hole in 7075-T6 aluminum.

This theory may be the most general of all theories discussed in Chapter IV.

Elasticity theory shows that the radial and tangential stresses,  $\sigma_r$  and  $\sigma_\theta$ , are equal in magnitude and opposite in sign. Since  $\sigma_z = 0$ , the elastic strain equation,

$$\epsilon_z = \frac{1}{E} \left[ \sigma_z - \nu(\sigma_r + \sigma_\theta) \right],$$

shows that the transverse strain,  $\epsilon_z$ , vanishes in the elastic region and at the elastic-plastic boundary. This means that there is no change in the plate thickness at the elastic-plastic boundary. In other words, the elastic-plastic boundary can be located precisely where the plate thickness starts to change.

#### 1.4 Coldworking Procedure

The coldworking procedure studied in this thesis has been developed by

J. O. King, Inc.  
711 Trabert Avenue, N.W.  
Atlanta, Georgia 30318

In this procedure a thin-walled sleeve is first inserted into the hole, after which a tapered mandrel is pulled through the sleeve. After the mandrel has been removed, the sleeve may or may not be removed before the fastener is inserted. The specific amounts of expansion used in this study, 0.076 (0.003 in.), 0.102 (0.004 in.), 0.127 (0.005 in.), and 0.152 (0.006 in.) mm. radial expansions of a 6.60 mm. (0.26 in.) hole were chosen to study their effects on the elastic-plastic boundary around the coldworked hole. None of the modern theories account for the presence of a sleeve. Accordingly,

and in order to avoid some errors of measurement for smaller amounts of coldwork, the sleeve was removed for these experiments.

It may be argued that if one wishes to evaluate theories of plastic radial expansion, one should match the boundary conditions as closely as possible. As mentioned earlier, one of the objectives of this thesis is to initially evaluate the theories. This will be done by examining (by comparison of experiments with theories) the capability of the theories to model this practical coldworking process. An experimental study in which one carefully generated a radial loading would be quite useful in deciding what simplifying assumptions are permissible. However, the industrial process would still have to be studied to determine the theory's applicability.

### 1.5 Overview of Dissertation

The materials used in this thesis are aluminum 7075-T6 and 1100, whose properties are given in Chapter 2. Care must be taken in preparing the original hole to exact dimensions and coldworking it in a manner that is similar to the industrial process and yet controlled enough to permit reproducible tests. The procedures for preparing and coldworking the specimens are given in Chapter 3. The background of the problem and the existing theories are discussed at some length in Chapter 4. Various possible techniques for locating  $r_p$ , including the instruments, precautions, and procedures are described in Chapter 5.

The results of a series of coldworking experiments for two specimen thicknesses and two kinds of aluminum are given in Chapter 6.

The comparison of the theories with the experimental results is discussed in Chapter 7, and closing comments are in Chapter 8.

## CHAPTER 2

### MATERIAL SPECIFICATIONS

The materials used for these studies were aluminum types 7075-T6 and 1100. Two thicknesses--6.35 mm. (1/4 in.) and 3.18 mm. (1/8 in.) for type 7075-T6 and 3.18 (1/8 in.) for type 1100 were tested. Aluminum type 7075-T6 is a "7XXX" series (Zn-Al) and high-strength alloy used for aircraft, space vehicles, and other applications where great strength is required. It is weldable but is subjected to stress corrosion and therefore must be protected by cladding or other surface protection methods. Generally, its precipitation hardening heat treatment begins with the solution heat treatment at 466<sup>0</sup>C. (870<sup>0</sup>F.) and then quenching at room temperature and reheating (artificial aging) at 121<sup>0</sup>C. (250<sup>0</sup>F.) for 25 hours. Typically, this material contains 7% Zn, 2-3% Mg, and up to 1.60% Cu plus a small amount of Cr to reduce stress corrosion susceptibility. Aluminum type 1100 is a pure aluminum of 99.00% or more purity with no special treatment.

Tension test specimens were cut from the same sheet as the specimens and tested according to ASTM E8 procedures. Foil gages were used to measure the strains. The stress-strain curves were obtained and are presented in Figures 2.1 and 2.2. Their mechanical

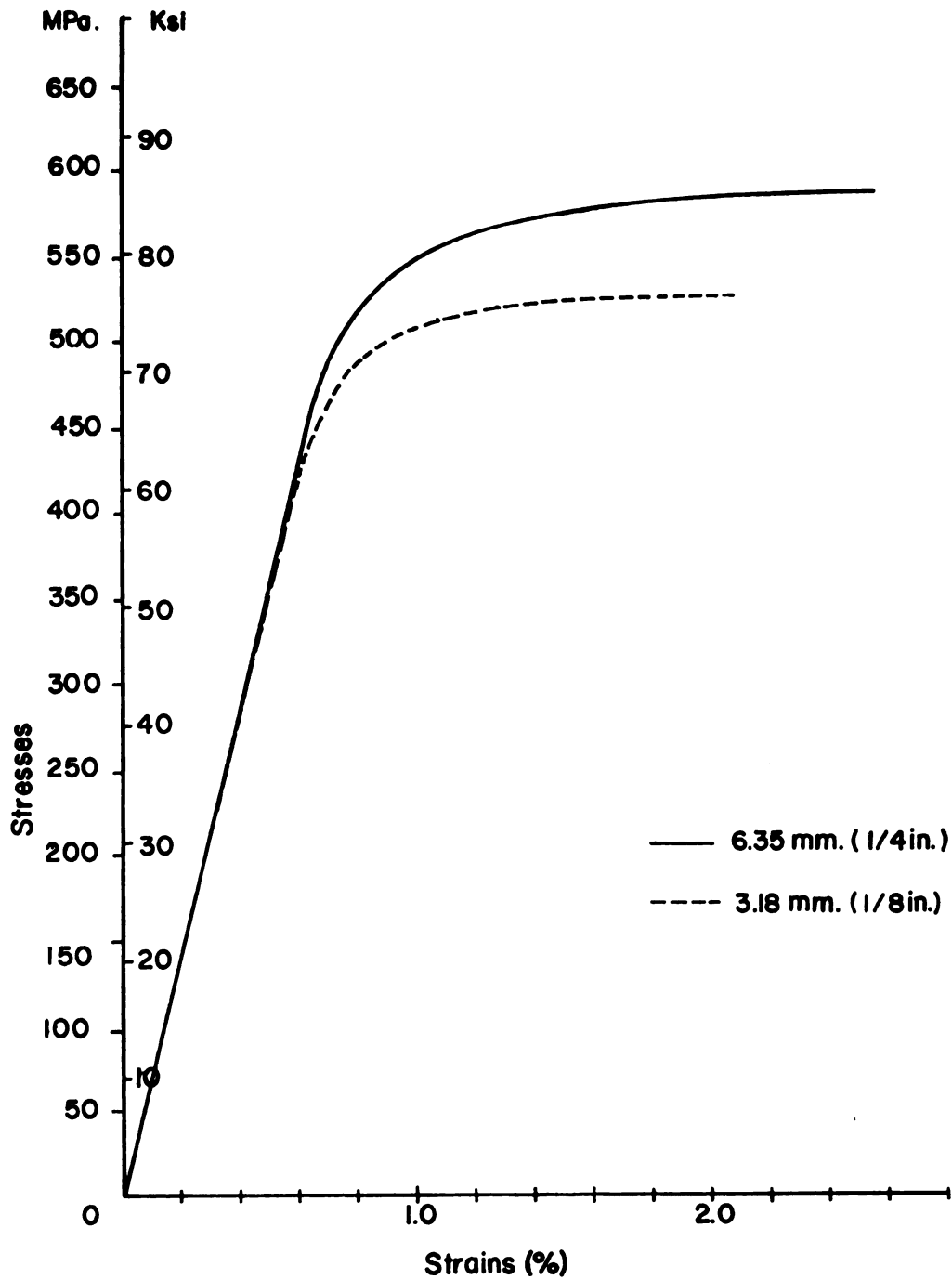


Figure 2.1.--Stress-strain curves for the two different sheets of 7075-T6 aluminum.

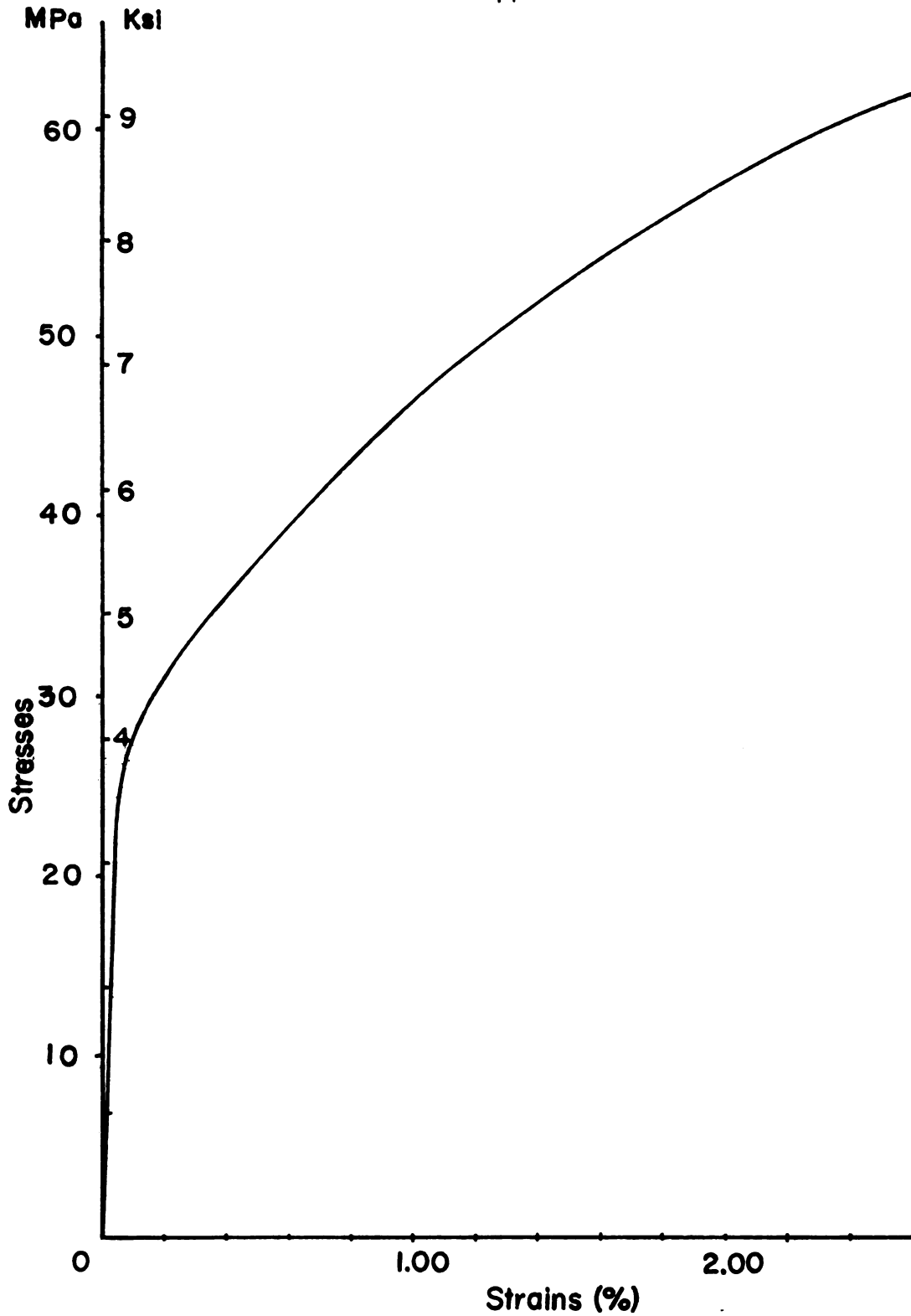


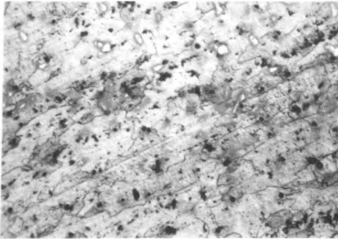
Figure 2.2.--Stress-strain curve for the 3.18 mm. (1/8 in.) thick, type 1100 aluminum.

properties, as obtained from the stress-strain curve and Rockwell hardness tester, are given in Table 2.1.

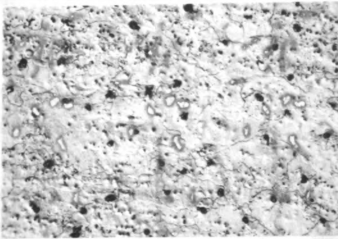
TABLE 2.1--Mechanical properties of materials used.

	Aluminum		
	6.35 mm. (1/4 in) thick, 7075-T6	3.18 mm. (1/8 in) thick, 7075-T6	3.18 mm. (1/8 in) thick, Type 1100
Ultimate Strength (MPa.)	589.1 (85.5 Ksi.)	527.1 (76.5 Ksi.)	79.2 (11.5 Ksi.)
Yield Strength at 0.2% offset (MPa.)	547.8 (79.5 Ksi.)	503.0 (73.0 Ksi.)	32.6 (4.73 Ksi.)
Modulus of Elasticity (MPa.)	$69.6 \times 10^3$ ( $10.1 \times 10^3$ Ksi.)	$68.2 \times 10^3$ ( $9.9 \times 10^3$ Ksi.)	$67.5 \times 10^3$ ( $9.8 \times 10^3$ Ksi.)
Poisson's ratio	0.31	0.31	0.28
Hardness	91R <sub>B</sub>	90R <sub>B</sub>	28R <sub>H</sub>

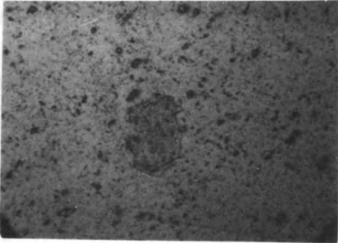
Photographs of their microstructures are presented in Figure 2.3 and it is seen that the microstructure is essentially the same for both thicknesses of 7075-T6 aluminum.



6.35 mm. (1/4 in.)  
thick, 7075-T6



3.18 mm. (1/8 in.)  
thick, 7075-T6



3.18 mm. (1/8 in.)  
thick, type 1100

Figure 2.3.--Photomicrographs of the two sheets of 7075-T6 aluminum (100X) and one sheet of 1100 aluminum (500X).

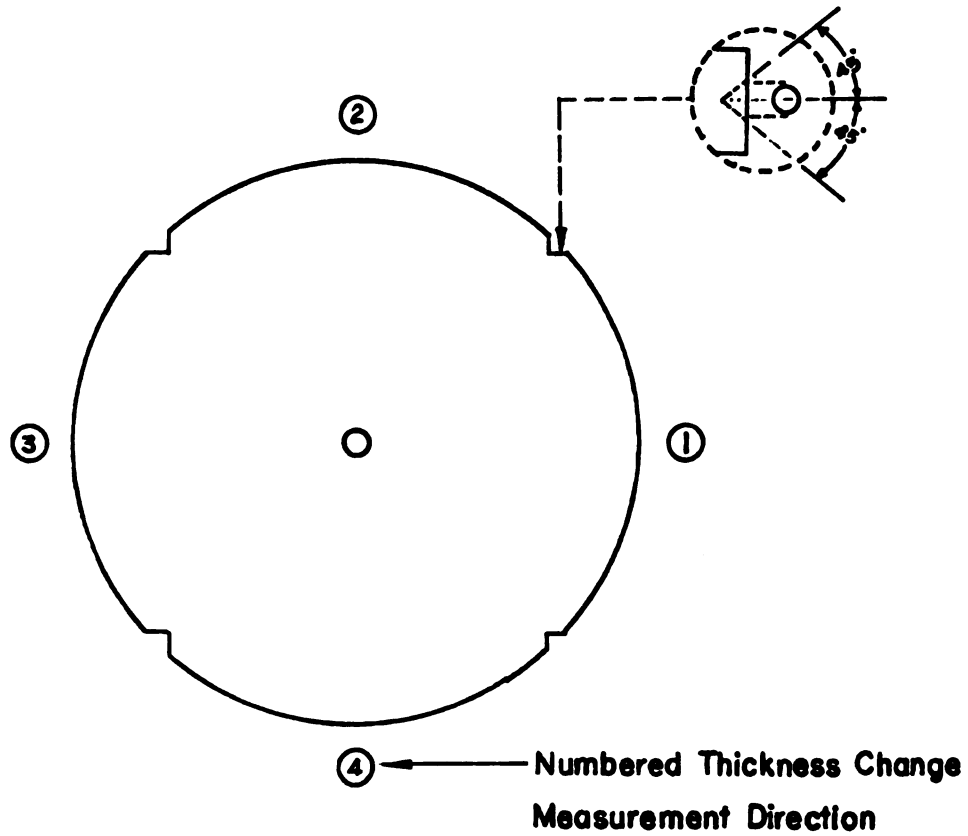
## CHAPTER 3

### HOLE PREPARATION AND COLDWORKING

#### 3.1 Hole Preparation

It is necessary to generate round, nontapered holes to a specific dimension in order to measure accurately the amount of coldworking deformation. A certain tolerance on the holes is required if one is to compare coldworking of various specimens. The variability in hole size and coldworking process that would be represented in an industrial atmosphere cannot be permitted here.

The specimens were circular plates of 178 mm. (7.00 in.) outside diameter, with a hole of 6.60 mm. (0.260 in.) typical diameter at the middle, as illustrated in Figure 3.1. The reason for selecting the 178 mm. circular plate is because of the limitation of the toolmaker's microscope in measuring the hole diameter of the plate. The ratio  $\frac{b}{a} = 27$  is large enough for treatment as an infinitely large plate (9). Holes were prepared by first drilling them with a 6.35 mm. (1/4 in.) drill and then using a honing machine to bring the diameter up to 6.60 mm. (0.260 in.). The honing machine produced straight sides in the hole (no evidence of spiraling) and square edges of the hole. The size was determined with a plug gauge with a "go" cylinder of 6.599 mm. (0.2598 in.) and a "no-go" cylinder of 6.609 mm. (0.2602 in.). Upon receipt from the machine shop, the holes in the specimens were measured with a toolmaker's microscope



**6.6 mm. (0.26 in.) Inside Diameter**

**178 mm. (7.0 in.) Outside Diameter**

Figure 3.1.--Specimen configuration.

equipped with an X-Y stage. The greatest uncertainty in this measurement is in locating the edge of the holes accurately. Measurements were made along diameters at  $45^{\circ}$  intervals, and each measurement was repeated at least three times. The variation in repeated measurements was usually less than 0.003 mm. (0.0001 in.). Original diameter measurements were made on both sides of the specimens. The values of the diameters on both sides were the same, so that only upper side original diameters of all specimens were recorded and are given in Tables 3.1, 3.2, and 3.3 for the 6.35 mm. (1/4 in.), 3.18 mm. (1/8 in.) thick 7075-T6 aluminum and 3.18 mm. (1/8 in.) thick aluminum type 1100, respectively. The measurements show that the holes are of acceptable roundness and diameter.

### 3.2 Coldworking Procedure

The J. O. King, Inc. ACRES coldworking sleeves part numbers:

JK 5535C08N04L for the 6.35 mm. (1/4 in.) thick specimens

JK 5535C08N0r for the 3.18 mm. (1/8 in.) thick specimens

were employed in the expansion of the initial hole diameter. Four associated mandrels were J. O. King, Inc. part numbers:

JK 6540-08-251 for the 0.076 mm. (0.003 in.) radial expansion

JK 6540-08-253 for the 0.102 mm. (0.004 in.) radial expansion

JK 6540-08-255 for the 0.127 mm. (0.005 in.) radial expansion

JK 6540-08-257 for the 0.152 mm. (0.006 in.) radial expansion.

The coldworking sleeves were supplied with the mild steel washer attached (see Figure 3.2), and a dry film lubricant of 0.013 mm. (0.0005 in.) thick applied to the inside and outside. The function of

TABLE 3.1.--Original diameters (in mm.) of holes for a typical set of 6.35 mm. (1/4 in.) thick, 7075-T6 specimens.

Specimen	(1)	(2)	(3)	(4)
P.1	6.622	6.622	6.619	6.624
P.2	6.619	6.619	6.619	6.619
P.3	6.614	6.607	6.609	6.614
P.4	6.614	6.614	6.612	6.609
P.5	6.612	6.612	6.607	6.609
P.6	6.622	6.619	6.614	6.617
P.7	6.629	6.629	6.627	6.629
P.8	6.624	6.624	6.624	6.624
P.9	6.619	6.619	6.619	6.619
P.10	6.614	6.617	6.619	6.617
P.11	6.619	6.622	6.617	6.622
P.12	6.622	6.614	6.614	6.619
P.13	Hole too big			
P.14	6.614	6.612	6.612	6.617
P.15	6.614	6.617	6.617	6.614
P.16	6.612	6.617	6.612	6.619
P.17	6.607	6.609	6.609	6.612
P.18	6.619	6.629	6.622	6.622

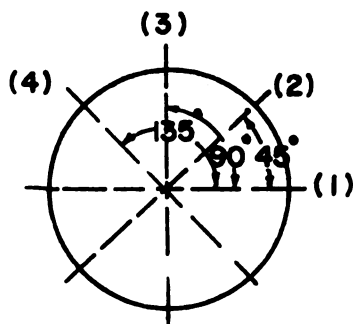
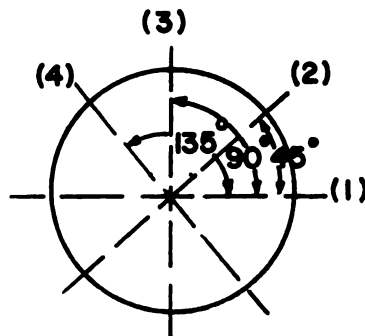




TABLE 3.3.--Original diameters (in mm.) of holes for a typical set of 3.18 mm. (1/8 in.) thick, type 1100 specimens.

Specimen	(1)	(2)	(3)	(4)
P.35	6.617	6.614	6.614	6.619
P.36	6.604	6.594	6.604	6.604
P.37	6.600	6.604	6.604	6.597
P.38	6.668	6.673	6.634	6.657
P.39	6.607	6.591	6.607	6.607
P.40	6.609	6.609	6.600	6.600
P.41	6.609	6.614	6.614	6.591
P.42	6.612	6.604	6.604	6.602
P.43	6.612	6.609	6.606	6.591
P.44	6.629	6.619	6.619	6.624
P.45	Hole too big			
P.46	6.614	6.627	6.629	6.624
P.47	6.622	6.606	6.584	6.612
P.48	6.612	6.591	6.624	6.624
P.49	6.586	6.624	6.627	6.617
P.50	6.627	6.629	6.627	6.602



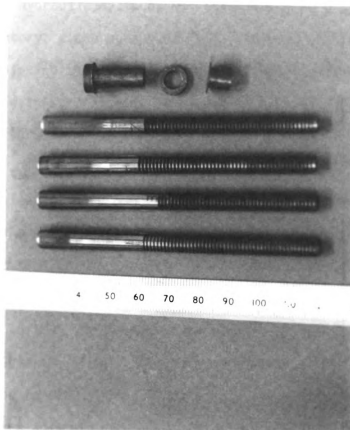


Figure 3.2.--Photograph of mandrels and sleeves.

the mild steel washer is simply to protect the sleeve and specimen as the mandrel is pulled through; it pops off after coldworking.

The coldworking process involves insertion of a sleeve into the hole and then drawing a tapered mandrel through the sleeve to expand the hole, as shown in Figure 3.3. A machine incorporating a hand-operated hydraulic cylinder was constructed to pull the mandrel in the laboratory; a photograph of it is included in Figure 5.2. The tension rod linking the mandrel to the cylindrical piston had been instrumented with strain gages to permit calibration of the force in terms of pressure. The peak force was 5357-7145 Newtons (1200-1600 pounds).

The sleeves, part number JK 5535C08N04, were provided only in the length of 6.35 mm. (1/4 in.). In order to prevent the unre-quired deformation on the upper surface of the 3.18 mm. (1/8 in.) thick specimens due to the longer sleeve, they were carefully cut with a lathe so that the length of the sleeve equaled the specimen thickness. Several sleeves were sectioned, and the average thick-ness was found to be 0.19 mm. (0.0075 in.), in agreement with Sharpe (10) and Adler-Dupree (11). This wall thickness is in fair accord with the sleeve wall thickness of  $0.216 \pm 0.013$  mm. (0.008  $\pm$  0.0005 in.) recorded in the manufacturer's literature. The radial expansion of the hole with the mandrel and sleeve inserted cannot be measured directly. It must be computed from the dimensions of the hole, mandrel, and sleeve, as follows:

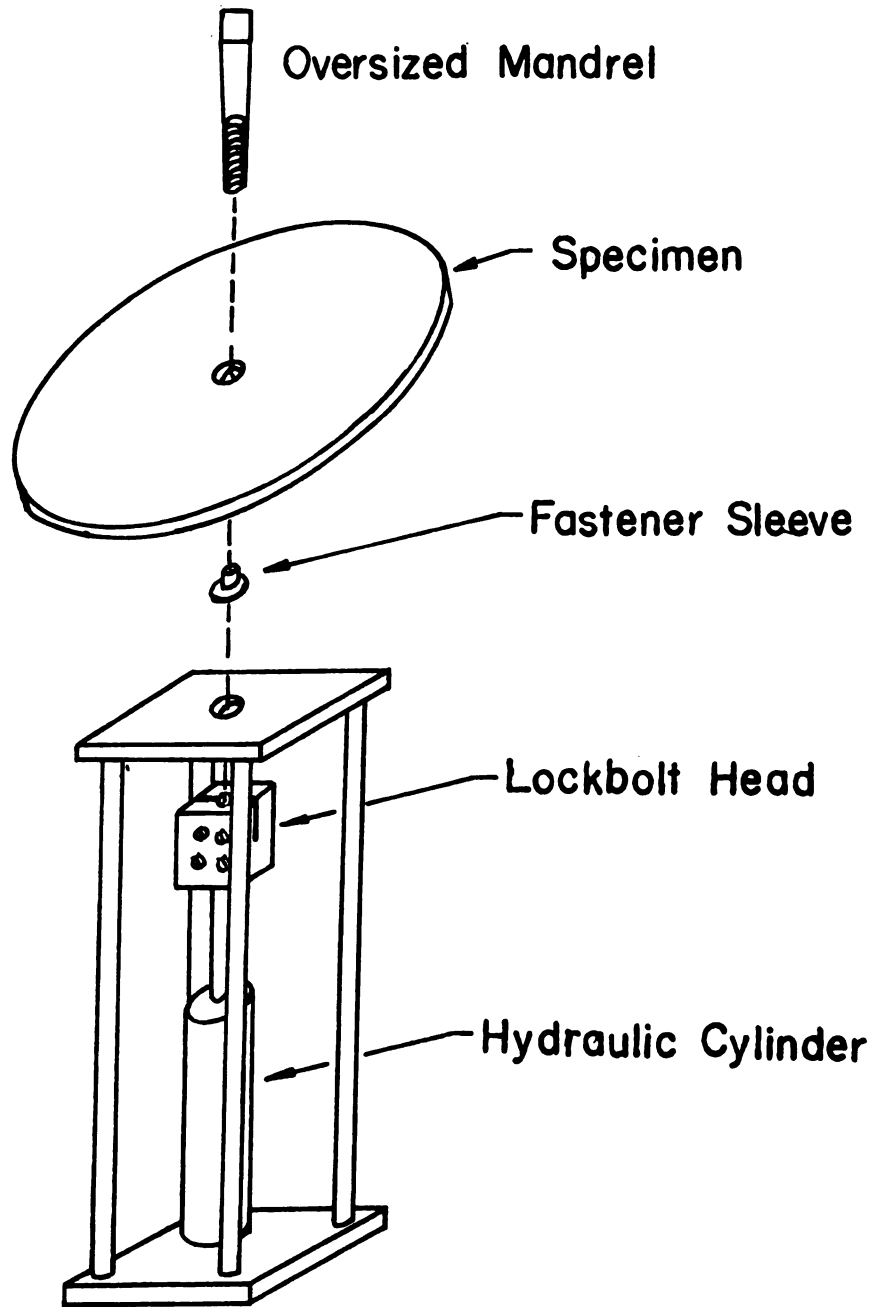


Figure 3.3.--Schematic of the J. O. King coldworking process.

$$\text{Radial Expansion} = \frac{\text{Mandrel Diameter} + 0.015 \text{ in.} - 0.260 \text{ in.}}{2}$$

The relations between hole diameters, mandrel sizes, and radial expansions are as follows:

Original Hole Diameter (mm.)	Mandrel Diameter (mm.)	Sleeve Thickness (mm.)	Radial Expansion (mm.)
	6.38 (0.251 in.)		0.076 (0.003 in.)
	6.43 (0.253 in.)		0.102 (0.004 in.)
6.604 (0.260 in.)		0.381 (0.015 in.)	
	6.48 (0.255 in.)		0.127 (0.005 in.)
	6.53 (0.257 in.)		0.152 (0.006 in.)

It is estimated that this computation expansion is accurate to  $\pm 0.013$  mm. (0.0005 in.). Note that the length of the final diameter of the mandrel is only 3.18 mm. (0.125 in.); it is not possible to uniformly expand a hole in 6.35 mm. (1/4 in.) thick plate.

## CHAPTER 4

### THEORIES OF RESIDUAL STRESSES AROUND A COLDWORKED HOLE

#### 4.1 Introduction

The normal geometry that has been considered by experiments and theories is a flat circular sheet of radius "b" with a circular hole of radius "a" in the center as shown in Figure 4.1. Many of the theories that have been developed assume "b" to be infinitely large, and some of them assume that the thickness of the sheet is sufficiently small relative to the dimension "b" that a condition of plane stress exists. Only two theories, those by Sachs (12) and Rich-Impellizzeri (13), assume a state of plane strain when a small ratio of  $\frac{b}{a}$  and a very large thickness of a plate are considered. Therefore, the ratio of  $\frac{b}{a}$  and  $\frac{t}{b}$  are important in considering a state of plane condition where t is the plate thickness. Potter-Grandt (9) considered the effect of  $\frac{b}{a}$  with a given thickness and found that the ratio of  $\frac{b}{a} > 10$  is relatively large enough for the state of plane stress. They did not consider the effect of  $\frac{t}{b}$ . There is still some question of how big the ratio of the outer radius "b" and the thickness of the sheet should be for plane stress. The solutions for the residual stresses around a coldworked hole have been obtained in the references (7,8,9,11,12,13,14,16,17,18,19). These theories differ in the yield criteria used and in plastic stress-strain relations. Some

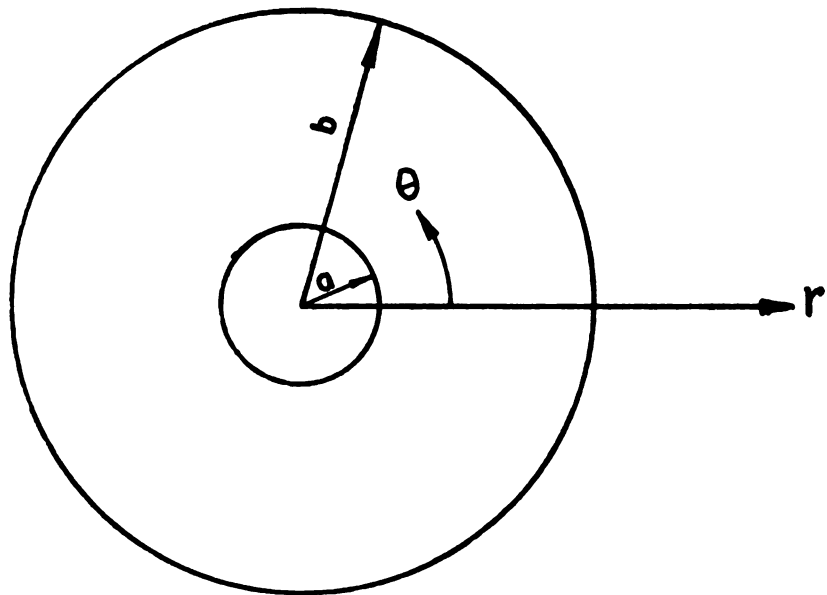


Figure 4.1.--Geometry and coordinate system used in coldworking hole theories.

theories use the Mises-Hencky yield criterion (7,8,9,11,12,13,14,16). Others use the Tresca yield criterion (17,19). Some theories, e.g., Hsu-Forman (8), Adler-Dupree (11), and Alexander-Ford (14) take into account strain hardening of the material. In the others no strain hardening is assumed.

Deformation of the sheet is caused by either a uniform positive radial displacement,  $u_a$ , or a uniform negative pressure,  $-p$ , at  $r=a$ . The shearing stress and strain vanish by symmetry. The stress equilibrium equation which must hold for either elastic or plastic stresses is:

$$\frac{d\sigma_r}{dr} + \frac{\sigma_r - \sigma_\theta}{r} = 0 \quad (4.1)$$

The strain-displacement relation with  $u$  as radial displacement is:

$$\begin{aligned} \epsilon_r &= \frac{du}{dr} \\ \epsilon_\theta &= \frac{u}{r} \end{aligned} \quad (4.2)$$

For a radial displacement,  $u_a$ , small enough that the material remains elastic everywhere, the stresses, strains, and displacements are given by (15) for the truly axisymmetric problems as:

$$\sigma_r = A\left(1 - \frac{b^2}{r^2}\right)$$

$$\sigma_\theta = A\left(1 + \frac{b^2}{r^2}\right)$$

$$\epsilon_r = \frac{A}{E} \left[ (1-\nu) - (1+\nu) \frac{b^2}{r^2} \right]$$

$$\epsilon_\theta = \frac{A}{E} \left[ (1-\nu) + (1+\nu) \frac{b^2}{r^2} \right]$$

$$u = \frac{A}{E} \left[ (1-\nu)r + (1+\nu) \frac{b^2}{r} \right]$$

where

$$A = \frac{Eu_a}{(1-\nu)a + (1+\nu) \frac{b^2}{a}} \quad (4.3)$$

$E$  and  $\nu$  are the modulus of elasticity and Poisson's ratio respectively. The boundary conditions are

$$u = u_a \text{ at } r=a$$

$$\sigma_r = 0 \text{ at } r=b \quad (4.4)$$

Using the plane stress condition ( $\sigma_z=0$ ), the Mises-Hencky yield criterion yields:

$$\sigma_r^2 + \sigma_\theta^2 - \sigma_r \sigma_\theta = \sigma_0^2 \quad (4.5)$$

where  $\sigma_0$  is the yield stress from the uniaxial stress-strain curve (which is taken at the 0.2 percent offset yield strength).

The largest radial displacement that can be applied to the hole without causing plastic deformation is:

$$u_{aE} = \frac{\sigma_0 a}{E(1+3\frac{b^4}{a^4})^{1/2}} \left[ 1-\nu + (1+\nu) \frac{b^2}{a^2} \right] \quad (4.6)$$

Once  $u_{aE}$  (or its equivalent pressure,  $p_E$ ) is exceeded, the material in the neighborhood of the edge of the hole becomes plastically deformed within the elastic-plastic boundary,  $r_p$ , around the hole. The solution of the problem is nonlinear and no longer easy. As  $u_a$  increases,  $r_p$  increases; i.e., the elastic-plastic boundary moves outward. If "b" is assumed to be large,  $\sigma_r = -\sigma_\theta$  outside of  $r_p$ . Therefore equation (4.5) yields, at  $r=r_p$ :

$$\sigma_r = -\sigma_\theta = -\frac{\sigma_0}{\sqrt{3}} \quad (4.7)$$

The solutions for the stresses and strains in plastic region,  $a < r < r_p$ , can be obtained from the theories, depending on which plane condition and yield criteria are used. The solutions in the plastic region must be found for which  $u=u_a$  at  $r=a$  (or  $\sigma_r = -p$  at  $r=a$ ) and the stresses, strains, and displacements match the elastic ones at  $r=r_p$ . The various theories fall into three classes: analytical, numerical, and finite element. The analytical theories produce closed-form equations based on either an elastic-perfectly-plastic stress-strain curve or a two-parameter plastic stress-strain curve. The numerical ones develop the solutions in terms of incremental rings between a and b corresponding to the increments on the plastic stress-strain curve or use a numerical integration to solve the two-point boundary value problem of finite rings for some range of  $\frac{a}{b}$ . The only finite element solution used an elastic-plastic computer code.

The solutions for stresses, strains, and displacements in the elastic region,  $r \geq r_p$ , are:

$$\sigma_r = -\frac{\sigma_0}{\sqrt{3}} \left(\frac{r_p}{r}\right)^2$$

$$\sigma_\theta = \frac{\sigma_0}{\sqrt{3}} \left(\frac{r_p}{r}\right)^2$$

$$\epsilon_r = -\frac{\sigma_0(1+\nu)}{E\sqrt{3}} \left(\frac{r_p}{r}\right)^2$$

$$\epsilon_\theta = \frac{\sigma_0(1+\nu)}{E\sqrt{3}} \left(\frac{r_p}{r}\right)^2$$

$$u = \frac{\sigma_0}{E\sqrt{3}} (1+\nu) \frac{r_p^2}{r} \quad (4.8)$$

Once the hole has been expanded to the prescribed conditions, the loading is then removed at  $r=a$ . This generates, because of the elastic relaxation of material outside and inside  $r_p$ , residual stresses and strains. These quantities can be found by superimposing an elastic distribution at  $r=a$  on the plastic distribution. The elastic distributions are:

$$\sigma_r = \sigma_m \left(\frac{a}{r}\right)^2$$

$$\sigma_\theta = -\sigma_m \left(\frac{a}{r}\right)^2 \quad (4.9)$$

where  $\sigma_m$  is the magnitude of the radial stress generated at  $r=a$  by the loading process. This guarantees that  $\sigma_r=0$  at  $r=a$  after unloading.

## 4.2 Nadai Theory

Nadai (7), in 1943, developed a theory of plastic expansion of small tubes fitted into steam condensers and high-pressure boilers. His paper focussed on a slight enlargement of a small tube, fitted into the plate of a boiler, by means of a device consisting of three hardened rollers with a slight taper which were mounted symmetrically around a long tapered pin. The pressure of the revolving rollers created a radial plastic distribution of stress in the tube wall and around the hole in a steel plate. After the removal of the roller, the residual stresses remain locked in near the edge of the hole, as well as in the tube, and guarantee a leak-free fit. He considered both the plastic deformation in the steel plate and copper alloy tubes. He also solved the plate problem, which is the one of interest here. His assumptions were:

1. Uniform pressure at the inside edge of the hole in an infinite plate
2. Mises-Hencky yield criterion
3. Perfectly plastic material response.

In his first investigation of the paper he predicted the yielding of the plate satisfied "the ellipse of plasticity," namely:

$$\sigma_r^2 + \sigma_\theta^2 - \sigma_r \sigma_\theta = \sigma_0^2 \quad (4.10)$$

and developed the following expression:

$$\sigma_r = \frac{2\sigma_0}{\sqrt{3}} \sin\left(\theta - \frac{\pi}{6}\right)$$

$$\sigma_{\theta} = \frac{2\sigma_0}{\sqrt{3}} \sin\left(\theta + \frac{\pi}{6}\right)$$

$$r^2 = \frac{e^{\sqrt{3}\theta}}{\cos\theta} r_p^2 \quad (4.11)$$

where  $\theta$  was any angle of the points on the ellipse of plasticity. He found that  $\theta=0^\circ$  at the onset of the yielding, and  $\theta = \frac{\pi}{3}$  was the maximum value. This gave the elastic-plastic boundary  $r_p=1.75a$ . Not much was gained in carrying the expansion of the plate beyond this point.

In his second investigation he used the same assumptions, but a linear approximation to the Mises-Hencky yield criterion was assumed instead. He developed the largest radial displacement that could be applied to the hole without causing plastic deformation as:

$$u_{aE} = \frac{\sigma_0 a}{\sqrt{3}E} (1+\nu) \quad (4.12)$$

In the plastic region,  $a < r \leq r_p$ , he developed the following expressions:

$$\sigma_r = \frac{\sigma_0}{\sqrt{3}} \left(-1 + 2 \ln \frac{r}{r_p}\right)$$

$$\sigma_{\theta} = \frac{\sigma_0}{\sqrt{3}} \left(1 + 2 \ln \frac{r}{r_p}\right)$$

$$u = u_{aE} r/a \left(1 + \frac{2}{3} \ln \frac{r}{r_p}\right)^3 \quad (4.13)$$

where the strains are given by:

$$\begin{aligned}\epsilon_r &= du/dr \\ \epsilon_\theta &= u/r\end{aligned}\tag{4.14}$$

After the roller device was removed, the residual stresses and strains were determined by superposing an elastic distribution of stresses of the tube joint at  $r=a$  on the plastic distribution.

Equation 4.13 is the radial plastic displacement during loading. One can locate the elastic-plastic boundary,  $r_p$ , by using this equation for a given radial displacement,  $u_a$ , at  $r=a$ .

#### 4.3 Swainger Theory

In 1945 Swainger (16) published a theory of plasticity and calculated the stresses and residual stresses around an expanded hole. He founded his theory on certain observations of plastic behavior that are well-known today, and treated the material as having a bilinear stress-strain curve with elastic slope and plastic slope. The material was assumed to yield according to the Mises-Hencky theory by a uniform pressure applied on the inside of the hole under plane stress conditions.

Two assumptions were made which permitted solution of the problem:

1. When the yield zone in the bilinear-strain curve is narrow enough, the plastic slope can be regarded as an approximate constant through it.
2. In general, when the yield zone is wide, it may be considered to vary step-by-step over narrow annuluses.

He developed the expressions for stresses and strains in his paper. He also introduced the relation between  $u$  and  $r$  from which one can compute  $r_p$  for his problem. As computed by Sharpe (10), the  $r_p$  was about  $1.50a$  for the radial expansion displacement of  $0.152$  mm. ( $0.006$  in.) for the 7075-T6 aluminum, which is very much smaller than the  $r_p$  predicted by other theories.

#### 4.4 Taylor Theory

G. I. Taylor (17) in 1947 published a theory of the expansion of a circular hole in a thin plastic sheet by radial pressure. His assumptions were:

1. Perfectly plastic material response
2. Tresca's yield criterion and a flow rule associated with Mises-Hencky yield criterion
3. Uniform pressure at the edge of the hole.

His solutions started with a pin-hole subjected to a uniform pressure, and three regions were considered. In the first region,  $a \leq r \leq r_2$ , large plastic strain occurred, and the plastic tangential stress was negative. The value of  $r_2$  was computed to be  $0.606r_p$ . The second region,  $r_2 \leq r \leq r_p$ , had small plastic strain in which tangential stress was positive. The third region was elastic for  $r \geq r_p$ . Since the initial hole was started with a pin-hole, this problem is not exactly like the coldworked hole problem.

In the second region,  $r_2 \leq r \leq r_p$ , he developed the expressions for stresses and strains as follows:

$$\sigma_r = \frac{\sigma_0}{2} (1 + 2 \ln \frac{r}{r_p})$$

$$\sigma_\theta = \frac{\sigma_0}{2} (1 + 2 \ln \frac{r}{r_p})$$

$$u = \frac{3\sigma_0 r}{4E} \left[ \frac{3}{2 \left[ 1 + \frac{1}{3} \ln \left( \frac{r}{r_p} \right)^2 \right]^2} - \frac{1}{2} \right] \quad (4.15)$$

$$\epsilon_r = \partial u / \partial r$$

$$\epsilon_\theta = u / r \quad (4.16)$$

One cannot compute  $r_p$  from the third equation of (4.15), because  $u$  at  $r=r_2$  is unknown. Therefore, this theory did not give an explicit relation between  $r_p$  and  $u_a$ . He also computed the predicted variation of thickness with  $r$  with experiments in which he slowly forced a rotating mandrel of very small taper into a hole in a thin lead sheet. The agreement was very good as the thickness change decreased to zero at  $r=r_2$ .

#### 4.5 Alexander-Ford and Mangasarian Theories

Alexander and Ford (14) in 1954 published a theory of expansion by uniform pressure of a hole from zero radius in an infinitely thin plate. They assumed that the material obeyed the Mises-Hencky yield criterion and associated Prandtl-Ruess relation for a specific uniaxial stress-strain curve. The expressions for stresses in the plastic zone were developed exactly the same as earlier theory of Nadai (7). For strains, they developed four simultaneous, nonlinear, ordinary differential equations and solved them by a numerical method.

The solutions by this theory are different from the coldworked hole problem due to zero initial radius of the hole, but one can obtain the solution to that problem by discarding the parts of the solutions around the hole that are not required.

Mangasarian (18) in 1960 computed the solutions by both deformation and incremental theories of plasticity, together with the Ramberg-Osgood uniaxial stress-strain relation, by a numerical method and found little difference between the two solutions.

These two theories did not predict  $r_p$ .

#### 4.6 Carter-Hanagud Theory

A. E. Carter and S. Hanagud (19) in 1974 performed an experimental investigation of the stress corrosion susceptibility of stress-coined (coldworked) fastener holes in AISI 7075-T651 aluminum. Their point was that the residual tensile stresses surrounding the hole could be above the threshold stress to cause stress corrosion cracking. They developed their own theory, which is similar to Taylor (17), to evaluate loading and unloading stresses. Their assumptions were:

1. Radial displacement at the edge of the hole
2. Tresca yield criterion
3. Elastic-plastic material response.

They also assumed the coldworking mandrel to be rigid and ignored thickness variations in the plastic region and developed the following relationship:

$$u_{aE} = \frac{1+\nu}{2E} \sigma_o a$$

$$u_a = u_{aE} + \frac{\sigma_0}{2E} \left[ \frac{3-\nu}{2a} (r_p^2 - a^2) - 2(1-\nu)a \ln \frac{r_p}{a} \right] \quad (4.17)$$

The elastic deformation was included in developing equation (4.17). The value of  $r_p$  can be computed from equation (4.17) for a given  $u_a$ . It must be noted that the predicted  $r_p$  by this theory are larger than other theories as shown in Figure 4.3 at the end of this chapter.

#### 4.7 Hsu-Forman Theory

In 1975, Y. C. Hsu and R. G. Forman (8) developed an exact elastic-plastic solution for stresses in an infinite sheet having a circular hole subjected to pressure on the basis of  $J_2$  deformation. Their work is basically the Nadai theory extended to account for work-hardening. Only small displacements were considered. They assumed:

1. Uniform pressure at the hole
2. The actual stress-strain curve represented by a modified uniaxial Ramberg-Osgood Law:

$$\epsilon = \frac{\sigma}{E} \text{ for } |\sigma| \leq \sigma_0$$

$$\epsilon = \frac{\sigma}{E} \left( \frac{\sigma}{\sigma_0} \right)^{n-1} \text{ for } |\sigma| \geq \sigma_0$$

3. Mises-Hencky yield criterion in which  $R=1$ , where  $R$  was the ratio of the transverse plastic strain in the plane of the sheet to the plastic strain through the thickness.

The solutions were developed in terms of a parameter  $\alpha$  which varies between  $\frac{\pi}{2}$  at elastic-plastic boundary and  $\alpha_a$  at the edge of the hole corresponding to a radial expansion  $u_a$ .

In plastic zone,  $a \leq r \leq r_p$ , they established the following equations:

$$\sigma_r = \left[ \frac{\sigma(2+2R)^{\frac{1}{2}}}{2} \right] \left[ \cos\alpha - (1+2R)^{-\frac{1}{2}} \sin\alpha \right]$$

$$\sigma_\theta = \left[ \frac{\sigma(2+2R)^{\frac{1}{2}}}{2} \right] \left[ \cos\alpha + (1+2R)^{-\frac{1}{2}} \sin\alpha \right]$$

$$\frac{\sigma}{\sigma_0} = \left[ \frac{(n-1)(1+2R)^{\frac{1}{2}}}{(n-1)(1+2R)^{\frac{1}{2}} \sin\alpha + (n+1+2R) \cos\alpha} \right]^\mu \cdot \exp \left[ \frac{(n-1)(1+2R)^{\frac{1}{2}}}{n^2+1+2R} \left( \alpha - \frac{\pi}{2} \right) \right]$$

$$\mu = \frac{n+1+2R}{n^2+1+2R}$$

$$\frac{r}{a} = \left( \frac{\sin\alpha_a}{\sin\alpha} \right)^{\frac{1}{2}} \left[ \frac{(n+1+2R) \cos\alpha + (n-1)(1+2R)^{\frac{1}{2}} \sin\alpha}{(n+1+2R) \cos\alpha_a + (n-1)(1+2R)^{\frac{1}{2}} \sin\alpha_a} \right]^\gamma \cdot \exp \left[ \frac{(n^2-1)(1+2R)^{\frac{1}{2}}}{2(n^2+1+2R)} (\alpha_a - \alpha) \right]$$

$$\gamma = \frac{n(1+R)}{n^2+1+2R}, \quad \frac{\pi}{2} \leq \alpha \leq \alpha_a \quad (4.18)$$

$$\epsilon_r = \frac{\sigma_r - \nu \sigma_\theta}{E} + \left( \frac{1}{E_s} - \frac{1}{E} \right) \left( \sigma_r - \frac{R}{1+R} \sigma_\theta \right)$$

$$\epsilon_\theta = \frac{\sigma_\theta - \nu \sigma_r}{E} + \left( \frac{1}{E_s} - \frac{1}{E} \right) \left( \sigma_\theta - \frac{R}{1+R} \sigma_r \right) \quad (4.19)$$

One can compute the elastic-plastic boundary,  $r_p$ , from the last equation of (4.18) by setting  $\alpha = \frac{\pi}{2}$  at  $r = r_p$ .

They also developed the expressions in terms of radial expansion as follows:

$$u_o = \frac{1+\nu}{\sqrt{3}E} \sigma_o a \quad (4.20)$$

which is exactly the same as Nadai (7) for the largest radial expansion for elastic deformation.

$$\frac{u_a}{u_o} = \frac{\sqrt{3}}{1+\nu} \left(\frac{\sigma}{\sigma_o}\right)^n [(1-\nu') \cos \alpha_a + \frac{1+\nu'}{\sqrt{3}} \sin \alpha_a] \quad (4.21)$$

$$\nu' = \frac{R}{1+R} - \left(\frac{R}{1+R} - \nu\right) / \left(\frac{\sigma}{\sigma_o}\right)^{n-1}$$

where  $E_s$  is the secant modulus on the uniaxial stress-strain curve at the effective stress  $\sigma$ :

$$\sigma = [\sigma_r^2 + \sigma_\theta^2 - \frac{2R}{1+R} \sigma_r \sigma_\theta]^{\frac{1}{2}} \quad (4.22)$$

After the removal of pressure, the residual stresses and strains could be computed by subtracting unloading stresses and strains from the loading ones.

In addition, this theory stated that the pressure at the edge of the hole must be known and  $\alpha_a$  could be determined from the third equation of (4.18). This is not possible for a practical coldworking process; no one can tell exactly what the pressure at the edge is. But he can solve the problem using a given  $u_a$  in equation (4.21) to determine  $\alpha_a$ . With the determined  $\alpha_a$  for each  $u_a$  he can compute  $r_p$  from the fourth equation of (4.18) by setting  $\alpha = \frac{\pi}{2}$  at the elastic-plastic boundary.

The 7075-T6 aluminum here are adequately represented by:

$n=15$ ,  $\sigma_0=73.0$  Ksi (503.0 MPa) for 3.18 mm. (1/8 in.) thick;

$n=15$ ,  $\sigma_0=79.5$  Ksi (548 MPa) for 6.35 mm. (1/4 in.) thick.

$u_a$ (mm.)	$\alpha_a$ (3.18 mm. thick)	$\alpha_a$ (6.35 mm. thick)
0.0762 (0.003 in.)	125.0°	123.8°
0.1016 (0.004 in.)	129.6°	128.7°
0.1270 (0.005 in.)	132.6°	131.8°
0.1524 (0.006 in.)	134.6°	133.9°

The values of the  $r_p$  predicted by this theory are shown at the end of this chapter (see Figure 4.3).

#### 4.8 Adler-Dupree's Finite Element Method

W. F. Adler and D. M. Dupree (11) in 1974 performed an elastic-plastic element analysis of the two-dimensional stress field around a coldworked hole. They assumed the plane stress condition and accounted for plastic behavior of the material by a Ramberg-Osgood relation which relates the equivalent plastic strain to the  $n$ th power of the equivalent stress. To insure the geometric symmetry of the elements, they divided the plate thickness into equal layers. The finite element mesh was made up of quadrilateral elements in nine concentric circles, which were divided into two triangular elements by a diagonal to different corners on each layer. This resulted in the elimination of the additional nodes at the diagonal intersection and four triangles in one quadrilateral. Furthermore, a data reduction method was used to average the strains of the four triangles within each quadrilateral area of the model to be the input

for the contour plots at middle location of that quadrilateral area. Therefore, the strains could not be determined right at the edge of the hole. The closest they could get to the hole edge was 0.64 mm. (0.025 in.).

They started the finite element computation with the principle of minimum potential energy for the elastic solution, and then connected the elastic solution to the plastic one with an accumulated prestrain associated with the Prandtl-Reuss flow rule and the assumptions used. The specific problem they considered was a 0.152 mm. (0.006 in.) radial expansion of a 6.6 mm. (0.26 in.) hole in 7075-T6 aluminum and then removal of expansion. This is the cold-working process of J. O. King Inc., which is the same as used in this thesis. Two-dimensional plots of stresses and strains, as a function of distance from the hole edge for the expanded hole, the relaxed hole, and an expanded hole subjected to remote uniaxial tensions, were given.

#### 4.9 Potter-Grandt Theory

R. M. Potter and A. F. Grandt (9) in 1975 applied the general solution of forced fitting by Potter-Ting (20) to coldworked holes with the following assumptions:

1. Uniform radial displacement at the hole
2. Mises-Hencky yield criterion
3. Elastic-plastic material response.

They used numerical integration to solve the two-point boundary value problem of finite rings of  $\frac{b}{a}$  ranging from  $\frac{b}{a}=3$  to  $\frac{b}{a}=40$ , and

presented all results in dimensionless forms. Besides the stresses around the hole, they also predicted the elastic-plastic boundary versus the radial displacements used. This is useful to the designer, as shown by one of their figures on the following page, Figure 4.2. Their work is similar to the earlier work of Nadai (7), except that they did not use a linearized yield criterion. The later work of Hsu-Forman contains their solution for loading as a special case.

There are, however, three important differences between the Potter-Grandt theory and these other two just mentioned:

1. Potter-Grandt computed the yielding associated with unloading, and did not simply superpose an elastic solution.
2. The geometry they considered was a finite ring of outer radius "b".
3. Their solution is not presented in closed-form; the differential equation is solved numerically.

The first version of the Nadai theory shows that there is a limiting value of  $r_p = 1.75a$  corresponding to the maximum allowable pressure. This restriction on the deformation shows up in the Potter-Grandt theory as a limitation on the allowable radial displacement. For the 7075-T6 aluminum used, the maximum radial displacement of 0.1346 mm. (0.0053 in.) is allowed by this theory; therefore the 0.152 mm. (0.006 in.) radial displacement of this experiment is not permitted. The plot of the  $r_p$  by this theory was depicted in Figure 4.3 for 3.18 mm. (1/8 in.), 6.35 mm. (1/4 in.) thick, 7075-T6 aluminums. Pure aluminum type 1100 is not permitted

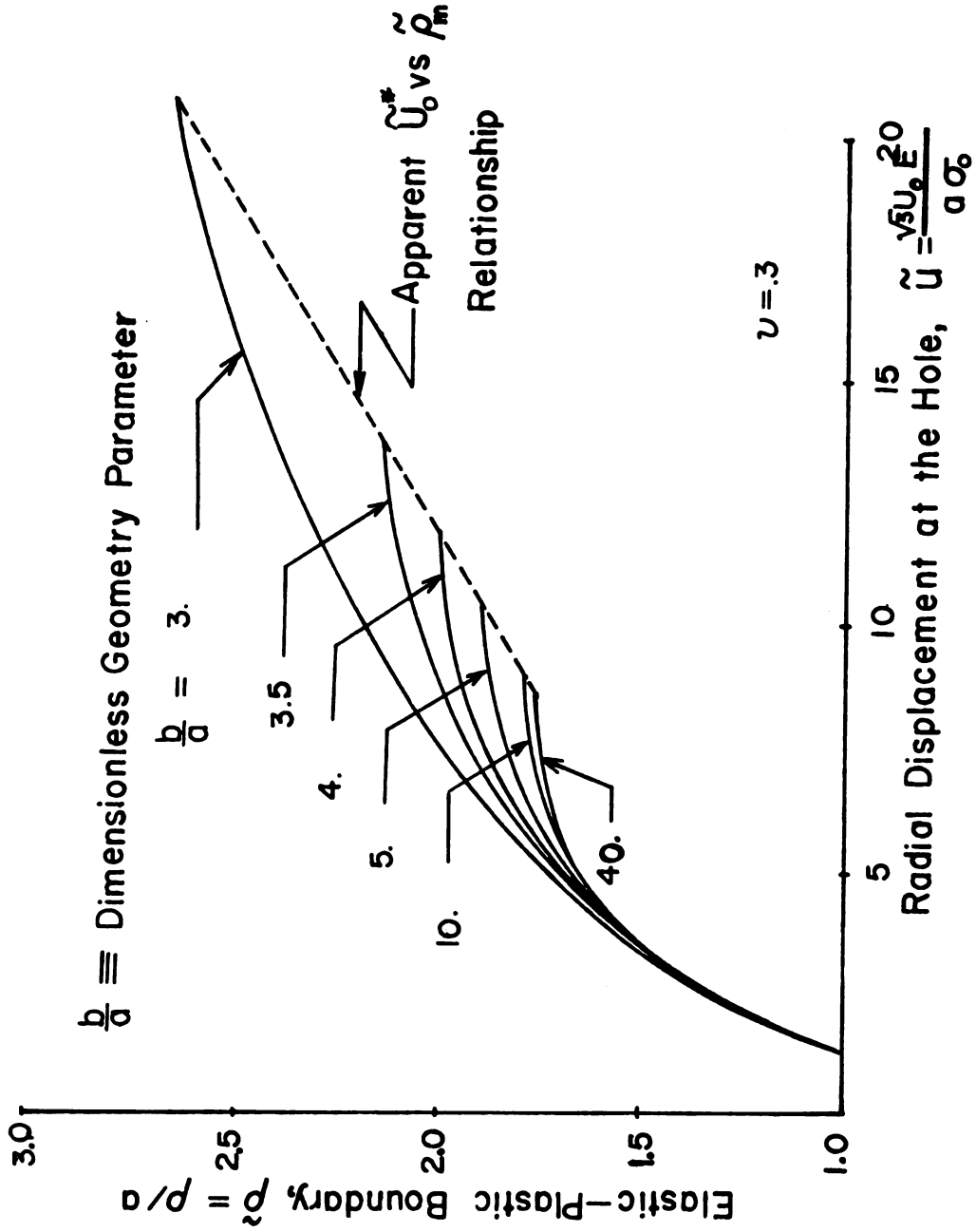


Figure 4.2.--Loading elastic-plastic boundary,  $\tilde{p}$ , vs. radial displacement at the hole,  $\tilde{u}$ , from reference 9.

due to the out-of-range of its yield stress and radial displacement used.

#### 4.10 Thick-Walled Tube Theory

In 1975, J. B. Chang (21) used the elastoplastic solution of a pressurized thick-walled cylinder (12) to evaluate the residual stress distribution adjacent to an open hole in a thick plate, before using it for an analytical prediction of fatigue crack growth of coldworked fastener holes. The assumptions of this theory were:

1. Perfectly plastic material
2. Uniform pressure at the edge of the hole
3. Plane strain condition
4. Mises Hencky yield criterion and flow rule associated with Saint-Venant's theory of plastic flow.

The elastoplastic solutions were developed in terms of stresses and also in terms of an amount of coldworking and plastic zone radii (for  $a \leq r \leq r_p$ ) as follows:

$$\sigma_r = \frac{\sigma_0}{\sqrt{3}} \left( 21n \frac{r}{r_p} - 1 + \frac{r_p^2}{b^2} \right)$$

$$\sigma_\theta = \frac{\sigma_0}{\sqrt{3}} \left( 21n \frac{r}{r_p} + 1 + \frac{r_p^2}{b^2} \right)$$

$$\sigma_z = \frac{\sigma_0}{\sqrt{3}} \left( 21n \frac{r}{r_p} + \frac{r_p^2}{b^2} \right)$$

$$p = \frac{\sigma_0}{\sqrt{3}} \left( 21n \frac{r_p}{a} + 1 - \frac{r_p^2}{b^2} \right)$$

$$u = \frac{\sigma_o r_p^2}{2\sqrt{3}Ga} \quad (4.23)$$

where  $p$  is the pressure applied at the edge of the hole.

Chang used these solutions for 12.7 mm. (1/2 in.) thick, 2024-T851 aluminum with 0.178 mm. (0.007 in.) radial expansion applied to a 12.7 mm. (0.5 in.) hole. The analytical crack growth behavior was predicted through the use of a computer. Reasonably good correlations were obtained when compared to those generated from B-1 fracture mechanics properties programs.

The prediction of  $r_p$  by this theory can be obtained from either the fourth or fifth equation of (4.23) if the applied pressure or radial expansion used is known. The plot of  $r_p$  depicted in Figure 4.3 was obtained from the fifth equation of (4.23). This theory gives slightly larger  $r_p$  for all three materials used.

#### 4.11 Rich-Impellizzeri Theory

D. L. Rich and L. F. Impellizzeri (13) in 1976 developed an approximate closed-form solution for residual stresses around cold-worked holes and interference fit fasteners in their determination of the improvement in fatigue life of structural components of aircraft. The solutions for loading stresses were taken from the elastoplastic analysis of the thick-walled tube with internal pressure (12) with  $\nu=0.5$  for the plate. For the residual stress, they did the same as others by simply superposing an elastic unloading on loading one. The residual stress distributions were valid as long as compressive

yield was not exceeded at the hole edge on elastic unloading. When the compressive yielding occurred, they developed an approximate compressive yield zone as:

$$r_c = \sqrt{\frac{a^2}{2(1-\frac{a^2}{b^2})} (21n\frac{r_p}{a} + 1 - \frac{r_p^2}{b^2})} \quad (4.24)$$

The residual tangential stress became maximum in magnitude at  $r=r_c$  and decreased to be:

$$(\sigma_\theta)_{RES} = \frac{2\sigma_o}{\sqrt{3}} (-2\gamma + \frac{a^2}{b^2} e^{2\gamma}) \quad (4.25)$$

$$\text{where } \gamma = \frac{1}{2} - \frac{a^2}{b^2} + \frac{1}{2} \frac{r_p^2}{b^2}$$

at the hole edge. This is the same shape as the residual tangential stress predicted by Potter-Grandt (9).

It must be noted that they worked on the tangential stress and took them from the tube analysis (12). By setting the radial interference fit equal to the sum of radial displacement of the mandrel and the plate, they introduced the relation between  $r_p$  and  $u$  as:

$$\frac{u}{a} = \frac{\sigma_o}{\sqrt{3}E_B} [0.52(21n\frac{r_p}{a} + 1 - \frac{r_p^2}{a^2}) + 1.5 \frac{r_p^2}{a^2} \frac{E_B}{E_p}] \quad (4.26)$$

where  $E_B$  and  $E_p$  were the modulus of elasticity of mandrel and plate, respectively.

The predicted  $r_p$ , for this theory, can be computed from equation (4.26) by using the trial and error method for a given  $u=u_a$ . For the tested

cases, the  $r_p$ 's were given in Figure 4.3 by assuming  $\nu = 0.3$  and  $E_B = 30 \times 10^6$  psi for the mandrel.

#### 4.12 Discussion

The theories for predicting the stresses and strains around a coldworked hole, as well as some for predicting  $r_p$ , fall into two classes: those that allow work-hardening (Alexander-Ford, Mangasarian, Hsu-Forman, and the finite element one), and those that do not (Nadai, Taylor, Carter-Hanagud, Sachs, and Rich-Impellizzeri). All of the theories considered, except the finite element solution and Mangasarian, are of the deformation, not incremental, type.

Figure 4.3 shows the elastic-plastic boundaries predicted by various theories for typical 7075-T6 aluminum.

In the non-workhardening theories (see Figure 4.3), Nadai assumes plane stress and linearized Mises-Hencky yield criterion in computing his relation between  $r_p$  and  $u$  which causes his  $r_p$  to be smaller than Carter-Hanagud, who assumed the Tresca yield criterion and included elastic deformation in computing  $r_p$ . The Potter-Grandt theory uses the Mises-Hencky yield criterion (not the linearized one) and gives a very much smaller value of  $r_p$ . The Rich-Impellizzeri theory assumes plane strain, linearized Mises-Hencky yield criterion and accounts for radial compressive displacement of the mandrel. It allows the assumption of elastic unloading, but computes a compressive yield zone to avoid the violation of yield criterion near the hole edge. The computed  $r_p$  by this theory are larger than those of the plane stress condition but smaller than predicted ones by the thick-walled tube solution. Within this class, the choice of yield

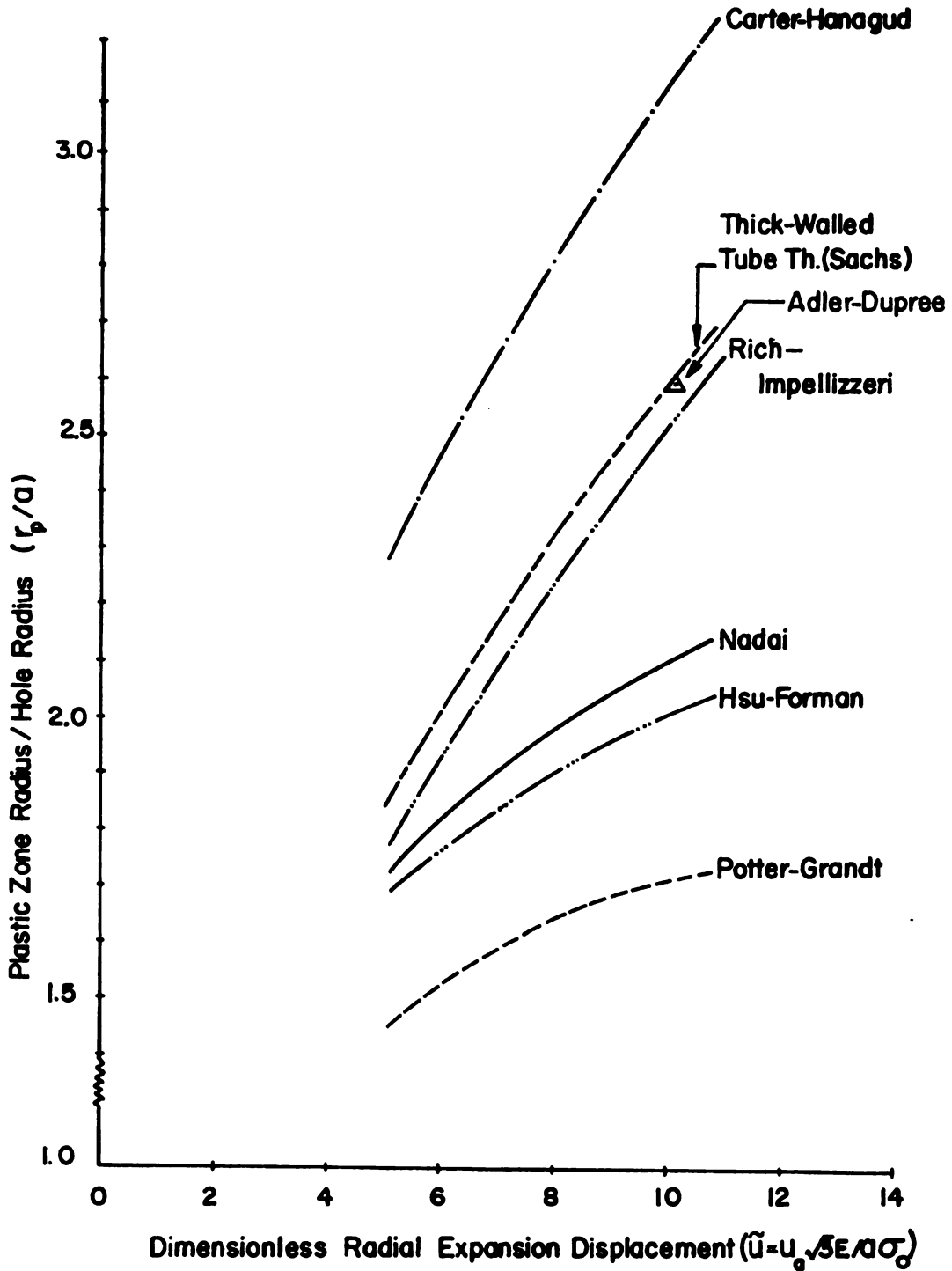


Figure 4.3.--Elastic-plastic boundaries predicted by various theories.

criterion, plane condition, and the decision on whether or not a rigid mandrel and elastic deformation are accounted for make a lot of difference. Mendelson (22) summarized much experimental data using these two yield criterions, and he found the Mises-Hencky yield criterion to be better. Therefore, the Potter-Grandt theory, in the sense of yield criterion, plane condition, accounting for elastic deformation in which the real material behaves, and computing yielding on unloading, is more complete.

The work-hardening theories account for elastic deformation inside the elastic-plastic boundary,  $r_p$ . Swainger works on the incremental rings over the plastic stress-strain curve and produces all equations in terms of an annulus thickness which is different from the others (8,11,14), while Mangasarian works on both  $J_2$ -deformation and incremental theories. The finite-element solution by Adler-Dupree suffers from an inability to produce values near the edge of the hole due to the quadrilateral area there, and also is not generally applicable. The Hsu-Forman theory is the most general of all theories developed; it produces all values needed for a cold-worked hole in workable closed-form that make for economical computation.

In all of these theories, small deformations are assumed. This raises a serious question concerning the large deformation of material near the edge of the hole. The strains computed by all theories are typically higher than 0.10 near the hole edge, which is certainly large enough to cause significant errors in small deformation assumptions.

The assumption of elastic unloading is not correct; the residual stresses violate the yield criterion near the edge of the hole. The Rich-Impellizzeri theory avoids this violation by the restriction of compressive yield zone near the edge, while the Potter-Grandt theory computes yielding upon unloading. A complete theory, depending on the real material behavior, would be the Hsu-Forman theory with computing upon unloading and accounting for radial compressive displacement of a mandrel instead of uniform pressure.

As to experimental verification of any of these theories, it would be very difficult to match the boundary conditions at the expanded hole due to the elastic deformation of the plate and mandrel used. Taylor did do this by pressing a rotating, slightly tapered mandrel into a very soft, thin sheet; but that is far removed from a practical coldworking process, and very soft materials are not used in structures.

## CHAPTER 5

### ELASTIC-PLASTIC BOUNDARY

#### MEASUREMENT TECHNIQUES

Three experimental techniques for locating the elastic-plastic boundary were examined. These were

- a) Foil Strain Gages
- b) Thickness Change Measurement,
- c) Photoelastic Coating.

The first two were used for the measurements reported in this thesis.

#### 5.1 Nature of Deformation Around a Coldworked Hole

Some preliminary experiments were run to verify that the cold-working process was working properly and to get an idea of the state of deformation around a coldworked hole. A photograph of the deformation area around the hole in a 6.35 mm. (1/4 in.) thick, 7075-T6 aluminum specimen is given in Figure 5.1. The most notable feature is the large amount of deformation near the edge of the hole which becomes smaller within a very short distance away from the edge. Furthermore, the deformation is so great that individual grains have rotated. Slip lines are easily visible in Figure 5.1. The material in the neighborhood of the edge of the hole cannot be considered as a homogeneous, isotropic continuum on a local scale.

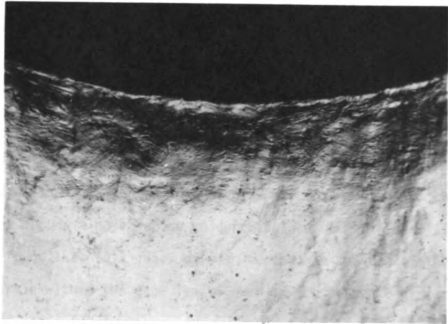


Figure 5.1.--Photograph of the deformed region around the hole in a 6.35 mm. (1/4 in.) thick specimen (100X).

## 5.2 Foil Strain Gage Techniques

The resistance strain gage is an excellent tool for measurement of strain in most structural material, as it closely approaches the characteristic requirement of strain measurement. A few researchers (3,23,24) used foil gages to measure the strains near interference-fit fasteners and were satisfied with the measurements. However, one report (24) questions the accuracy of data obtained near a fastener with short gage-length strain gages. Recently, Sharpe (10) used foil gages with a gage length of 0.38 mm. (0.015 in.) to measure the strains around a hole during coldworking and due to a static load. He found that foil gages gave an acceptable measure of the average strain within the gage length even in the presence of large strains and large gradients.

For this technique, the following gages and cements were purchased from Micro-Measurement Co., Romulus, Michigan:

Foil gages: Gage type EP-08-031ME-120 for radial strain  
EP-08-031MF-120 for tangential strain

Resistance 120  $\pm$ 0.50% ohms

Gage length 0.79 mm. (0.031 in.)

Gage factor 2.14  $\pm$ 1.0%

Cements: M-bond 200 Adhesive and 200 Catalyst

There are ten gages in one strip, with 2.13 mm. (0.08 in.) between gage centerlines. Due to the limited number of channels of the amplifier, three gages were carefully cut out of each strip with small scissors and used.

Electrical circuit used:

6-Channel Amplifier with a Wheatstone bridge circuit in each channel, by B. & F. Instrument Inc., Philadelphia, Pennsylvania

Recorder:

Minicomputer - Computer Automation model LSI 2

X-Y Recorder - Hewlett Packard, model 7046 A

The instruments are shown in Figure 5.2 for the setup.

The specimens were polished with silicon carbide grinding papers, grit numbers 320 and 400, followed by 600 grit to insure a smooth surface. Surfaces were finally cleaned with acetone. Three-gage sets were bonded to specimens following the bonding procedure as suggested by the manufacturer. The measured strains were in the neighborhood of the elastic-plastic boundary which was far away from the edge of the hole. The nearest location to the edge of the hole of the centerline of the first gage was at least 1 mm. from the edge, and the third one was 5.30 mm. The prepared specimen is shown in Figure 5.3.

Two attempts were made to measure the strains. First, both radial and tangential strains were measured by bonding both kinds of gages at 90° apart to the upper side of the specimen as shown in Figure 5.3. Secondly, only radial strains were measured by bonding the radial foil gages to the upper and lower sides of specimens in the same radial line of the hold. In both attempts to gage locations were measured with a microscope, and gage resistance was checked. Then the following procedure was used after the gages were connected to the signal conditioner:



Figure 5.2.--Photograph of equipment set up for the foil gage technique. Minicomputer (1), teletype (2), X-Y recorder (3), 6-channel amplifier (4), bonded specimen (5), coldworking apparatus (6), hydraulic pump (7), Bridge Amplifier Meter (8).

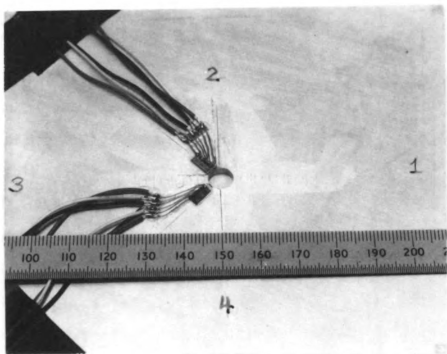


Figure 5.3.--Photograph of bonded specimen with radial and tangential foil gages on the upper side.

- a) Balanced all Wheatstone bridges to get zero output;
- b) Calibrated all gages with  $\epsilon = \frac{-R_g}{F(R_g + R_{cal})}$ ;
- c) Set the gain of the 6-Channel amplifier to 5 volts per 1.00% strain.

The voltage change as the mandrel was pulled through the hole was temporarily recorded by the minicomputer and was later plotted on the X-Y recorder. Typical plots, as given in Figures 5.4 to 5.11, of the loading strains versus applied load were obtained from the foil gages applied on the upper side of the specimens (P. 18,20). The forces required to pull the mandrel through the hole were about 5357-7143 N (1200-1600 lb.) and 4464-5357 N (1000-1200 lb.) for the 6.35 mm. and 3.18 mm. thick, 7075-T6 aluminum respectively.

Strains at the peak of the average strain (typical plots are in Figures 5.4 to 5.11) were plotted (as in Figures 5.12 and 5.13) versus gage location to establish the elastic-plastic boundary. The elastic-plastic boundary,  $r_p$ , would be where the radial and tangential strains were equal in magnitude to the maximum elastic strain before yielding when radial and tangential strains were measured. The elastic strain is given as

$$\epsilon_r = -\epsilon_\theta = \frac{1+\nu}{\sqrt{3}E} \sigma_o$$

which were 0.60, 0.56, 0.04% for the 6.35 mm. (1/4 in.), 3.18 mm. (1/8 in.) thick, 7075-T6 aluminum, and 3.18 mm. (1/8 in.) thick, 1100 aluminum, respectively.

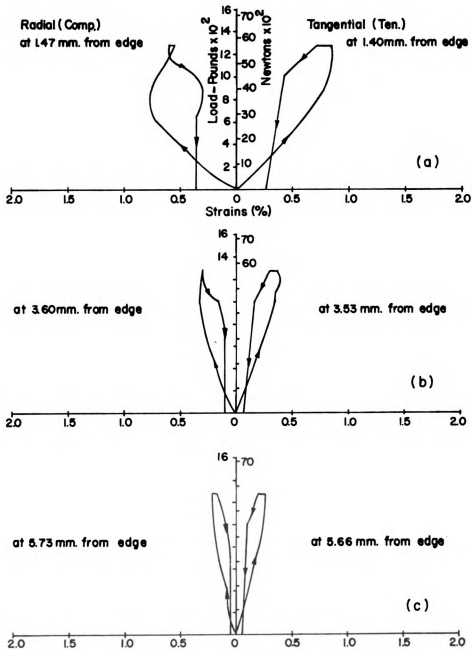


Figure 5.4.--Radial and tangential strains measured with foil gages on the upper side of the 6.35 mm. (1/4 in.) thick, 7075-T6 aluminum (P.18) as the mandrel of 0.076 mm. (0.003 in.) radial expansion was pulled through the hole.

- (a) . . . the first (nearest) gage
- (b) . . . the second gage
- (c) . . . the third gage.

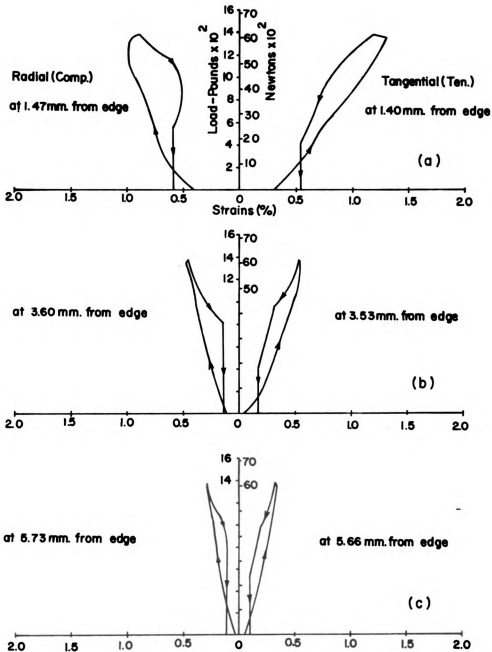


Figure 5.5.--Radial and tangential strains measured with foil gages on the upper side of the 6.35 mm. (1/4 in.) thick, 7075-T6 aluminum (P.18) as the mandrel of 0.102 mm. (0.004 in.) radial expansion was pulled through the hole.  
 (a) . . . the first (nearest) gage  
 (b) . . . the second gage  
 (c) . . . the third gage.

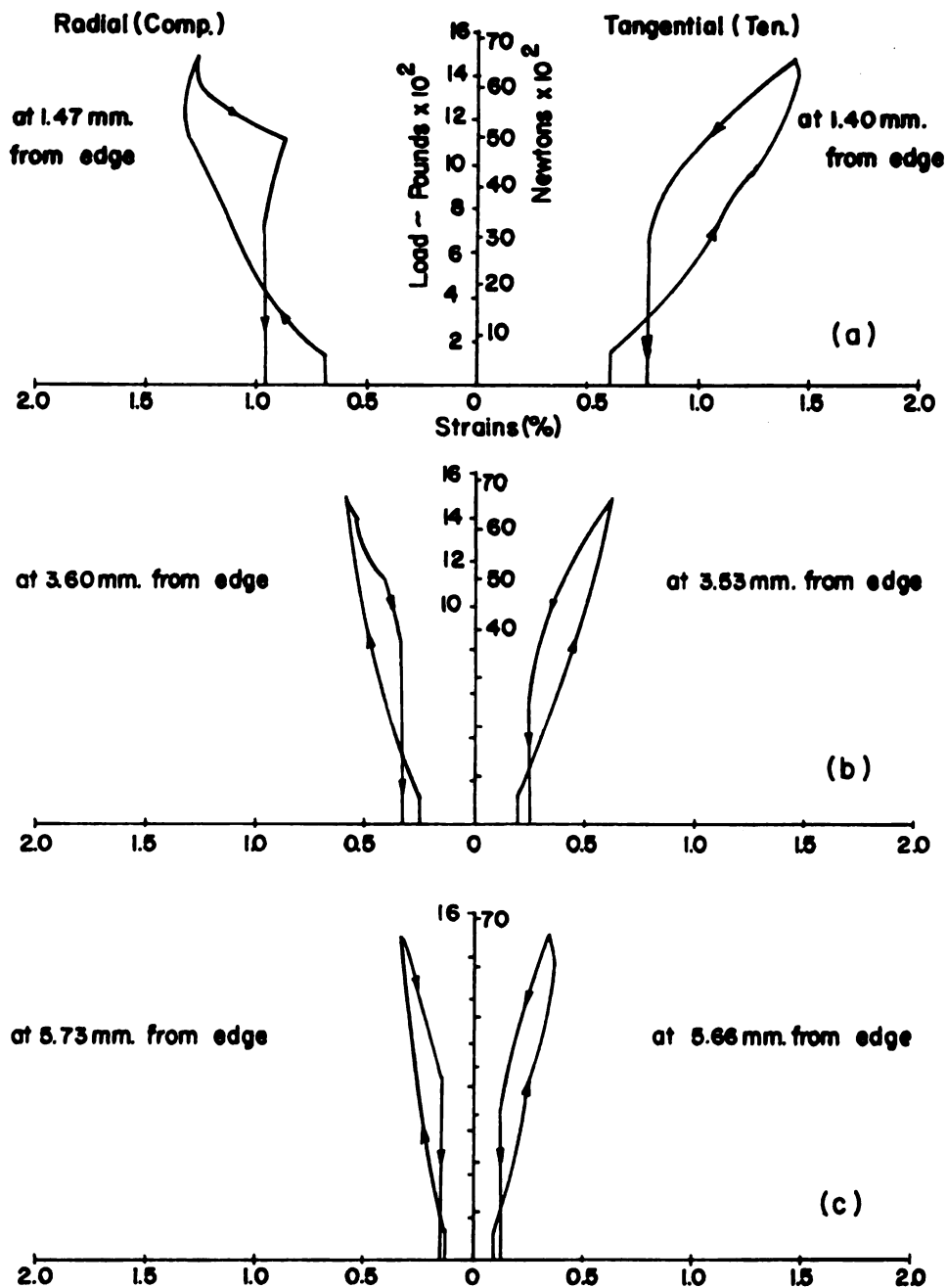


Figure 5.6.--Radial and tangential strains measured with foil gages on the upper side of the 6.35 mm. (1/4 in.) thick, 7075-T6 aluminum (P.18) as the mandrel of 0.127 mm. (0.005 in.) radial expansion was pulled through the hole.

- (a) . . . the first (nearest) gage
- (b) . . . the second gage
- (c) . . . the third gage.

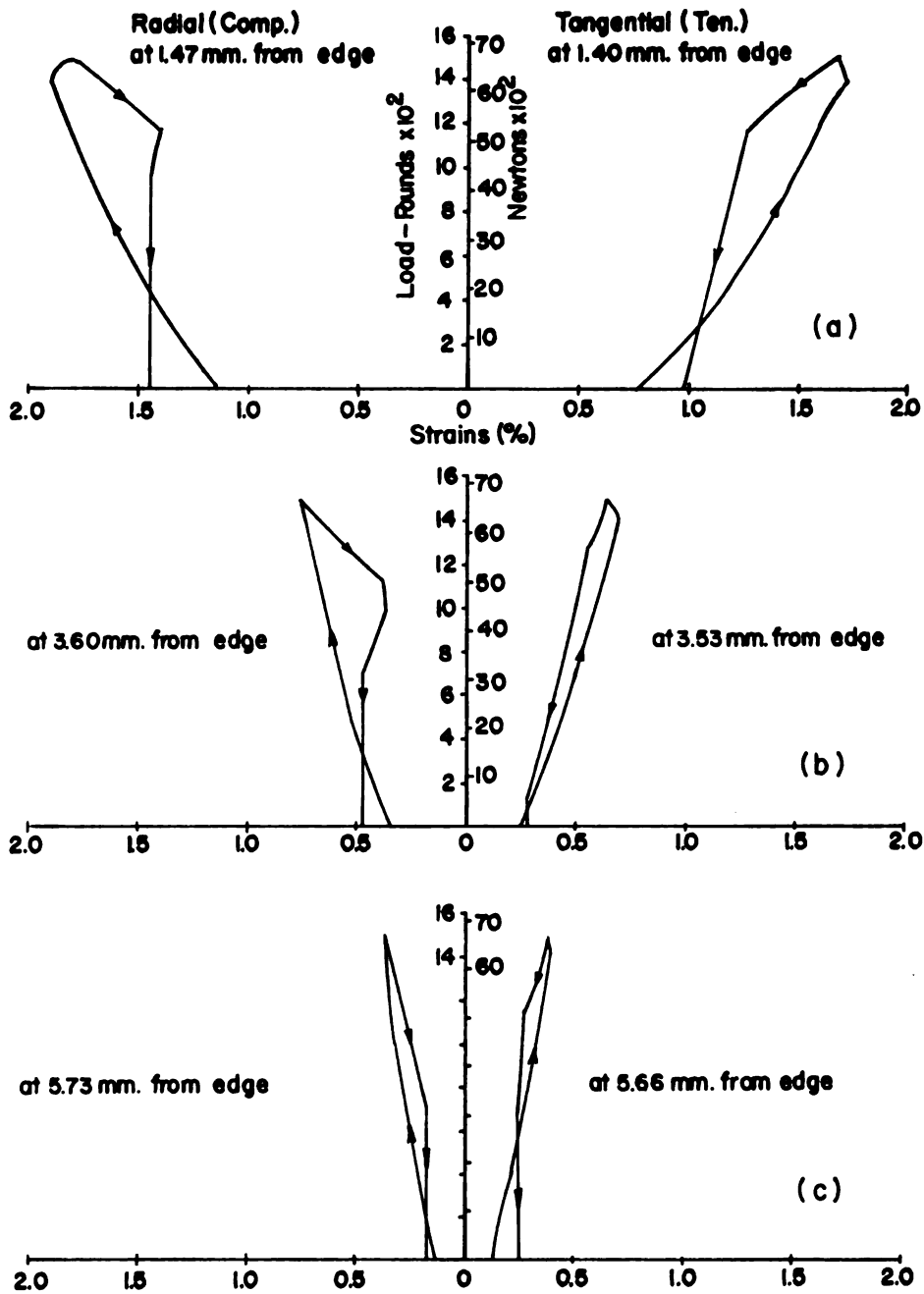


Figure 5.7.--Radial and tangential strains measured with foil gages on the upper side of the 6.35 mm. (1/4 in.) thick, 7075-T6 aluminum (P.18) as the mandrel of 0.152 mm. (0.006 in.) radial expansion was pulled through the hole.  
 (a) . . . the first (nearest) gage  
 (b) . . . the second gage  
 (c) . . . the third gage.

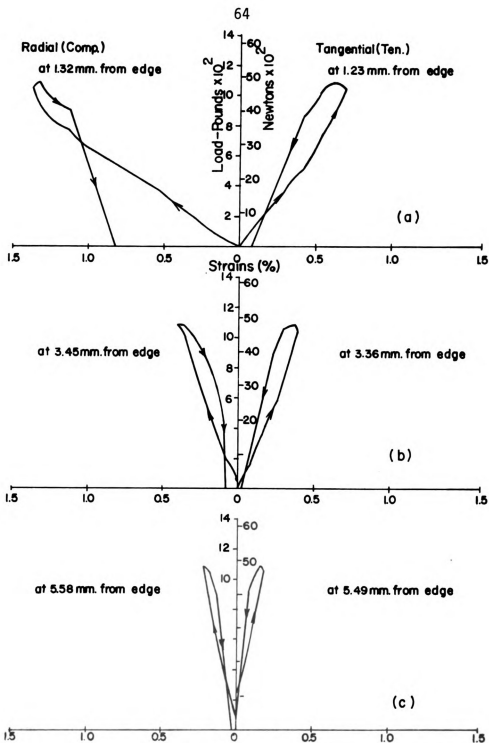


Figure 5.8.--Radial and tangential strains measured with foil gages on the upper side of the 3.18 mm. (1/8 in.) thick, 7075-T6 aluminum (P.20) as the mandrel of 0.076 mm. (0.003 in.) radial expansion was pulled through the hole.  
 (a) . . . the first (nearest) gage  
 (b) . . . the second gage  
 (c) . . . the third gage.

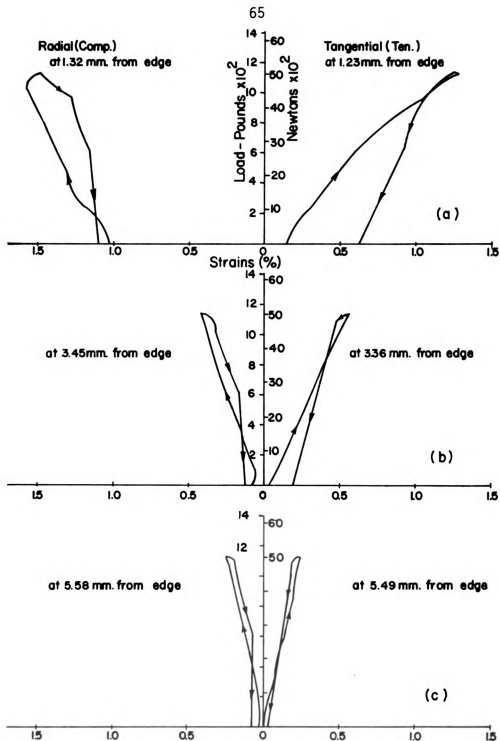


Figure 5.9.--Radial and tangential strains measured with foil gages on the upper side of the 3.18 mm. (1/8 in.) thick, 7075-T6 aluminum (P.20) as the mandrel of 0.102 mm. (0.004 in.) radial expansion was pulled through the hole.  
 (a) . . . the first (nearest) gage  
 (b) . . . the second gage  
 (c) . . . the third gage.

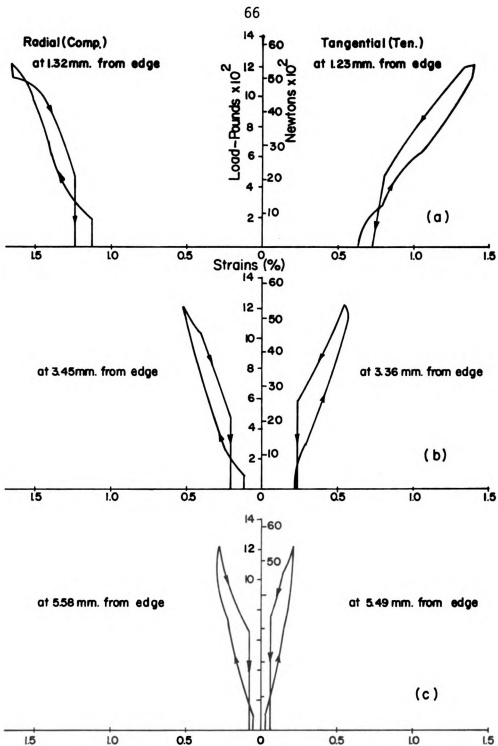


Figure 5.10.--Radial and tangential strains measured with foil gages on the upper side of the 3.18 mm. (1/8 in.) thick, 7075-T6 aluminum (P.20) as the mandrel of 0.127 mm. (0.005 in.) radial expansion was pulled through the hole.  
 (a) . . . the first (nearest) gage  
 (b) . . . the second gage  
 (c) . . . the third gage.

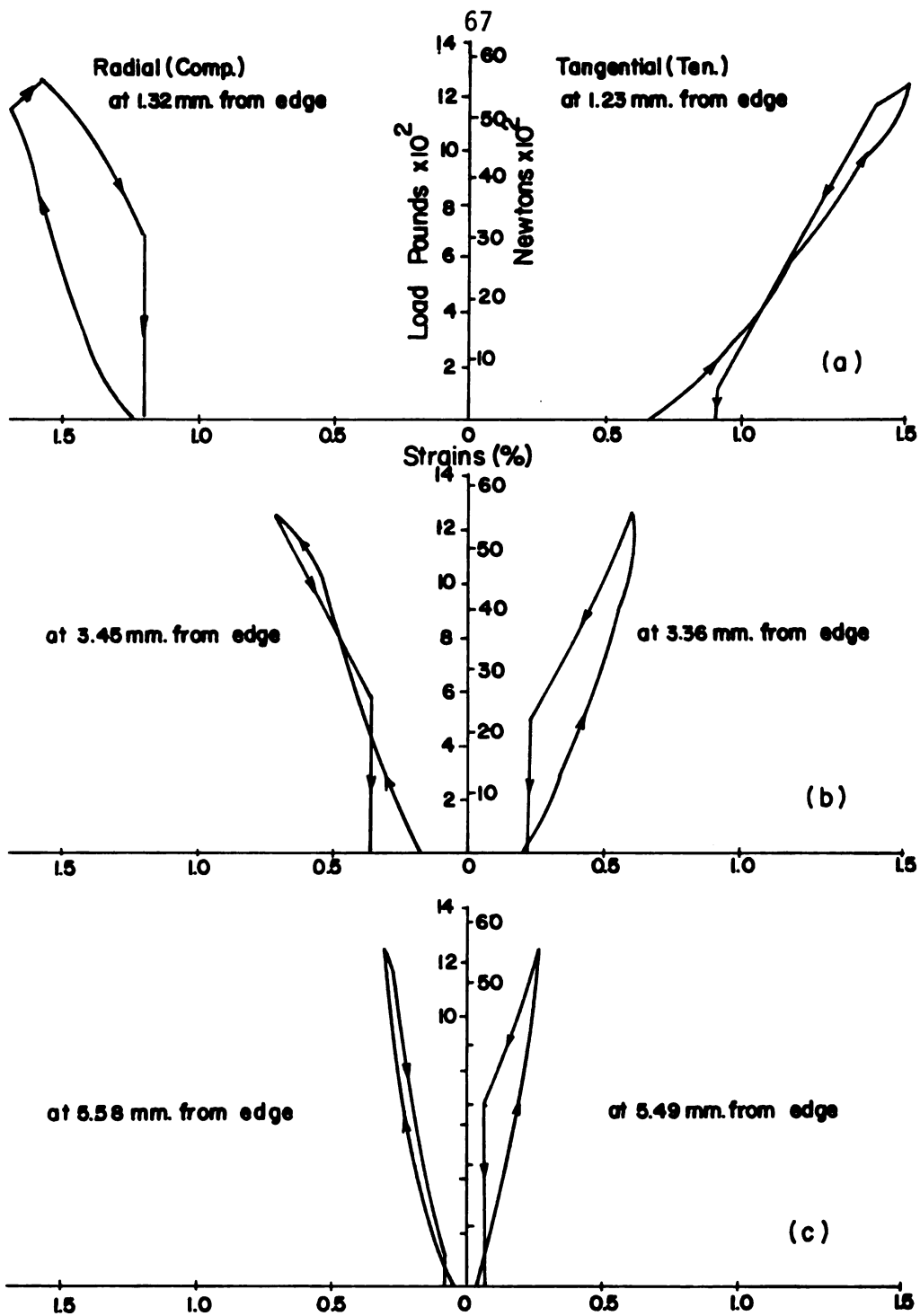


Figure 5.11.--Radial and tangential strains measured with foil gages on the upper side of the 3.18 mm. (1/8 in.) thick, 7075-T6 aluminum (P.20) as the mandrel of 0.152 mm. (0.006 in.) radial expansion was pulled through the hole.

- (a) . . . the first (nearest) gage
- (b) . . . the second gage
- (c) . . . the third gage.

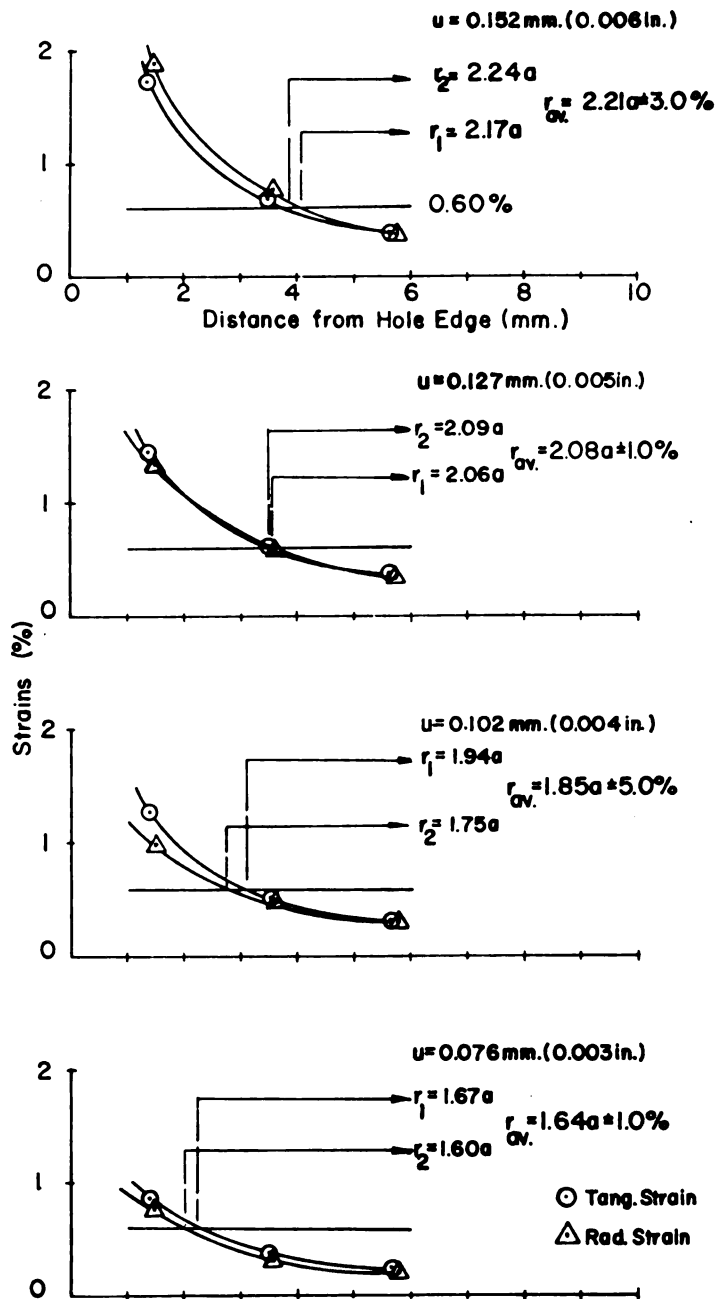


Figure 5.12.--Typical method used to locate the elastic-plastic boundary,  $r_p$ , of typical 6.35 mm. (1/4 in.) thick, 7075-T6 aluminum (P.18) in which foil gages were applied on the upper side only.  
 $r_1$  . . .  $r_p$  located by tangential strain  
 $r_2$  . . .  $r_p$  located by radial strain.

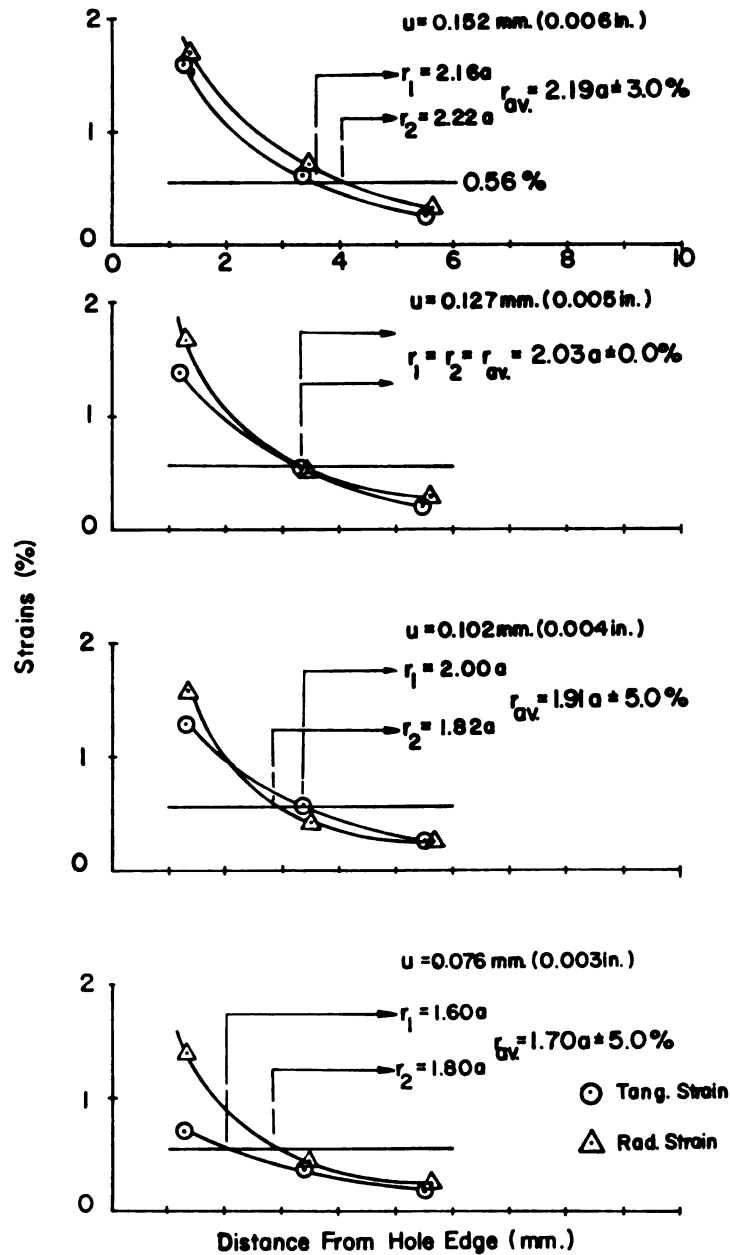


Figure 5.13.--Typical method used to locate the elastic-plastic boundary,  $r_p$ , of typical 3.18 mm. (1/8 in.) thick, 7075-T6 aluminum (P.20) in which foil gages were applied on the upper side only.

$r_1$  . . .  $r_p$  located by tangential strain  
 $r_2$  . . .  $r_p$  located by radial strain.

As found by Sharpe (10), the lower side strains are significantly larger than the upper side strains. This leads to an error of the  $r_p$  location by measuring the upper side strains only. Another important factor is that the radial and tangential gages were bonded to the specimen on different radial lines from the hole where the  $r_p$  are not exactly equal, as later found by the thickness change measurement technique; therefore the equal value of  $\epsilon_r$  and  $\epsilon_\theta$  on the plot cannot be found at the same location. For these reasons, a second procedure was examined. Two three-gage sets of radial foil gage were bonded to the specimen in the same radial line of the hole on both sides. Following the same procedure, strains at the peak of the average radial strains on both sides of the specimen were plotted versus gage location. The elastic-plastic boundary,  $r_p$ , would be where the measured strains were equal in magnitude to the maximum elastic strain before yielding (see Figure 5.14 and 5.15). A significant difference of the  $r_p/a$  obtained from the first and second attempts occurred on the smaller amounts of coldwork as listed in Tables 6.1 and 6.2.

The advantages of applying radial foil gages on both sides of a specimen relative to radial and tangential on one side may be stated as follows:

- a) Foil gages can be applied in the same radial line of the hole, with the result that the strains in the same direction are obtained.
- b) It is more accurate to locate the elastic-plastic boundary around a coldworked hole which is slightly different

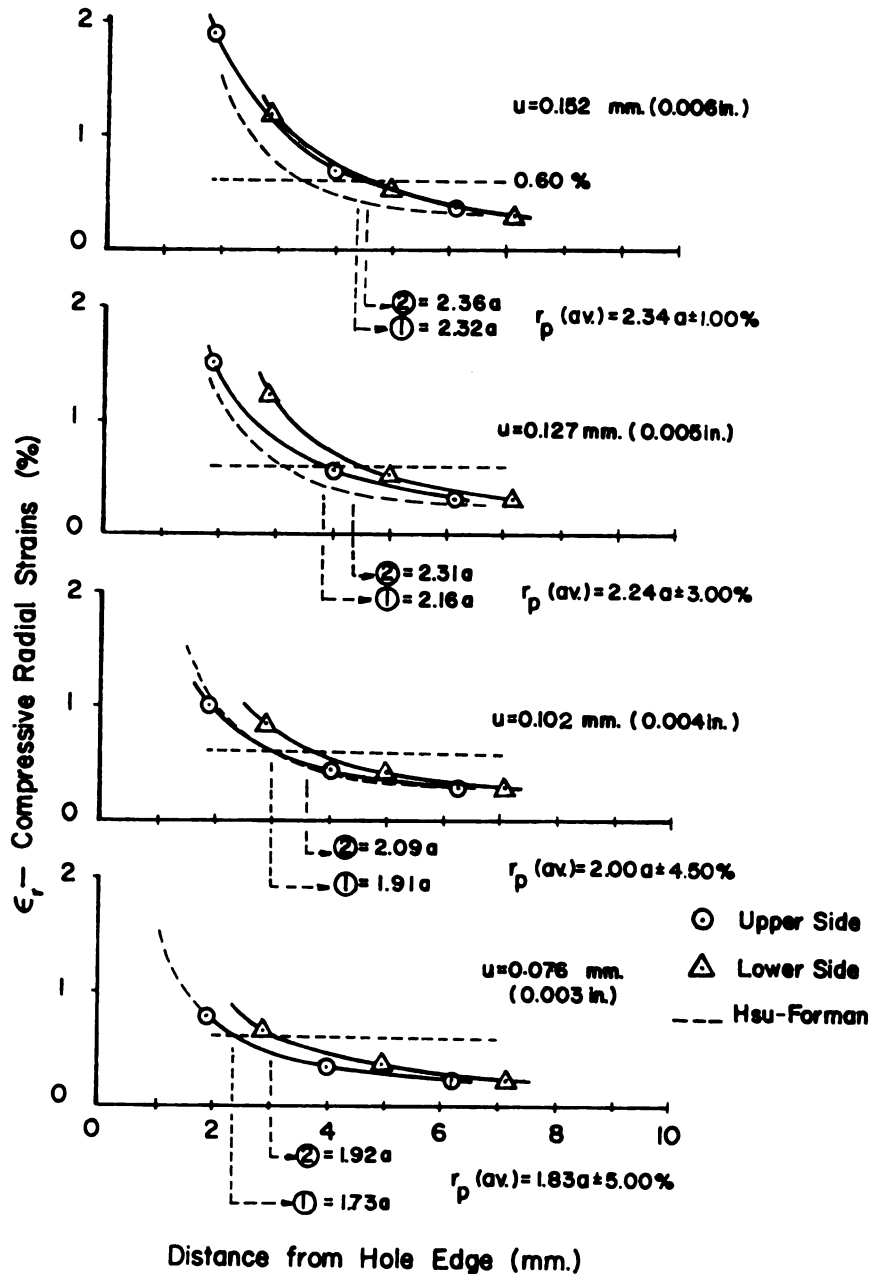


Figure 5.14.--Typical method used to locate the elastic-plastic boundary,  $r_p$ , of typical 6.35 mm. (1/4 in.) thick, 7075-T6 aluminum (P.14).  
 (1) . . .  $r_p^u$  located by the upper strain  
 (2) . . .  $r_p^l$  located by the lower strain.

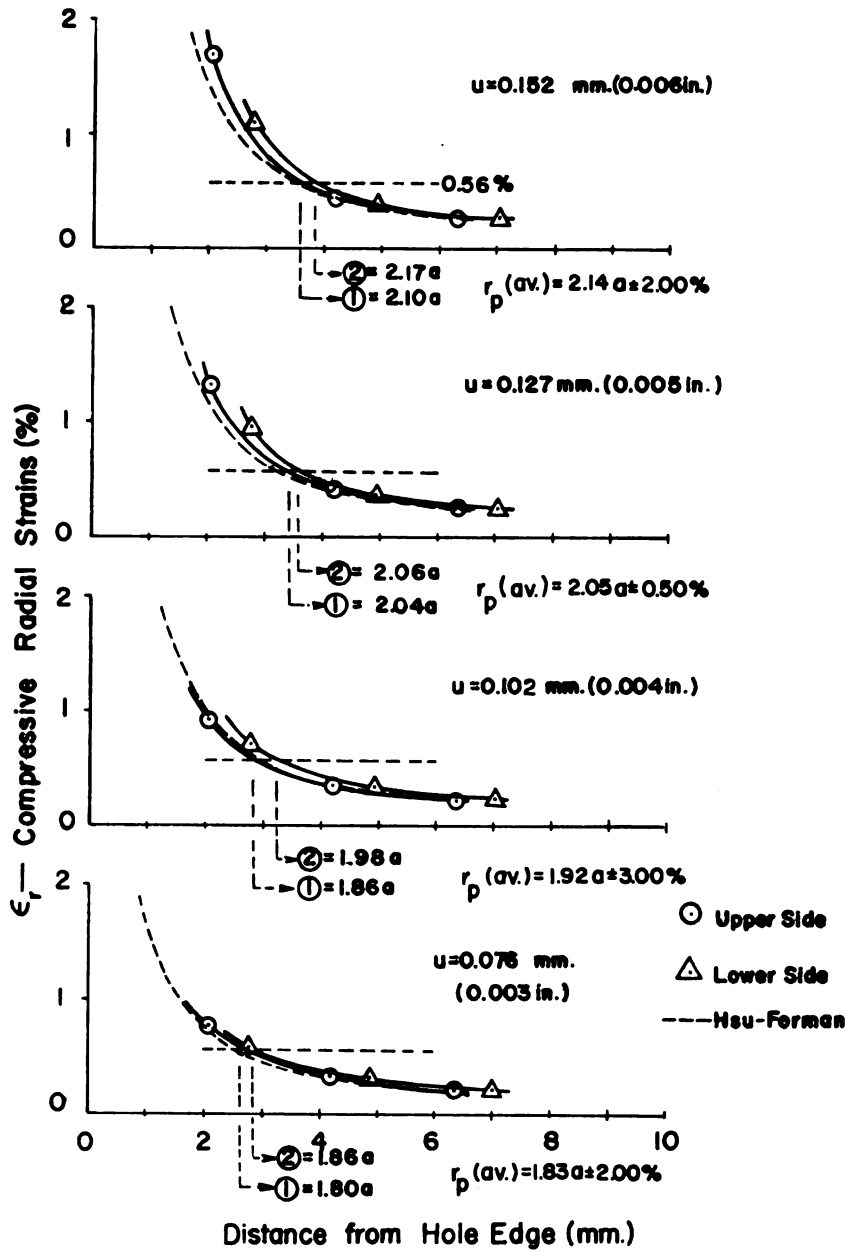


Figure 5.15.--Typical method used to locate the elastic-plastic boundary,  $r_p$ , of typical 3.18 mm. (1/8 in.) thick, 7075-T6 aluminum (P.28).  
 (1) . . .  $r_p$  located by the upper strain  
 (2) . . .  $r_p$  located by the lower strain.

from uniform pressure or radial expansion displacement assumed theories.

- c) The elastic-plastic boundary can be quickly obtained by averaging the upper and lower  $r_p$ , giving an actual average  $r_p$  of the coldworked hole.

Figures 5.4 to 5.7, the typical radial and tangential strains obtained from the gages applied on the upper side of a 6.35 mm. (1/4 in.) thick, 7075-T6 aluminum (P.18) as the mandrel (0.076, 0.102, 0.127, 0.152 mm.) was pulled through its hole are shown as a function of applied load.

Figures 5.8 to 5.11 are also the typical radial and tangential strains on the upper side. These are obtained from the 3.18 mm. (1/8 in.) thick, 7075-T6 aluminum (P.20).

These plots are similar. The strains start to increase as the mandrel is first pulled through the hole and decrease to residual strains as the mandrel is completely pulled through the hole. As the second, third, and fourth mandrels are used, the loading strains will start to increase from the residual strains of the last mandrel used. Figures 5.12 and 5.13 show the typical method used to locate  $r_p/a$ . The radial and tangential strains are taken from Figures 5.4 to 5.7 and Figures 5.8 to 5.11, respectively. The uncertainty (plus or minus sign in the figures) is computed from the offset of the  $r_p/a$  located by the radial and tangential strains from the averaged  $r_p/a$ .

Figures 5.14 and 5.15 illustrate the typical method used to locate  $r_p/a$  when strains were measured on both sides. The strains plotted here are taken from the specimens (P.14, 28) with the radial

foil gages applied on both sides as all mandrels were pulled through their holes. In these plots, the strains predicted by the most general theory by Hsu-Forman (as stated in Chapter 4) are also shown. The experimental strains on the upper surface show very good agreement with the theory on the smaller amounts of coldwork. The  $r_p/a$  located by the lower side strain are somewhat larger than the one by the upper side strain for the 6.35 mm. thick specimen and very close to each other on the larger amounts of coldwork. For the thinner specimen, the  $r_p/a$  located by both side strains are not very much different. The final  $r_p/a$  is computed by averaging the  $r_p/a$  located by the measured strains on both sides. The uncertainty (plus or minus sign in the figures) is computed from the offset of the  $r_p/a$  located by the strains on both sides from the actual  $r_p/a$  and also listed later in Tables 6.1 and 6.2.

### 5.3 Thickness Change Measurement Technique

When a circular hole in a plate is expanded by a uniform pressure or radial displacement, the metal near the edge of the hole is thickened and extended out along both sides of the surface, due to the condition of volume constancy ( $\epsilon_r + \epsilon_\theta + \epsilon_z = 0$ ).

Based on elasticity theory, during coldworking process the well-known transverse strain is given as

$$\epsilon_z = \frac{1}{E} \left( \sigma_z - \nu(\sigma_r + \sigma_\theta) \right)$$

which is valid everywhere in the elastic region around the hole. At a given radial loading, all theories described in Chapter 4 agree that the values of radial and tangential stresses are equal in

magnitude but opposite in sign in the elastic region. Since  $\sigma_z = 0$ , the above equation leads to  $\epsilon_z = 0$ . This means that there is no change in thickness of the plate in the elastic region. The plate thickness will start to change right at the elastic-plastic boundary, due to the condition of volume constancy and inequality of the stresses in the plastic region. Therefore, a thickness change of the plate exists in the plastic region and vanishes in the elastic region. The elastic-plastic boundary of a coldworked hole can be found at the location where the thickness first starts to change. Sharpe (10) measured the thickness change of a coldworked hole by J. O. King coldworking process, which is the same as this experiment, by focusing the 100X-lens on a microscope for some indentations marked along a radial line of the hole. This technique suffers from inaccuracy in focusing the lens and does not measure total thickness change.

Among displacement-measuring devices, the linear variable differential transformer (LVDT) is an appropriate one. Durelli et al (25), in 1966 used a LVDT as one of their methods to determine the sum of principal stresses in two-dimensional problems. They used an LVDT of  $10^{-6}$  in. sensitivity to measure a change in thickness at a point of a loaded plate, and then the proportionality relationship was used to determine the sum of principal stresses. In 1968 Coleman and Ward (26) also used two LVDT for the change in specimen cross section in inhomogeneous deformation measurement. The diameter change could be measured over 0.2 in. with a maximum resolution of better than  $10 \times 10^{-6}$  in.

The LVDT used in this technique was purchased from the R.I.S. Incorporated Sales and Service, 20245 Van Dyke, Detroit, Michigan, and was model R.I.S. DT-100-2-A with 0.04 in. (1.02 mm.) carbide ball contact point. The operating range is  $\pm 0.05$  in. (1.27 mm.) with 0.05% at  $\pm 0.02$  in. (0.51 mm.) linearity. A Daytronic amplifier model 300C was modified to accept the DT-100-2-A transducer to have output of 10 volts D.C. A linear potentiometer by Bourns Inc., Riverside, California, with maximum range of 1.00 in. (25.4 mm.) was used to locate the radial distance from the edge of the hole.

Four thickness change measurements were run in each specimen along the numbered directions shown in Figure 3.1. The LVDT and linear potentiometer were checked and the linearity found satisfactory. The calibration curves of the LVDT on the  $\pm 0.005$  and  $\pm 0.001$  in. scales of Daytronic amplifier are given in Figures 5.16 and 5.17. The best resolution obtained was  $50 \times 10^{-6}$  in. and  $10 \times 10^{-6}$  in. on the  $\pm 0.005$  and  $\pm 0.001$  in. scales, respectively. The finer scales of  $\pm 0.0005$  and  $\pm 0.0001$  in. were checked, but the linearity was found to be unsatisfactory. The calibration curve of the linear potentiometer is shown in Figure 5.18 with a calibration factor of 0.183 in. per volt.

The setup is shown in Figure 5.19. The specimen was held by a sturdy C-clamp attached to a stationary X-Y translation stage, which could be moved in and out between two identical carbide balls that activated the LVDT. The lowest ball was attached to the steel frame and could not move. This ball was designed to be in the same vertical line as the LVDT's contact point. The second ball was

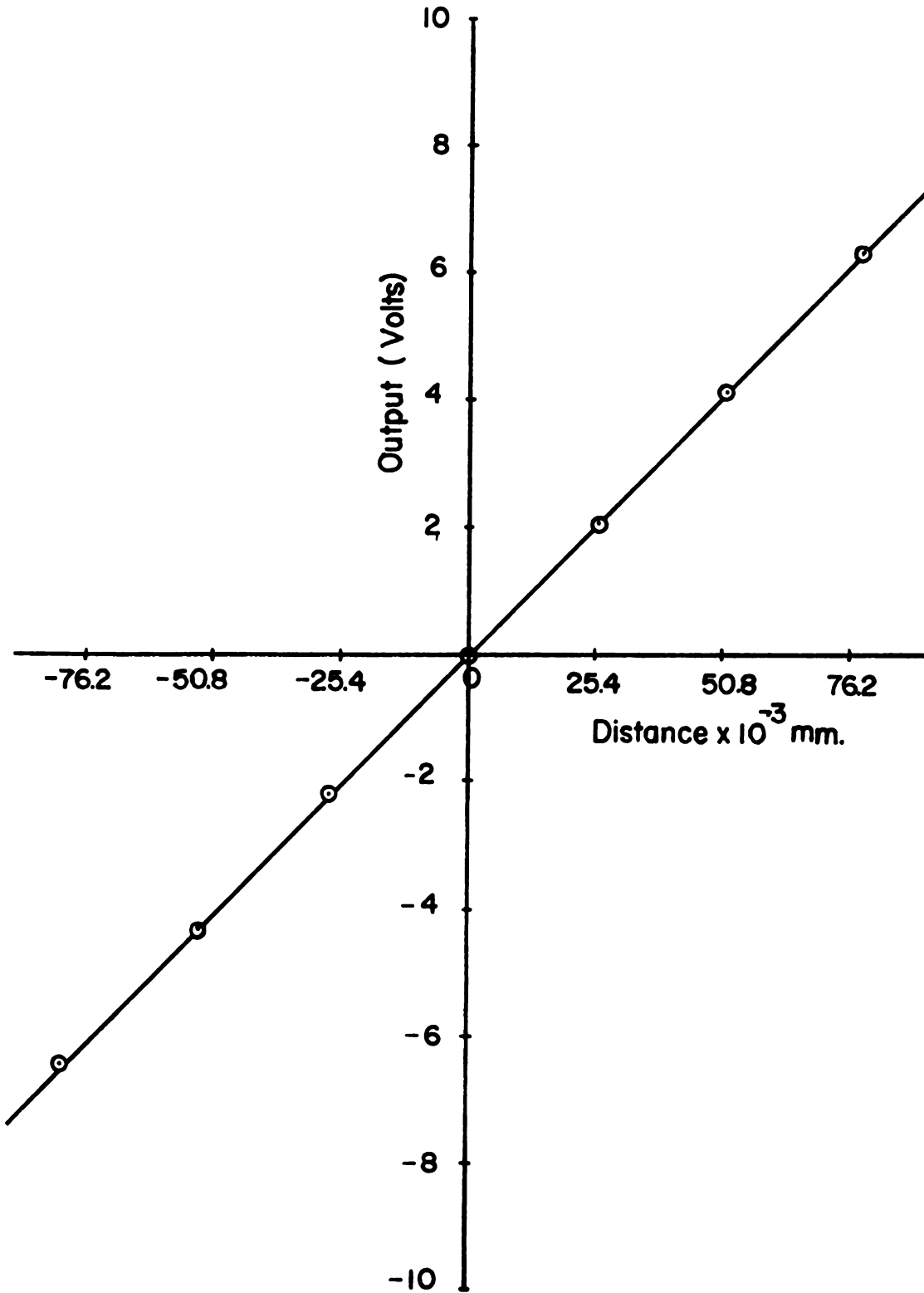


Figure 5.16.--Calibration curve of the LVDT on  $\pm 0.005$  in. scale of Daytronic amplifier model 300C.

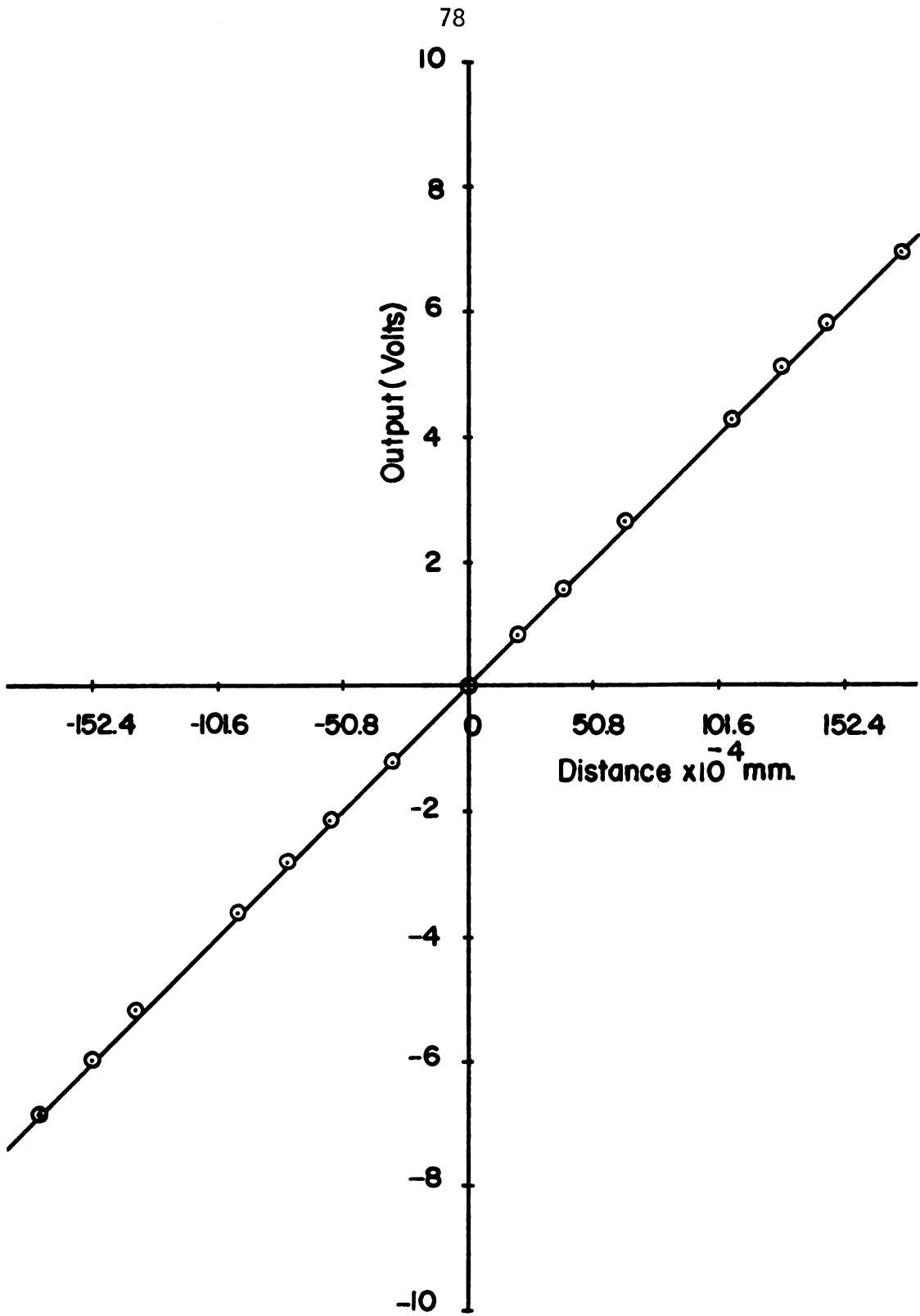


Figure 5.17.--Calibration curve of the LVDT on  $\pm 0.001$  in. scale of Daytronic amplifier model 300C.

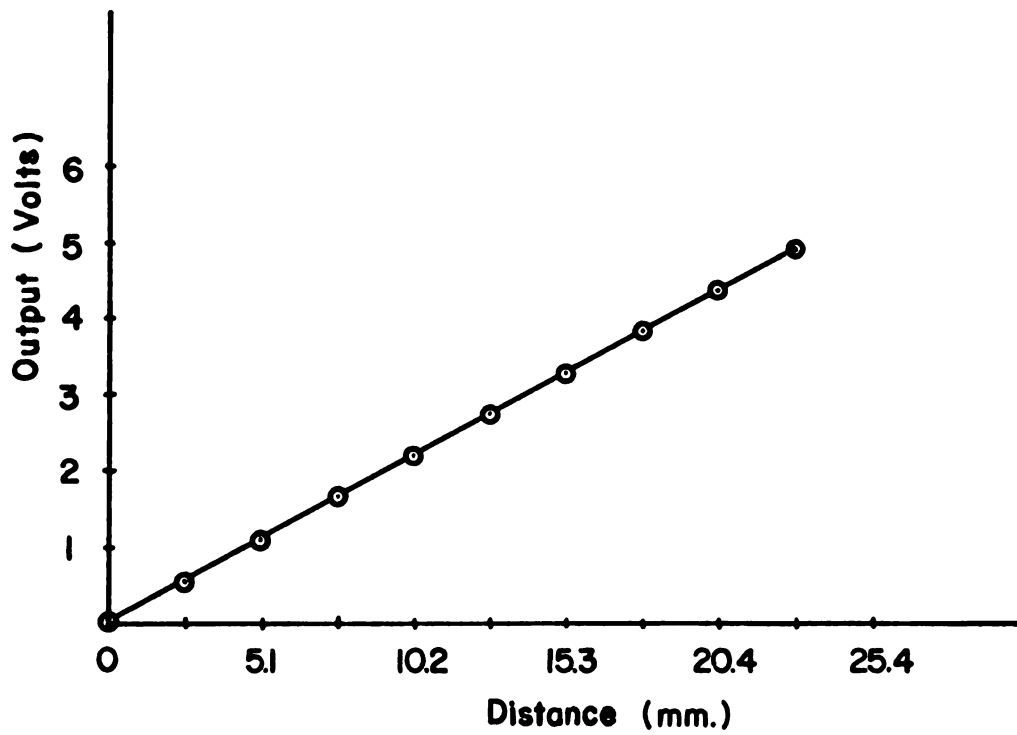


Figure 5.18.--Calibration curve of linear potentiometer.

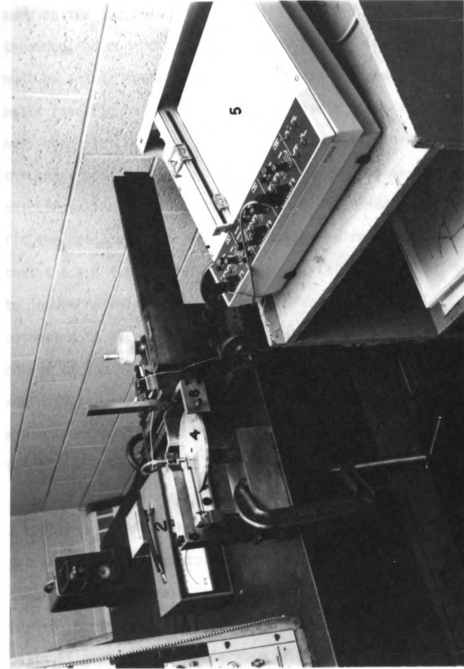


Figure 5.19.--Photograph of the thickness change measurement setup, consisting of the LVDT (1), Daytronic amplifier (2), the LVDT holder (3), specimen (4), X-Y recorder (5), X-Y translation stage (6), linear potentiometer (7), and the specimen holder (8).

attached to a horizontal small strip sheet. This sheet was tightened on the steel spacer block and used to control the LVDT spring pressure on the specimen by lifting its free end up and down with a small threaded rod connecting it with the steel block. This middle ball must be set in the same vertical line as the lowest and the LVDT's balls (see Figure 5.20) in order to have a measurement of the thickness change at the same point. The horizontal level for specimen thickness was adjusted by two steel spacer blocks--one for each thickness--that control the position of the middle contact ball to fit the specimen. The most important requirement of the setup is that the X-Y translation stage and the LVDT holder must be tightened to insure no relative motion during testing. The LVDT output was connected to the X-Y recorder from Daytronic amplifier output. The output of the linear potentiometer, mounted on the specimen holder, was directly connected to the same recorder so that it could provide a permanent profile of the change in thickness of a specimen as a function of the distance from the edge of the hole.

Since only one LVDT was used, the ideal original thickness of a specimen would be the zero volt output (null) line when the null was set at a starting point; but it was very difficult to have a uniform thickness in the real specimen. Two precautionary steps must be made before the testing. First, one must set the contact point of the balls as close to the centerline of the hole as possible in order to get the real  $r_p$  around the hole. Second, the null of the LVDT should be set at the nearest location to the original starting point to obtain the same path as the original one when the coldworking process was completely done.

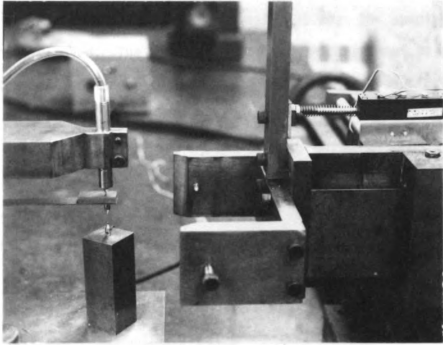


Figure 5.20.--Photograph of the LVDT and linear potentiometer mounted in holders.

The following procedure was used for the test:

a) The original thickness of the non-coldworked specimen was recorded, using the methods described above. A small weight was used to balance the specimen weight on the lowest ball when the specimen was horizontally moved. The starting point was made at about 20 mm. away from the edge to insure that it would not be in the plastic region.

b) After each mandrel was pulled through the hole, the sleeve was removed for final diameter measurement and to avoid the possibility of contact of the lowest ball and sleeve lip edge near the edge of the hole. The same procedure was then followed to record the thickness change by each mandrel.

c) The thickness profile recorded in b) was superimposed on the original one. The point in which the second curve deviated from the first one was the elastic-plastic boundary around the cold-worked hole by each mandrel.

This technique is straightforward. Only one suggestion may be pointed out: the first deviation of the thickness profile of the 6.35 mm. (1/4 in.) thick coldworked specimen from the original one came from change in thickness due to non-uniform deformation. The locations where the thickness started to change on each surface were checked by using a very thin piece of glass attached to the other surface in both original thickness and the thickness after each mandrel was pulled through the hole. The small marks on the left and the right sides of the arrow index (see Figure 5.21) are the actual

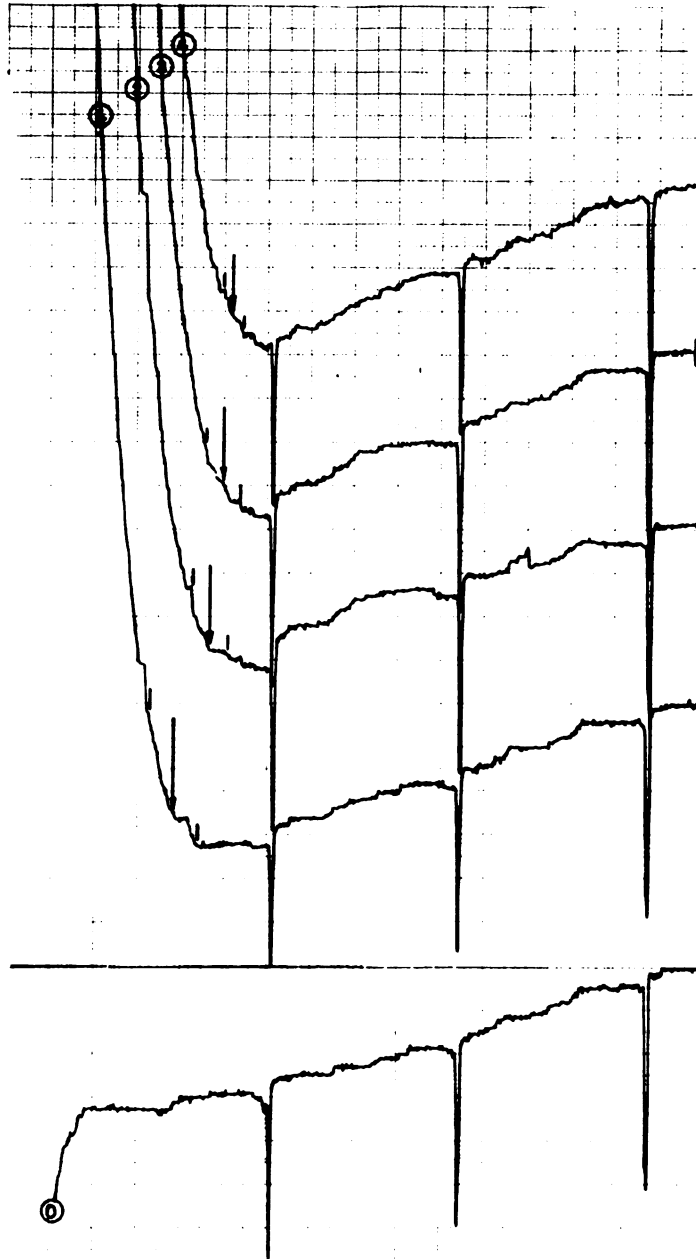


Figure 5.21.--Typical method used to locate the elastic-plastic boundary,  $r_p$ , from the thickness profile of the 6.35 mm. (1/4 in.) thick, 7075-T6 aluminum (P.12) on direction number 2 and  $\pm 0.001$  in. scale after four different sizes of oversize mandrels were pulled through the hole.

- (0) . . . original thickness of non-coldworked hole.
- (1) . . . after 0.076 mm. (0.003 in.) mandrel
- (2) . . . after 0.102 mm. (0.004 in.) mandrel
- (3) . . . after 0.127 mm. (0.005 in.) mandrel
- (4) . . . after 0.152 mm. (0.006 in.) mandrel.

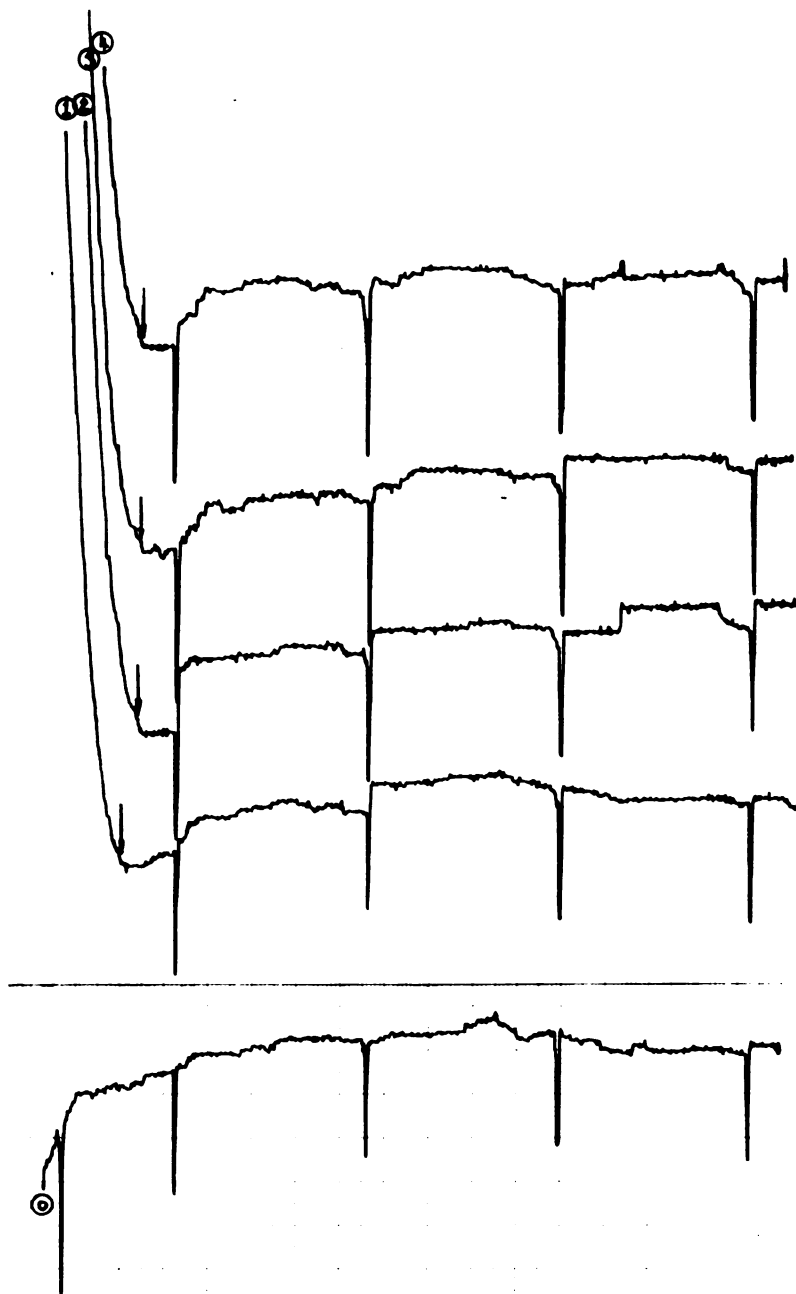


Figure 5.22.--Typical method used to locate the elastic-plastic boundary,  $r_p$ , from the thickness profile of the 3.18 mm. (1/8 in.) thick, 7075-T6 aluminum (P.28) on direction number 2 and  $\pm 0.001$  in. scale after four different sizes of oversize mandrels were pulled through the hole.

- (0) . . . original thickness of non-coldworked hole
- (1) . . . after 0.076 mm. (0.003 in.) mandrel
- (2) . . . after 0.102 mm. (0.004 in.) mandrel
- (3) . . . after 0.127 mm. (0.005 in.) mandrel
- (4) . . . after 0.152 mm. (0.006 in.) mandrel.

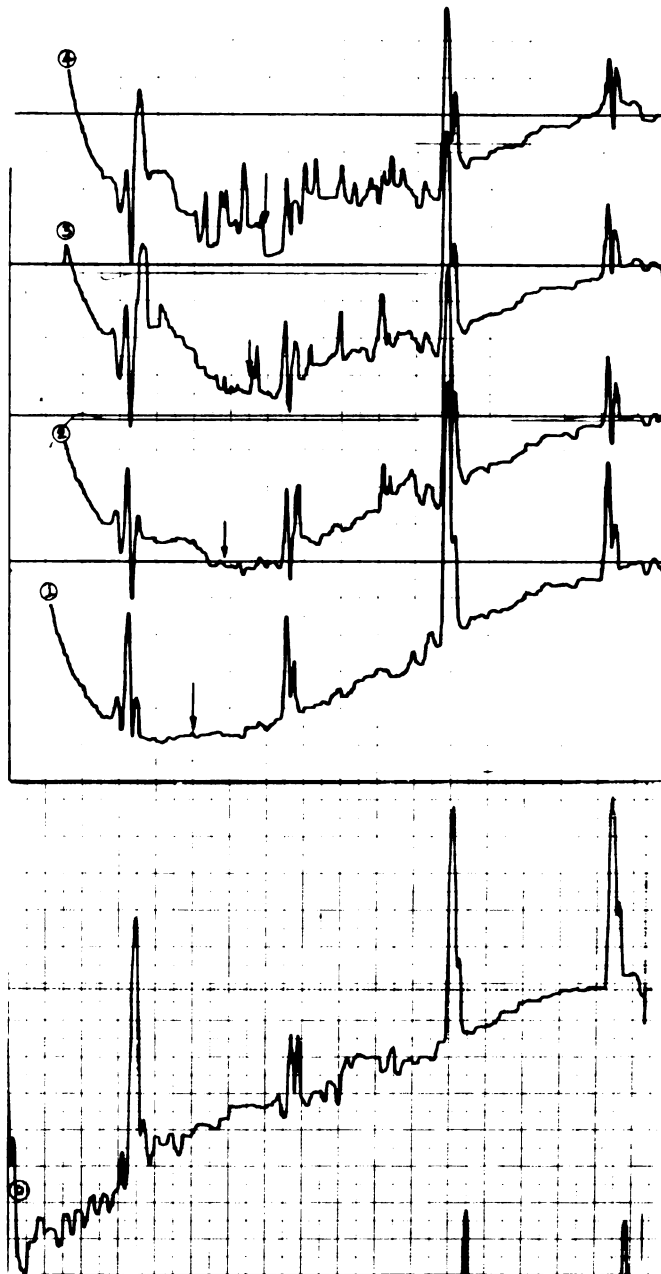


Figure 5.23.--Typical method used to locate the elastic-plastic boundary,  $r_p$ , from the thickness profile of the 3.18 mm. (1/8 in.) thick, type 1100 aluminum (P.36) on direction number 2 and  $\pm 0.005$  in. scale after four different sizes of oversize mandrels were pulled through the hole.

(0) . . . original thickness of non-coldworked hole  
 (1) . . . after 0.076 mm. (0.003 in.) mandrel  
 (2) . . . after 0.102 mm. (0.004 in.) mandrel  
 (3) . . . after 0.127 mm. (0.005 in.) mandrel  
 (4) . . . after 0.152 mm. (0.006 in.) mandrel.

locations where the thickness started to change. The actual  $r_p$  around the hole of the thicker specimen could be located by averaging the upper and lower  $r_p$ . This was not done on the 3.18 mm. (1/8 in.) thick specimen because the starting changes in thickness on both sides are very close to each other.

Figures 5.21 to 5.23 illustrate the typical methods used to locate the  $r_p$  in each kind of specimen. Only one of four directions is shown. The spikes (as seen in the plots) occur at the location of the scale marks scribed on the specimen. This enables one to compare the various graphs. The arrow index is the final location of the elastic-plastic boundary measured with this technique.

#### 5.4 Photoelastic Coating Technique

Photoelastic coating is a simple technique. A thin layer of birefringent coating is bonded to the surface of a metallic specimen. When the specimen is loaded and strained, the birefringent coating responds; and the resulting fringe pattern observed in a reflected-light polariscope can be interpreted in terms of the surface strains of the metallic specimen. An important advantage of the birefringent coating over other means of strain measurement is that the strains are obtained over the entire coated area in a single picture. But the thickness effect of the coating and the high strain gradients constitute limitations (27,28,29,30).

Dixon and Visser (31) used this method to measure the stress distribution and plastic deformation ahead of a crack in aluminum alloy and mild steel; but, admittedly, their fringe orders at the

tip of the crack, where the strain gradients were very high, suffered from the inaccuracy of the birefringent coating method. Calcote and Bowman (32) used this method of isochromatics to predict the elastic-plastic boundary of a rectangular beam having a single concentrated load acting at its free end, but they found good agreement only on the tension side. Recently the same method was used to visualize the deformation around holes (33) and on interference-fit fastener (23) but was found to be unsatisfactory. This method would be useful only when the elastic-plastic boundary is far away from the hole.

The plastic coating used was purchased from Photoelastic Inc.

Plastic sheet type PS-1D with  $0.022 \pm 0.002$  in. thick as suggested by references 29,31, and 0.15 K-factor

Cements: resin type PC-8

hardener type PCH-8

A polariscope model LF/MU by Instruments Budd Division and a Nikon F-100 camera with Kodak film Panatonic-X were used.

Specimens were polished with silicon carbide grinding papers, grit number 320, and then followed by 400 grit. The fringe order at the elastic-plastic boundary is given as

$$N = \frac{2(1+\nu)}{\sqrt{3}Ef} \sigma_0$$

which were 3.37, 3.24, and 0.2 for the 6.35 mm. (1/4 in.), 3.18 mm. (1/8 in.) thick, 7075-T6 aluminum, and the 3.18 mm. (1/8 in.) thick, aluminum 1100, respectively.

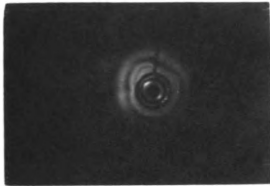
It was quickly discovered that the photoelastic coating would not stick in the very high gradient area near the edge of a

cold-worked hole. Some preliminary experiments were tried, by cutting a hole on plastic the same size as the original hole of the specimen, to get an idea of fringe patterns at the elastic-plastic boundary. The bonding procedure as suggested by the manufacturer was used. The fringe orders on the specimen, when observed through the analyzer on the polariscope, showed up and then disappeared during the cold-working process. Peeling of the plastic from the adhesive was found at the edge of the hole. The maximum elongation of the plastic itself is about 10 percent so that it cannot stand for the very high strain gradient there.

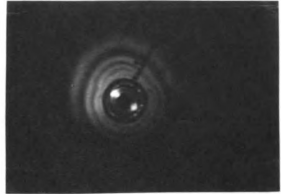
A 6.35 mm. thick, 7075-T6 specimen was tried. The hole in the plastic was cut about 2 mm. bigger than the original hole diameter of the specimen. Some photographs were taken through the analyzer with camera attached to the telemicroscope on the polariscope during the coldworking process with "mandrel in" condition as shown in Figure 5.24. The  $r_p$ 's located by this technique (see Figure 5.24) were located at the location of the calculated isochromatic fringe order, which was the same as all mandrels were pulled through the hole. The  $r_p$  measured by this technique is smaller than the foil gage technique with foil gage on the upper side surface. This means that it is certainly smaller than the actual  $r_p$  found by two previous techniques.

Therefore, photoelastic coating is not applicable for measuring the elastic-plastic boundary around the coldworked hole, due to the following limitations:

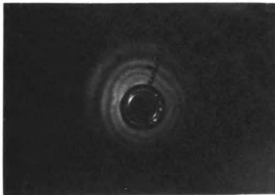
- a) The plastic bent along the specimen surface near the



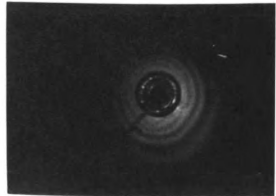
(a) 0.0762 mm. (0.003 in.)  
Rad. Exp.  $r_p = 1.61 a$



(b) 0.1016 mm. (0.004 in.)  
Rad. Exp.  $r_p = 1.91 a$



(c) 0.127 mm. (0.005 in.)  
Rad. Exp.  $r_p = 2.06 a$



(d) 0.1524 mm. (0.006 in.)  
Rad. Exp.  $r_p = 2.21 a$

Figure 5.24.--Isochromatic-fringe patterns and elastic-plastic boundaries obtained around the coldworked 6.35 mm. (1/4 in.) thick specimen (P.4) as four different sizes of oversize mandrels were pulled through the hole.

edge of the hole leading to errors in reading the fringe order;

- b) It is difficult to apply the plastic on both sides of the specimen surface;
- c) The outer diameter of sleeve lip on the lower side of the specimen is about 11 mm., which is large enough to cause some trouble in reading the fringe order in case the plastic is applied on both sides.

## CHAPTER 6

### ELASTIC-PLASTIC BOUNDARY MEASUREMENTS

In this chapter the elastic-plastic boundary, as measured by foil gages and thickness change, are compared. The photo-elastic coating was no longer employed after the debonding was found around the coldworked hole.

#### 6.1 Elastic-Plastic Boundary Measurement with Foil Gages

##### 6.1.1 6.35 mm. (1/4 in.) Thick, 7075-T6 Specimen Data

The elastic-plastic boundary measurements by this technique were made on seven coldworked 6.35 mm. (1/4 in.) thick specimens, four specimens for gages applied on one side and three specimens for gages applied on both sides. Table 6.1 lists the measured  $r_p/a$  for different expansions and specimens. The original hole diameter in these specimens was very slightly oversized, as shown in Table 3.1. The  $r_p$  was located after each mandrel was pulled through the hole. Since the gage application was made on different radial lines of the hole for gages on one side, the uncertainty of the measurements of  $r_p/a$  located by the one side strains is larger than of the one located by both sides strains (see Table 6.1). This uncertainty is computed from the offset of the  $r_p/a$  located by the radial and tangential strains (or by the radial strains on both sides) from the actual  $r_p/a$ .

Figure 6.1 illustrates the difference in the measured  $r_p/a$  by both procedures. The average of the measured  $r_p/a$  was plotted (four measurements by upper side foil gages and three by both sides foil gages) as a function of radial expansion displacement used. This plot shows that the actual  $r_p/a$  obtained by averaging the measured  $r_p/a$  on both sides was significantly larger than the  $r_p/a$  obtained using the foil gages on the upper side only, and this was to be expected by Sharpe AFOSR report (10).

TABLE 6.1--Measured  $r_p/a$  and its uncertainty obtained from foil gage technique when foil gages were applied on one side and on both sides surfaces of the 6.35 mm. (1/4 in.) thick, 7075-T6 aluminum specimens.

Specimen	Upper side foil gage ( $r_p/a$ )				Both sides foil gage ( $r_p/a$ )		
	P.7	P.8	P.9	P.18	P.11	P.12	P.14
Radial Displacement (mm.)							
0.076 (0.003 in.)	1.62 ±5.0%	1.65 ±1.0%	1.72 ±2.0%	1.64 ±1.0%	1.91 ±4.0%	1.69 ±0.0%	1.83 ±5.0%
0.102 (0.004 in.)	1.84 ±7.0%	1.95 ±2.0%	1.96 ±3.0%	1.85 ±5.0%	2.16 ±5.0%	2.05 ±2.5%	2.00 ±4.5%
0.127 (0.005 in.)	2.13 ±9.0%	2.12 ±7.0%	2.23 ±6.0%	2.08 ±1.0%	2.21 ±3.0%	2.27 ±2.0%	2.24 ±3.0%
0.152 (0.006 in.)	2.30 ±12.0%	2.30 ±9.0%	2.29 ±7.0%	2.21 ±3.0%	2.45 ±1.0%	2.39 ±2.0%	2.34 ±1.0%

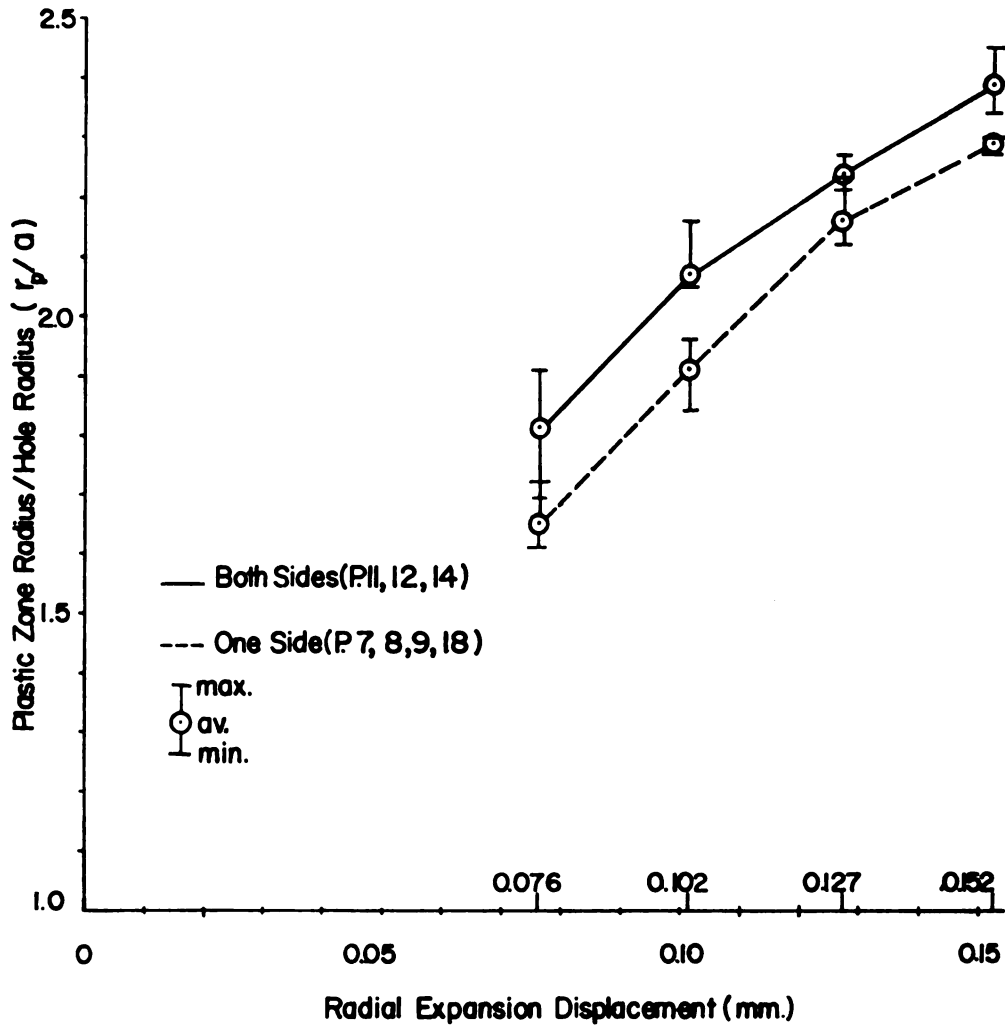


Figure 6.1.--Comparison of the measured  $r_p/a$  obtained from foil gages applied on one side and both sides of the 6.35 mm. (1/4 in.) thick, 7075-T6 aluminum.

### 6.1.2 3.18 mm. (1/8 in.) Thick, 7075-T6 Specimen Data

Elastic-plastic boundary measurements were made on four specimens for gages applied on one side and three specimens for gages applied on both sides as listed in Table 6.2. The plot of  $r_p/a$  versus radial expansion displacement in Figure 6.2 was taken from Table 6.2. The differences of the measured  $r_p/a$  by both procedures are not as large as the ones of the 6.35 mm. thick specimens. This is true because the thickening of the metal near the hole of thinner specimens, when the mandrel is pulled through, is less than for the thicker specimens. In addition, the force required to pull the mandrel through the hole is reduced. The result is less sleeve washer effect, which explains the smaller difference in strains on both sides. This plot agrees with the thicker specimens in that the  $r_p/a$  measured on both sides was larger than the  $r_p/a$  measured on the upper side only. The scattering of the measurements is not as wide as in the previous specimens. Even allowing for the biggest difference in the 0.076 mm. (0.003 in.) radial expansion, this technique gives a close agreement in both procedures. This means that the coldworking process by J. O. King does give more uniform deformation around a coldworked hole in the thinner specimen.

### 6.1.3 3.18 mm. (1/8 inch) Thick, Aluminum type 1100 Specimen

The foil strain gage technique was used on some specimens of type 1100 aluminum, but the coldworking process was not successful. Radial strain of these specimens became smaller on the free upper surface and larger on the lower surface as bigger mandrels were used.

TABLE 6.2--Measured  $r_p/a$  and its uncertainty obtained from foil gage technique with foil gages applied to one side and to both sides of the 3.18 mm. (1/8 inch) thick, 7075-T6 aluminum specimen.

Specimen	Upper side foil gage ( $r_p/a$ )				Both sides foil gage ( $r_p/a$ )		
	P.19	P.20	P.22	P.24	P.25	P.28	P.30
Radial Displacement (mm.)							
0.076 (0.003 in.)	1.71 ±3.0%	1.70 ±5.0%	1.68 ±4.5%	1.72 ±6.0%	1.86 ±2.0%	1.83 ±2.0%	1.76 ±2.0%
0.102 (0.004 in.)	1.87 ±2.0%	1.91 ±5.0%	1.89 ±1.0%	1.90 ±5.0%	1.95 ±3.0%	1.92 ±3.0%	1.96 ±2.5%
0.127 (0.005 in.)	2.02 ±1.0%	2.03 ±0.0%	2.12 ±1.5%	2.00 ±0.0%	2.01 ±1.5%	2.05 ±0.5%	2.02 ±0.0%
0.152 (0.006 in.)	2.09 ±1.0%	2.19 ±3.0%	2.12 ±1.5%	2.16 ±3.0%	2.05 ±1.5%	2.14 ±2.0%	2.12 ±3.0%

The bending of the metal itself occurred and caused thickening on the lower surface much more than on the upper surface. In addition, the sleeve was tightly wedged into the hole and the metal at the edge surface was also pulled from the upper to the lower surface by friction between the sleeve and the edge surface. Thus the coldworking process by J. O. King did not give uniform deformation in the very soft metal and caused a lot of shearing effect during processing. Usable data were not obtained for type 1100 aluminum with the foil gage technique.

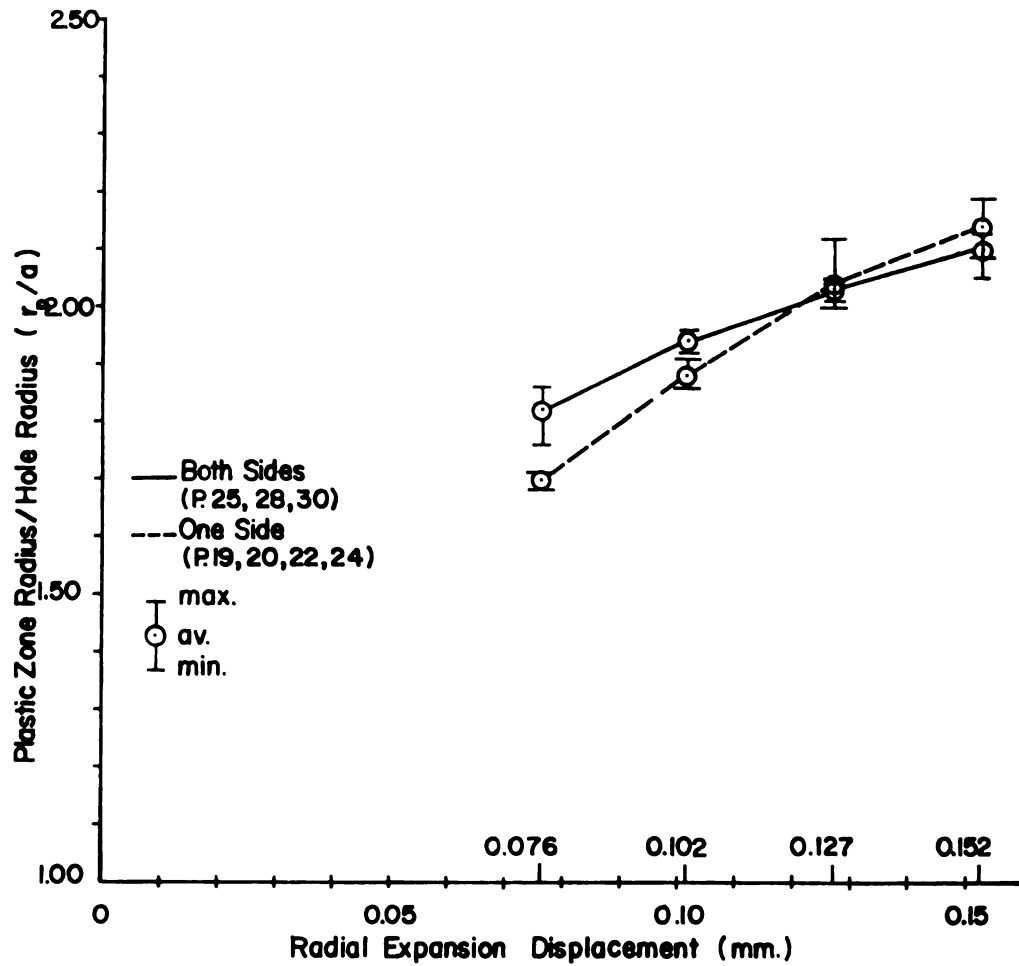


Figure 6.2.--Comparison of the measured  $r_p/a$  obtained from foil gages applied on one side and both sides of the 3.18 mm. (1/8 in.) thick, 7075-T6 aluminum.

## 6.2 Elastic-Plastic Boundary Measurement by Thickness Change Measurement

### 6.2.1 6.35 mm. (1/4 in.) Thick, 7075-T6 Specimen Data

Thickness change measurements were made on the same specimens that were used for the foil gage technique. In each case the thickness change measurement was taken after the foil gage technique for each mandrel used. For seven (P.7,8,9,11,12,14,18) specimens, four successively larger mandrels were used, measurements being taken after each coldworking operation. For eight (P.1,2,3,5,10,15,16,17) specimens, only one mandrel was used; i.e. the coldworking was not done in an incremental manner. The specimen numbers associated with the measured  $r_p/a$  are given in Table 6.3. Three specimens (P.7,8,9) were tested using both scales ( $\pm 0.005$  and  $\pm 0.001$  in.) on the Daytronic amplifier. The overall  $r_p/a$  obtained from both scales were similar. The average of  $r_p/a$  by both scales is the measured  $r_p/a$  by this technique. The  $r_p/a$  measurements were made for four radial directions around the coldworked hole. One value of the  $r_p/a$  represents one measurement. The average of the scattering of measurements was computed by using a standard deviation method (34) based on 25 measurements for each amount of coldwork.

Figure 6.3 compares the average  $r_p/a$  obtained from seven specimens in which four mandrels were pulled through the hole of each specimen, with that obtained from two sets of specimens in which only one mandrel was pulled through the hole. The plot shows a very

TABLE 6.3.--Measured  $r_p/a$  obtained from thickness change measurement technique for the 6.35 mm. (1/4 in.) thick, 7075-T6 aluminum specimens.

Radial Expansion Displacement (mm.)	P.7		P.8		P.9		P.11		P.12		P.14	
	0.005	0.001	Av.	0.005	0.001	Av.	0.005	0.001	Av.	0.001	0.001	0.001
0.076 (0.003 in.)	1.95	2.00	1.98	1.85	1.85	1.85	1.94	1.93	1.94	1.85	1.82	1.94
	1.94	1.93	1.94	1.90	1.91	1.91	1.95	2.02	1.99	1.91	1.86	2.10
	1.95	1.94	1.95	1.86	1.86	1.86	2.02	1.92	1.97	1.92	1.85	1.86
	1.90	1.99	1.94	1.92	1.91	1.92	1.86	1.89	1.88	1.87	1.89	1.93
0.102 (0.004 in.)	2.20	2.19	2.20	2.04	2.13	2.09	2.16	2.10	2.13	2.16	2.05	2.09
	2.12	2.14	2.13	2.13	2.14	2.14	2.23	2.27	2.25	2.16	2.11	2.27
	2.13	2.16	2.14	2.00	2.02	2.01	2.22	2.22	2.22	2.14	2.16	2.11
	2.16	2.28	2.22	2.13	2.12	2.13	2.16	2.18	2.17	2.18	2.18	2.19
0.127 (0.005 in.)	2.31	2.33	2.32	2.11	2.29	2.20	2.24	2.26	2.25	2.25	2.17	2.28
	2.25	2.28	2.26	2.23	2.28	2.26	2.34	2.34	2.34	2.26	2.25	2.37
	2.25	2.30	2.27	2.11	2.17	2.14	2.35	2.35	2.35	2.27	2.24	2.16
	2.24	2.37	2.31	2.26	2.31	2.29	2.24	2.25	2.25	2.33	2.27	2.24
0.152 (0.006 in.)	2.40	2.40	2.40	2.23	2.36	2.30	2.38	2.42	2.40	2.36	2.30	2.33
	2.30	2.37	2.34	2.30	2.37	2.33	2.37	2.37	2.37	2.32	2.38	2.49
	2.44	2.37	2.41	2.28	2.28	2.28	2.46	2.46	2.46	2.36	2.30	2.23
	2.32	2.39	2.35	2.38	2.41	2.39	2.33	2.25	2.29	2.40	2.39	2.41



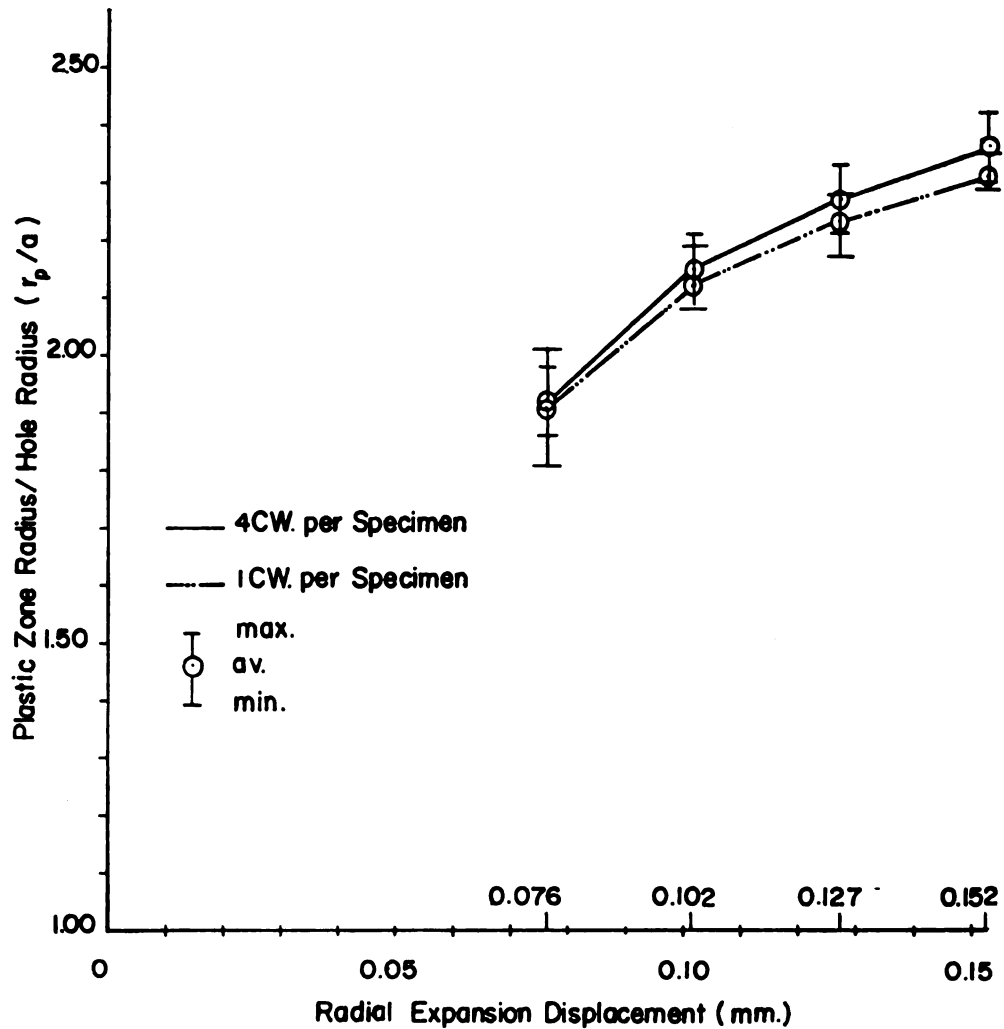


Figure 6.3.--Comparison of the measured  $r_p/a$  obtained from thickness change measurement technique with 1 CW. and 4 CW. on one specimen of the 6.35 mm. (1/4 in.) thick, 7075-T6 aluminum.

similar elastic-plastic boundary around the coldworked hole for the two coldworking procedures. In other words, it makes little difference whether a given radial expansion is achieved in one step or several steps. However, the  $r_p/a$  for each mandrel in four directions was not equal, indicating that the elastic-plastic boundary around these coldworked holes was not truly round because the original hole was not perfectly round, as shown in Table 3.1.

#### 6.2.2 3.18 mm. (1/8 in.) Thick, 7075-T6 Specimen Data

Elastic-plastic boundary measurements were made on nine coldworked 3.18 mm. (1/8 in.) thick specimens after four mandrels were pulled through the hole of each specimen. Three of them were tested on both scales as for the thicker specimens. Two specimens (P.19 and 22) were tested by employing all three examining techniques. The photoelastic coating failed and only one direction  $r_p$  could be measured, as given in Table 6.4. Furthermore, only one set of specimens was tested with one coldworking operation per specimen (four specimens for four coldworking levels).

Figure 6.4 shows no difference in the elastic-plastic boundary around the coldworked hole for incremental coldworking versus single coldworking. This plot was made using the average  $r_p/a$  of the nine specimens (30 measurements) which were coldworked incrementally, and the average  $r_p/a$  of four specimens (four measurements per one specimen) which were coldworked in one operation.

TABLE 6.4.--Measured  $r_p/a$  obtained from thickness change measurement technique for the 3.18 mm. (1/8 in.) thick, 7075-T6 aluminum specimens.

Radial Expansion Displacement (mm.)	P.19	P.20		P.22	P.24		P.25	P.27	P.28
	0.001	0.005	0.001	Av.	0.001	0.005	0.001	Av.	0.001
0.076 (0.003 in.)	1.73	1.80	1.77	1.79	1.74	1.76	1.79	1.81	1.75
	1.75	1.76	1.76	1.75	1.79	1.77	1.78	1.80	1.82
	1.80	1.79	1.78	1.75	1.73	1.76	1.78	1.76	1.75
	1.72	1.78	1.75	1.76	1.74	1.75	1.70	1.87	1.79
0.102 (0.004 in.)	1.91	1.91	1.91	1.90	1.91	1.91	1.89	1.94	1.92
	1.92	1.95	1.94	1.89	1.93	1.91	1.91	1.92	1.94
	1.92	1.93	1.93	1.86	1.92	1.92	1.97	2.00	1.97
	1.97	1.96	1.97	1.85	1.88	1.87	1.92	1.95	1.93
0.127 (0.005 in.)	2.02	2.02	2.02	1.97	1.98	1.98	1.96	1.99	2.02
	2.01	2.02	2.02	2.01	2.00	2.01	1.99	1.99	1.97
	2.02	2.02	2.02	2.01	2.04	2.04	2.09	2.06	2.05
	2.03	2.00	2.02	2.00	2.00	2.00	2.00	2.02	1.98
0.152 (0.006 in.)	2.13	2.12	2.13	2.11	2.09	2.10	1.98	2.05	2.07
	2.08	2.10	2.09	2.08	2.07	2.08	2.05	2.06	1.98
	2.09	2.11	2.10	2.11	2.10	2.11	2.12	2.15	2.09
	2.11	2.10	2.11	2.11	2.08	2.10	2.08	2.09	2.02

TABLE 6.4 (Continued).--Measured  $r_p/a$  obtained from thickness change measurement technique for the 3.18 mm. (1/8 in.) thick, 7075-T6 aluminum specimens.

Radial Expansion Displacement (mm.)	P.29		P.30		Overall Average	S.D.	1 CW per specimen				
	0.005	0.001	Av.	0.001			0.005	0.001	P.31	P.32	P.33
0.076 (0.003 in.)	1.78	1.81	1.80	1.75	1.77	0.04	1.78	1.81	1.80	Average = 1.76	
	1.82	1.84	1.83	1.70			1.78	1.78	1.78		
	1.68	1.68	1.68	1.73			1.75	1.74	1.74		
	1.78	1.80	1.79	1.71			1.72	1.76	1.74		
0.102 (0.004 in.)	1.88	1.91	1.90	1.92	1.92	0.04	1.89	1.89	1.89	Average = 1.88	1.89
	1.94	1.94	1.94	1.91			1.85	1.88	1.87		
	1.80	1.82	1.81	1.92			1.92	1.92	1.92		
	1.94	1.91	1.93	1.92			1.82	1.85	1.84		
0.127 (0.005 in.)	2.02	2.02	2.02	2.01	2.01	0.03	1.94	1.98	1.98	Average = 1.97	1.96
	2.04	2.02	2.03	2.00			1.98	1.95	1.96		
	1.95	1.89	1.92	2.02			2.00	2.04	2.02		
	1.98	2.04	2.01	2.02			1.94	1.94	1.94		
0.152 (0.006 in.)	2.06	2.05	2.06	2.10	2.08	0.04	2.08	2.11	2.11	Average = 2.10	2.09
	2.08	2.08	2.08	2.12			2.10	2.10	2.10		
	2.00	2.04	2.02	2.12			2.11	2.07	2.09		
	2.08	2.11	2.10	2.09			2.13	2.13	2.13		

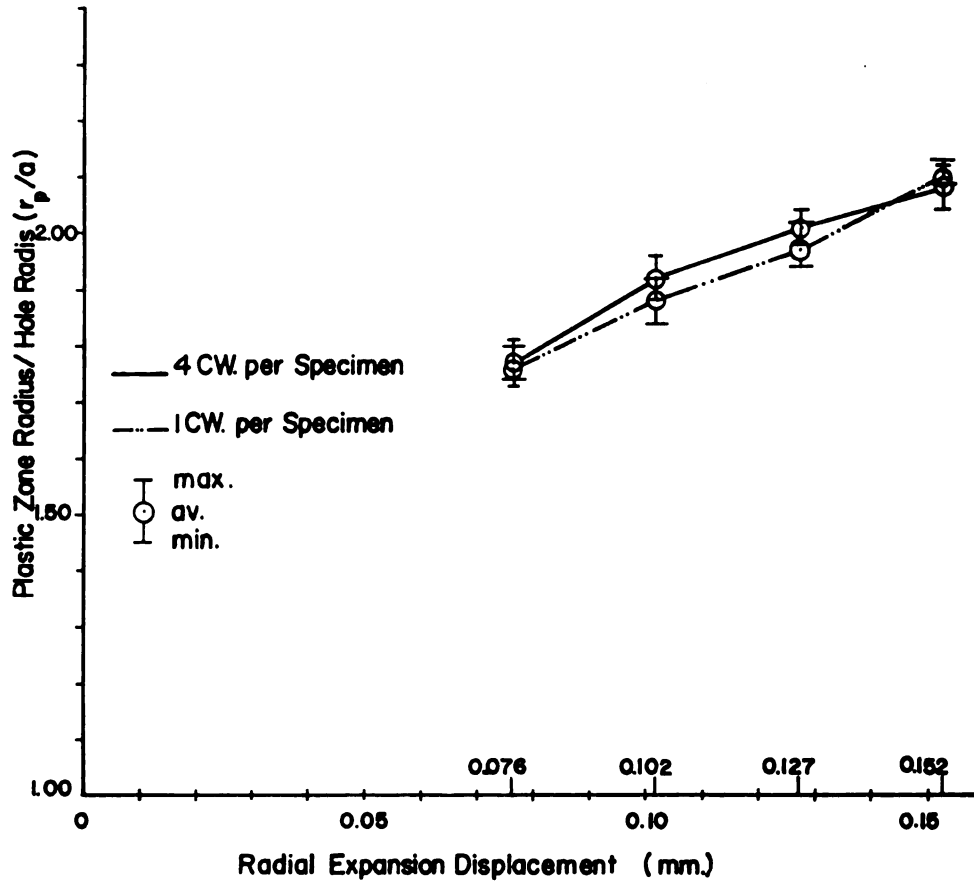


Figure 6.4.--Comparison of the measured  $r_p/a$  obtained from thickness change measurement technique with 1 CW. and 4 CW. on one specimen of the 3.18 mm. (1/8 in.) thick, 7075-T6 aluminum.

### 6.2.3 3.18 mm. (1/8 in.) Thick, Aluminum Type 1100 Specimen Data

Elastic-plastic boundary measurements were made on four 3.18 mm. (1/8 inch) thick, aluminum 1100 specimens after four mandrels were pulled through the hole of each specimen. The scattering of the measurements was very large due to the softness of the metal. The surfaces on both sides were scratched by the carbide balls during the movement of the specimen. This made too many ripples on the final plot from the X-Y recorder. Careful judgment must be made to decide where the thickness change starts. All specimens were run with  $\pm 0.005$  in. scale to have a better curve from the X-Y recorder. A final plot from the X-Y recorder is shown in Figure 5.21.

Table 6.5 lists the numbers of the specimens and the cold-working used for each. The table shows that the measured  $r_p/a$  around the coldworked holes are relatively larger than the  $r_p/a$  obtained for the 7075-T6 samples. This is because the yield stress of this specimen is much lower.

Figure 6.5 illustrates the comparison of the elastic-plastic boundary around the coldworked holes caused by incremental and single coldworking operations. This plot also indicates the consistency of no difference in the  $r_p/a$  obtained from the incremental and single cold-working operations.

## 6.3 Discussion

As for the techniques used to measure the elastic-plastic boundary around the coldworked hole by the J. O. King coldworking

TABLE 6.5.--Measured  $r_p/a$  obtained from thickness change measurement technique for the 3.18 mm. (1/8 in.) thick, type 1100 aluminum specimens with  $\pm 0.005$  in. scale of Daytronic Amplifier.

Radial Expansion Displacement (mm.)	P.35	P.36	P.47	P.50	Av.	S.D.	P.38	P.39	P.40	P.41	P.42	P.43	P.44	P.46	Av.	S.D.
0.076 (0.003 in.)	3.42	3.48	3.52	3.44	3.48	0.02	3.59	3.34	3.36	3.40	3.64	3.51	3.36	3.62	3.50	0.01
0.102 (0.004 in.)	--	3.38	3.45	3.40	3.48	0.02	3.63	3.59	3.62	3.40	3.64	3.59	3.55	3.62	3.50	0.01
0.127 (0.005 in.)	3.49	3.59	3.70	3.55	3.55	0.01	3.49	3.66	3.66	3.66	3.66	3.66	3.66	3.66	3.66	0.02
0.152 (0.006 in.)	3.17	3.63	3.50	--	3.66	0.01	3.66	3.65	3.66	3.66	3.66	3.66	3.66	3.66	3.66	0.02
	3.58	3.75	3.65	3.61	3.66	0.01	3.65	3.65	3.66	3.66	3.66	3.66	3.66	3.66	3.66	0.02
	--	3.68	3.66	3.54	3.66	0.01	3.65	3.65	3.66	3.66	3.66	3.66	3.66	3.66	3.66	0.02
	3.53	3.82	3.73	3.66	3.66	0.01	3.66	3.66	3.66	3.66	3.66	3.66	3.66	3.66	3.66	0.02
	3.52	3.86	3.65	--	3.66	0.01	3.66	3.66	3.66	3.66	3.66	3.66	3.66	3.66	3.66	0.02
	3.63	3.96	3.73	3.78	3.76	0.02	3.66	3.66	3.66	3.66	3.66	3.66	3.66	3.66	3.66	0.02
	--	3.93	3.70	3.65	3.76	0.02	3.66	3.66	3.66	3.66	3.66	3.66	3.66	3.66	3.66	0.02
	3.60	3.96	3.75	3.74	3.76	0.02	3.66	3.66	3.66	3.66	3.66	3.66	3.66	3.66	3.66	0.02
	3.63	3.93	3.71	--	3.76	0.02	3.66	3.66	3.66	3.66	3.66	3.66	3.66	3.66	3.66	0.02
	3.75	4.06	3.75	3.90	3.84	0.02	3.66	3.66	3.66	3.66	3.66	3.66	3.66	3.66	3.66	0.02
	--	4.06	3.74	3.80	3.84	0.02	3.66	3.66	3.66	3.66	3.66	3.66	3.66	3.66	3.66	0.02
	3.64	3.98	3.80	3.78	3.84	0.02	3.66	3.66	3.66	3.66	3.66	3.66	3.66	3.66	3.66	0.02
	3.67	3.95	3.81	--	3.84	0.02	3.66	3.66	3.66	3.66	3.66	3.66	3.66	3.66	3.66	0.02

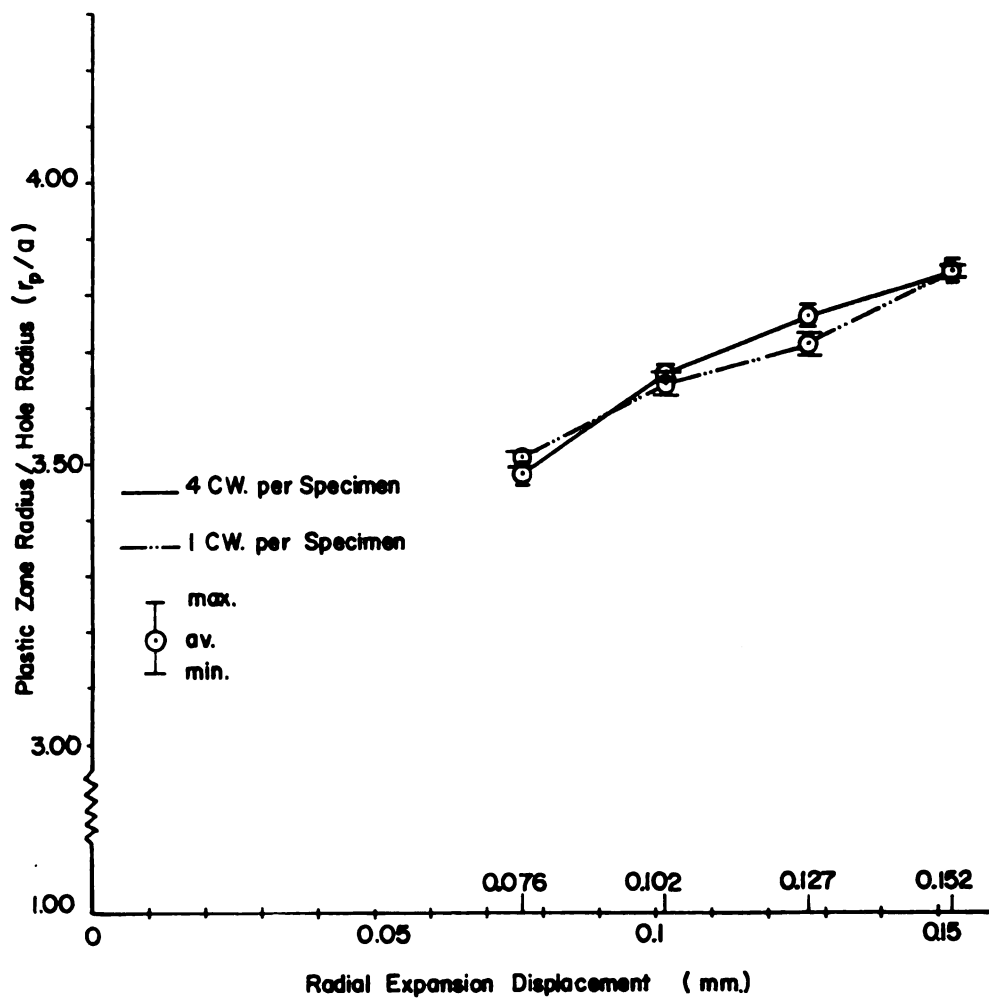


Figure 6.5.--Comparison of the measured  $r_p/a$  obtained from thickness change measurement technique with 1 CW. and 4 CW. on one specimen of the 3.18 mm. (1/8 in.) thick, type 1100 aluminum with  $\pm 0.005$  in. scale of Daytronic amplifier.

process, only two techniques--the foil strain gage and the thickness change measurement--are workable. The photoelastic coating is not usable due to its limitation as explained in section 5.4. Besides the limitation of using it with a very soft metal, the foil strain gage technique has another limitation: only three gages can be used within 4.26 mm. This method would give more accurate  $r_p$  if more and smaller gages could be used within the same distance. However, the strains obtained from the 7075-T6 aluminum increase monotonically from the elastic region to the first gage location. None of them deviates much from the smooth curve connecting those three points (see Figures 5.12 to 5.15). This means that the strains obtained from this method and the curve connecting them can be a good representation of strain distribution around the coldworked hole. As discussed in Chapter 4, the Hsu-Forman is the most general of all present theories developed. The strains on the upper free surface of the specimen agree well with the predicted strains by this theory (see Figure 5.14 and 5.15) for smaller amounts of coldwork. The nearest gage location to the edge of the hole was between 1 and 2 mm, whereas the predicted strains by most theories are less than 2%. The obtained strains were also never more than 2%, yet the foil strain gages had a maximum strain range of  $\pm 10$  percent. With its excellent characteristic of measuring infinitesimal strain, the foil strain gage is an accurate technique for the measurement of elastic-plastic boundary around the coldworked hole.

The lack of uniform deformation through the specimen thickness in the experimentally measured surface strains makes it impossible

to locate  $r_p$  by determining surface strains ( $\epsilon_r$  and  $\epsilon_\theta$ ) on only one side. The actual average  $r_p$  of the coldworked hole was finally determined by averaging the  $r_p$  of both side surfaces of the specimen. The thickness change measurement, though tedious on the very soft metal, is workable in all metals. However, both techniques give useful data on the harder metal 7075-T6 aluminum. The measured  $r_p/a$  obtained from both techniques have been shown here to be consistent with each other.

In order to clarify their accuracies, two extra plots are plotted in Figures 6.6 and 6.7. Figure 6.6 is the plot of average  $r_p/a$  obtained from the 6.35 mm. thick, 7075-T6 specimens, taken from Tables 6.1 and 6.3. The average  $r_p/a$  obtained from the thickness change measurement were made from twelve measurements (four measurements per one specimen) while three measurements were taken from the foil gage (one measurement per one specimen). Percentage differences are based on the distance between  $r_p$  and the edge of the hole and are 11.00, 7.50, 1.60, and 2.00 for the 0.076 (0.003 in.), 0.102 (0.004 in.), 0.127 (0.005 in.) and 0.152 (0.006 in.) mm. radial expansion displacements, respectively.

Figure 6.7, the average  $r_p/a$  obtained from both techniques of the 3.18 mm. thick, 7075-T6 specimens are taken from Tables 6.2 and 6.4 and compared. The percentage differences are 8.50, 1.00, 2.00 and 2.73 for the incremental mandrel sizes, respectively.

Results from both techniques are in excellent agreement for larger deformation, but show somewhat greater variations for smaller deformation. The overall percentage differences of both techniques are 5.52 and 3.56 for the 6.35 and 3.18 mm. thick specimens, which

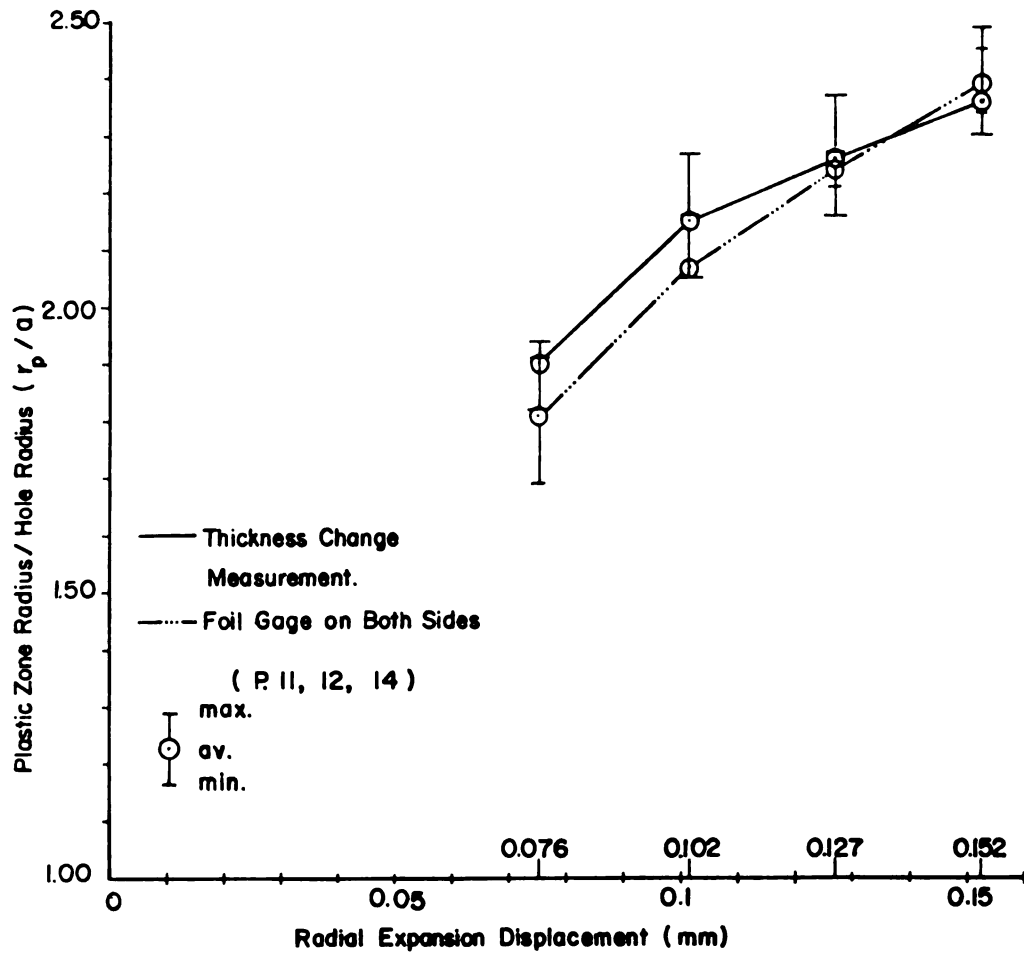


Figure 6.6.--Comparison of the measured  $r_p/a$  obtained from thickness change measurement and foil gage (both sides) techniques of the 6.35 mm. (1/4 in.) thick, 7075-T6 aluminum (P.11,12,14).

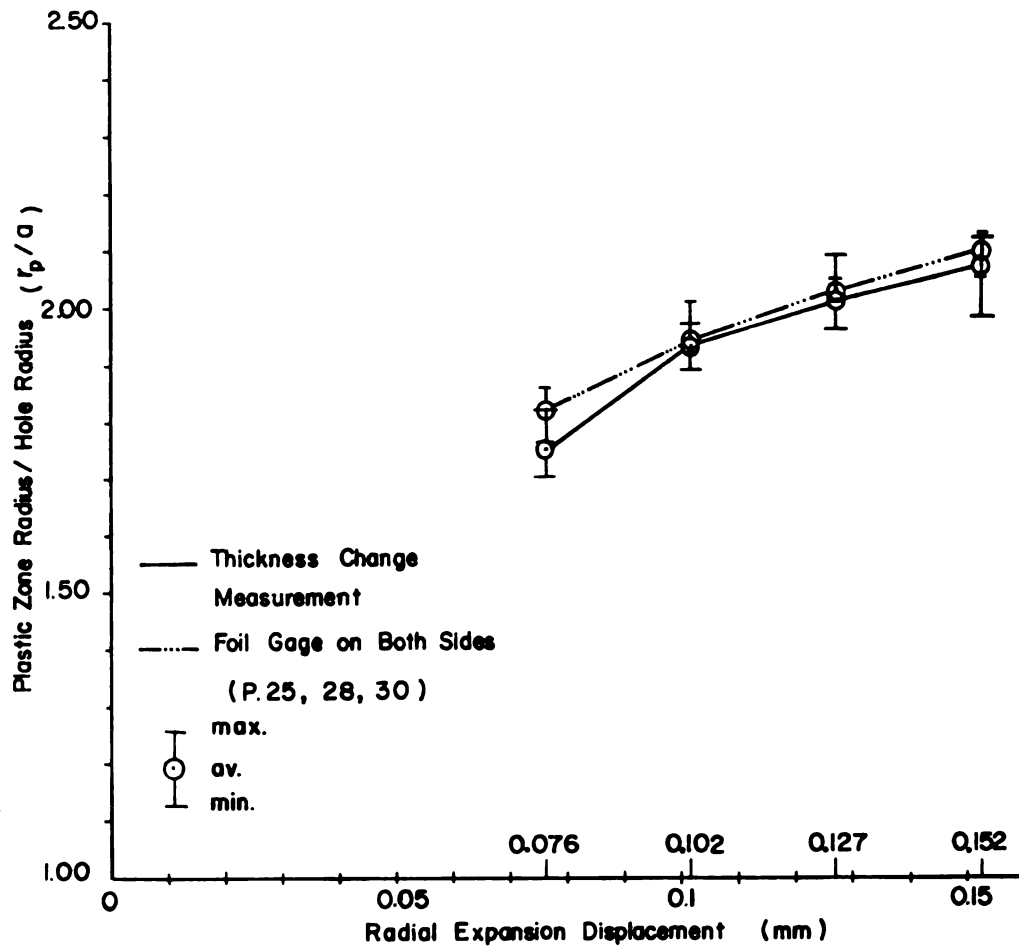


Figure 6.7.--Comparison of the measured  $r_p/a$  obtained from thickness change measurement and foil gage (both sides) techniques of the 3.18 mm. (1/8 in.) thick, 7075-T6 aluminum (P.25,28,30).

are well within the acceptable range of experimental accuracy. Therefore, the thickness change measurement is also an accurate technique for the elastic-plastic boundary measurement. With its advantages of being reusable and efficient, the thickness change measurement may be recommended for elastic-plastic boundary measurement in the future.

## CHAPTER 7

### COMPARISON OF THEORIES WITH EXPERIMENTS

The seven theories used for comparison in the experiments are the Potter-Grandt, Hsu-Forman, Nadai, Rich-Impellizzeri, Adler-Dupree, Sachs, and Carter-Hanagud. The predicted  $r_p/a$  were computed on a typical specimen of each material for the particular expansion considered and were separately plotted on a dimensionless form in Figure 4.3, and replotted in Figure 7.1 for comparison with the experiments. This is a general form in which the predicted  $r_p/a$  associated with different amounts of coldwork for each theory can be concisely compared. Only one value of  $r_p/a$  predicted by Adler-Dupree is given, due to the fact that only one specimen thickness and radial expansion were computed via the finite-element method in their report. Regardless of yield criteria used, the seven theories fall into two classes: plane stress and plane strain conditions. As shown in the plot in Figure 7.1, the predicted  $r_p/a$  by plane strain theories (Rich-Impellizzeri and Sachs) are larger than the ones by plane stress theories assumed (except the ones by Carter-Hanagud and Adler-Dupree). Rich-Impellizzeri modified the thick-walled tube theory (12) by including the compressive radial displacement of the mandrel under the same assumptions which cause smaller  $r_p/a$  than the

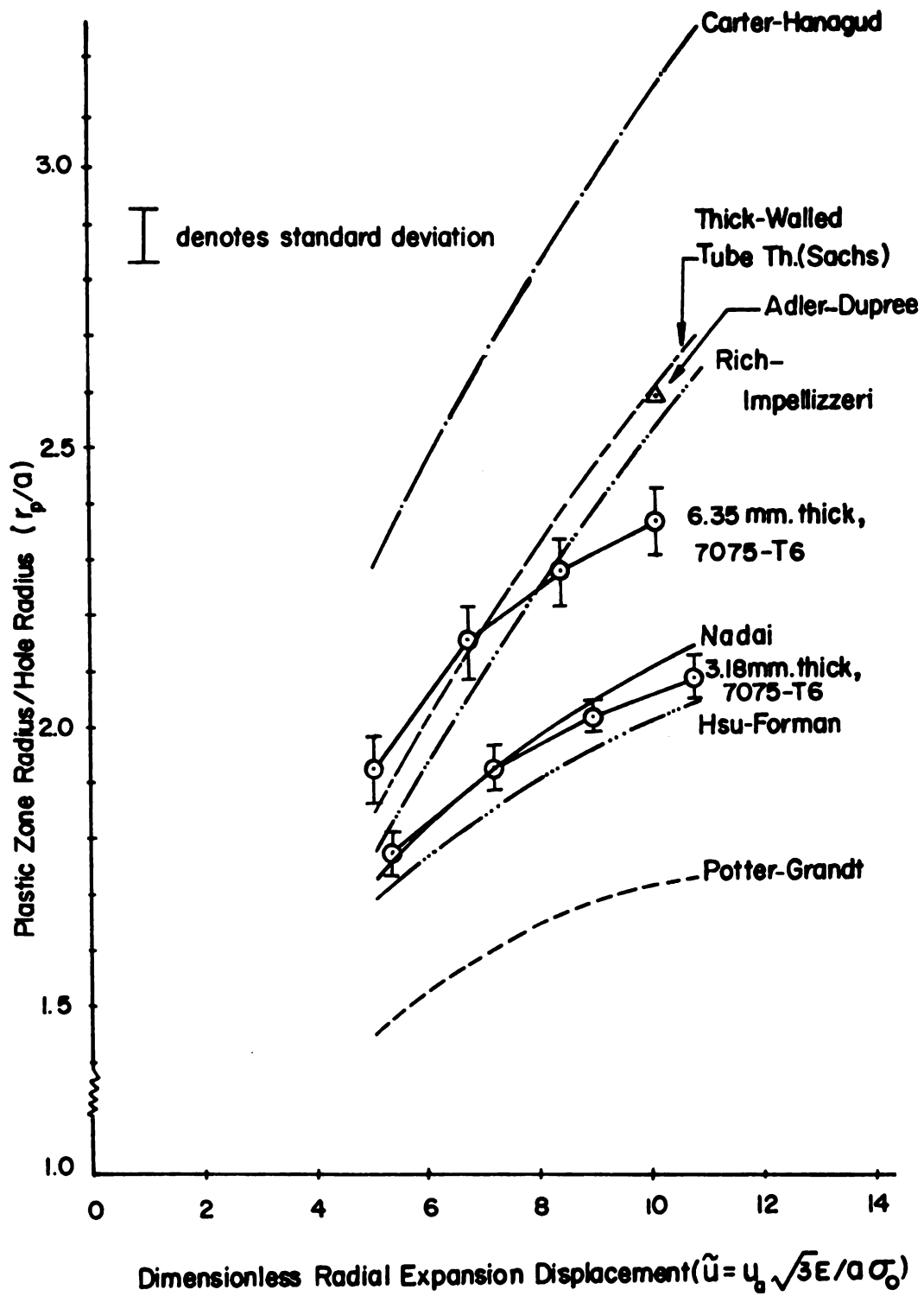


Figure 7.1.--Comparison of the elastic-plastic boundaries predicted by various theories and experiments for 7075-T6 aluminum.

original Sachs solution. Nadai considers the perfectly plastic material response and produces a higher  $r_p/a$  than the predicted value by the work-hardening theory of Hsu-Forman. The Potter-Grandt theory predicts the smallest  $r_p/a$  under the perfectly plastic material while Carter-Hanagud predict the largest value of all theories under Tresca yield criterion assumption.

Figure 7.1 compares the theories with experiments for the 7075-T6 aluminum. The measured  $r_p/a$ , with the thickness change measurement, are taken from Table 6.3 and 6.4 for the 6.35 mm. (1/4 in.) and 3.18 mm. (1/8 in.) thick, 7075-T6 specimens respectively. The comparison of 3.18 mm. thick specimen data with the theories is excellent. The experimental data lie between the two plane stress theories (Nadai and Hsu-Forman). The percentage differences between the average experimental and the predicted  $r_p/a$  by these two theories are given in Table 7.1. The percentage difference is based on the distance from the edge of the hole to the elastic-plastic boundary, and a positive sign means that the experimental value is larger than the value predicted by theory. By this comparison, only two plane stress theories agree quite well with the experiments. The Nadai theory, in which perfectly plastic material is assumed, is in nearly complete agreement with the experiments. As found by the foil gage technique, the experimental strains on the upper side of the specimen, where the supposed uniform deformation should be, agreed with the predicted strains by the Hsu-Forman theory better than the ones by Nadai. This means that the Hsu-Forman theory has the best chance of agreeing with experiments if uniform deformation exists through the thickness of

TABLE 7.1--Percentage differences between the measured  $r_p/a$  obtained from thickness change measurement for the 3.18 mm. (1/8 in.) thick, 7075-T6 aluminum and the Nadai and Hsu-Forman theories.

Radial Displacement (mm.)	% Difference of Experiments with	
	Nadai	Hsu-Forman
0.076 (0.003 in.)	+1.32	+6.95
0.102 (0.004 in.)	0.0	+8.24
0.127 (0.005 in.)	-2.89	+5.21
0.152 (0.006 in.)	-5.26	+3.85

the specimen. According to the measured strains obtained from the foil gage on both sides of the specimen, the difference between the strains on each surface became smaller as a bigger mandrel was pulled through the hole. One may suggest that for larger amounts of cold-work a nearly uniform deformation exists through the thickness of 3.18 mm. (1/8 in.) thick, 7075-T6 specimen, and a condition of plane stress is attained. In consideration of conservative design, two optimum theories (Nadai and Hsu-Forman) may be suggested to a designer for spacing the hole locations in practice. He may predict the plastic zone size around a coldworked hole by the Nadai theory when requiring more precision on 3.18 mm. (1/8 in.) thick plate.

The comparison of the experiments with the theories shows the non-existence of plane stress condition on the 6.35 mm. (1/4 in.) thick specimens. It tends to be either plane strain or generalized plane strain condition. The experimental  $r_p/a$ , in the plot, are very much larger than the predicted  $r_p/a$  of the plane stress theories.

The experimental results do not vary as greatly with the amount of coldwork as do the predicted  $r_p/a$  of the plane strain theories. Two plane strain theories (Sachs and Rich-Impellizzeri) agree fairly well with the experiments as shown in Table 7.2 and Figure 7.1. For the same reason as given for the thinner specimens, these two theories may be the only ones which have a better chance to agree with the experiments on the smaller amounts of coldwork if the deformation is uniform. The experiments on this thickness do not agree with any theory for the larger amount of coldwork used, 0.152 mm. (0.006 in.), which is the largest amount typically employed on the 6.35 mm. (1/4 in.) thick plate. Two theories--Sachs and Rich-Impellizzeri--may be used to predict  $r_p/a$  around a coldworked hole of the 6.35 mm. (1/4 in.) thick plate for smaller amounts of coldwork. But one must make measurements to get the actual  $r_p/a$  if a larger coldwork is required, in order to avoid an overlap of the  $r_p$  with an adjacent coldworked hole.

TABLE 7.2--Percentage differences between the measured  $r_p/a$  obtained from thickness change measurement for the 6.35 mm. (1/4 in.) thick, 7075-T6 aluminum and the Thick-Walled Tube and Rich-Impellizzeri theories.

Radial Displacement (mm.)	% Difference of Experiments with	
	Thick-Walled Tube	Rich-Impellizzeri
0.076 (0.003 in.)	+9.52	+17.95
0.102 (0.004 in.)	+1.77	+8.49
0.127 (0.005 in.)	-8.00	-2.31
0.152 (0.006 in.)	-15.00	-11.11

Table 7.3 shows the predicted  $r_p/a$  by some theories (Nadai, Carter-Hanagud, Sachs, and Rich-Impellizzeri) and the average  $r_p/a$  by thickness change measurement of the 3.18 mm. (1/8 in.) thick, aluminum type 1100 specimens. The predicted  $r_p/a$  computed from three of these theories, as shown in this table, are incredibly large. Only the Nadai theory gives results that compare closely to the experimental work for the soft 1100 aluminum specimens. The variations in the  $r_p/a$  values are about 20%, this difference perhaps caused either by an error in locating  $r_p/a$  from thickness change curves or by the theory itself. As explained in the chapter on techniques, many extra ripples are caused by the scratched surface; this leads to difficulty in locating the change in thickness. Pure aluminum, however, is rarely used for industrial applications.

TABLE 7.3--Average measured  $r_p/a$  obtained from thickness change measurement and predicted  $r_p/a$  from four theories for the 3.18 mm. (1/8 in.) thick, type 1100 aluminum.

Average $r_p/a$	Nadai	Carter-Hanagud	Sachs	Rich-Impellizzeri
3.47	3.08	8.52	7.43	7.39
3.66	3.19	9.80	8.57	8.54
3.76	3.27	10.93	9.59	9.55
3.84	3.33	11.96	10.50	10.47

Another experimental condition which can be compared with the theories is the final diameter of the relaxed hole after unloading. Such data also help the designer to determine the amount of coldwork

needed for his final hole size before fabricating in practice. Two researchers (9,11) have determined these data. Potter-Grandt computed the residual radial displacement of a coldworked hole after unloading and plotted this information in dimensionless form as a function of the amount of coldwork. The final diameters of the relaxed holes of the 7075-T6 specimens were computed by this theory and are shown in Figure 7.2. Adler-Dupree compared experimental relaxed hole diameters with the computed ones by the finite-element method on the 6.35 mm. (1/4 in.) thick, 7075-T6 aluminum. The experimentally permanent radial deformation of 0.112 mm. (0.0044 in.) was found after a 6.53 mm. (0.257 in.) mandrel was pulled through a 6.60 mm. (0.26 in.) hole, while a final deformation of 0.127 mm. (0.005 in.) was found in this experiment.

The final relaxed hole diameters are given in Tables 7.4, 7.5 and 7.6 for all kinds of the specimens. Those values are the average of four measurements around the hole (the same as the original hole measurement). Four theories (Nadai, Hsu-Forman, Potter-Grandt, and Adler-Dupree) are compared with the experiments. The predicted relaxed hole diameters, by the Nadai and Hsu-Forman theories, were computed from the residual tangential strains right at the edge of the hole.

Figure 7.2 compares the experiments and the theories. Only one curve of the 3.18 (1/8 in.) thick, 7075-T6 aluminum predicted by each theory is plotted for clarity. The computed values by the Hsu-Forman and Nadai theories vary with the amount of coldwork as a straight line connecting those values, and so do the experiments.

Only one value is given by the Adler-Dupree theory, due to the reason stated earlier.

Table 7.7 and Figure 7.2 show larger values in the experiments, which is the same as the result of Adler-Dupree (11). This may stem from the difficulty of matching boundary conditions at the experiment hole with theories, and from lack of a precise theory for computing the finite strains near the edge of the coldworked hole. The Nadai theory, as computed on the aluminum type 1100, shows unusable data. For computation on very low yield stress material, the Nadai theory gives an exaggerated residual strain at the edge of the hole, and results in a too large relaxed hole as compared with the experiments. Therefore, there is no comparison on the aluminum type 1100 in Figure 7.2.

TABLE 7.4.--Measured final diameters of 6.35 mm. (1/4 in.) thick, 7075-T6 specimens after the mandrel was pulled through the holes.

Specimen	Orientation	Final diameters (mm.) by radial expansion of			
		0.076	0.102	0.127	0.152 mm.
P.1	(1)	6.721			
	2	6.721			
	3	6.718			
	4	6.726			
P.2	1	6.729			
	2	6.723			
	3	6.723			
	4	6.716			
P.3	1		6.782		
	2		6.772		
	3		6.787		
	4		6.785		
P.5	1			6.795	
	2			6.807	
	3			6.782	
	4			6.797	
P.7	1	6.734	6.795	6.856	6.883
	2	6.739	6.795	6.840	6.871
	3	6.736	6.792	6.835	6.792
	4	6.739	6.797	6.848	6.863
P.8	1	6.731	6.784	6.835	6.871
	2	6.736	6.782	6.835	6.868
	3	6.739	6.784	6.838	6.873
	4	6.741	6.787	6.833	6.876
P.10	1				6.873
	2				6.864
	3				6.873
	4				6.876
P.11	1	6.729	6.805	6.838	6.886
	2	6.718	6.800	6.828	6.886
	3	6.726	6.789	6.825	6.861
	4	6.711	6.782	6.822	6.868
P.12	1	6.736	6.777	6.833	6.858
	2	6.736	6.795	6.835	6.881
	3	6.731	6.787	6.835	6.878
	4	6.739	6.784	6.825	6.863
P.15	1		6.751		
	2		6.746		
	3		6.762		
	4		6.759		
P.16	1			6.830	
	2			6.802	
	3			6.825	
	4			6.833	
P.17	1				6.838
	2				6.838
	3				6.838
	(4)				6.843
Average		6.729 (0.2649 in.)	6.782 (0.2670 in.)	6.825 (0.2687 in.)	6.868 (0.2704 in.)
St. Deviation		±0.008 (±0.0003 in.)	±0.016 (±0.0006 in.)	±0.018 (±0.0007 in.)	±0.0127 (±0.0005 in.)

TABLE 7.5.--Measured final diameters of 3.18 mm. (1/8 in.) thick, 7075-T6 specimens after the mandrel was pulled through the holes.

Specimen	Orientation	Final diameters (mm.) by radial expansion of			
		0.076	0.102	0.127	0.152 mm.
P.25	(1)	6.736	6.782	6.807	6.873
	2	6.764	6.795	6.820	6.873
	3	6.739	6.787	6.815	6.878
	4	6.772	6.782	6.820	6.871
P.27	1	6.731	6.792	6.840	6.864
	2	6.723	6.787	6.845	6.864
	3	6.731	6.769	6.822	6.873
	4	6.746	6.792	6.830	6.881
P.28	1	6.729	6.784	6.840	6.863
	2	6.721	6.774	6.835	6.868
	3	6.726	6.792	6.843	6.863
	4	6.718	6.784	6.840	6.863
P.31	1	6.713			
	2	6.716			
	3	6.726			
	4	6.716			
P.32	1		6.789		
	2		6.795		
	3		6.782		
	4		6.784		
P.33	1			6.863	
	2			6.843	
	3			6.822	
	4			6.848	
P.34	1				6.864
	2				6.871
	3				6.871
	(4)				6.866
Average		6.731 (0.2650 in.)	6.787 (0.2672 in.)	6.833 (0.2690 in.)	6.871 (0.2705 in.)
St. Deviation		±0.018 (±0.0007 in.)	±0.008 (±0.0003 in.)	±0.016 (±0.0006 in.)	±0.005 (±0.0002 in.)

TABLE 7.6--Measured final diameters of 3.18 mm. (1/8 in.) thick, type 1100 aluminum specimens after the mandrel was pulled through the holes.

Specimen Orientation		Final diameters (mm.) by radial expansion of			
		0.076	0.102	0.127	0.152 mm.
P.38	(1)	6.802			
	2	6.804			
	3	6.777			
	4	6.792			
P.39	1		6.862		
	2		6.894		
	3		6.855		
	4		6.873		
P.40	1	6.789			
	2	6.820			
	3	6.762			
	4	6.784			
P.41	1		6.825		
	2		6.840		
	3		6.805		
	4		6.820		
P.42	1			6.863	
	2			6.853	
	3			6.853	
	4			6.853	
P.43	1				6.894
	2				6.904
	3				6.909
	4				6.922
P.44	1			6.952	
	2			6.929	
	3			6.911	
	4			6.911	
P.46	1				6.927
	2				6.888
	3				6.891
	4				6.927
P.47	1	6.779	6.845	6.876	6.906
	2	6.772	6.837	6.864	6.919
	3	6.817	6.858	6.878	6.909
	4	6.807	6.850	6.888	6.906
P.50	1	6.789	6.840	6.919	6.967
	2	6.815	6.840	6.914	6.942
	3	6.784	6.833	6.909	6.960
	(4)	6.822	6.858	6.914	6.980
Average		6.795 (0.2675 in.)	6.845 (0.2695 in.)	6.891 (0.2713 in.)	6.922 (0.2725 in.)
St. Deviation		±0.018 (±0.0007 in.)	±0.020 (±0.0008 in.)	±0.023 (±0.0009 in.)	±0.025 (±0.001 in.)

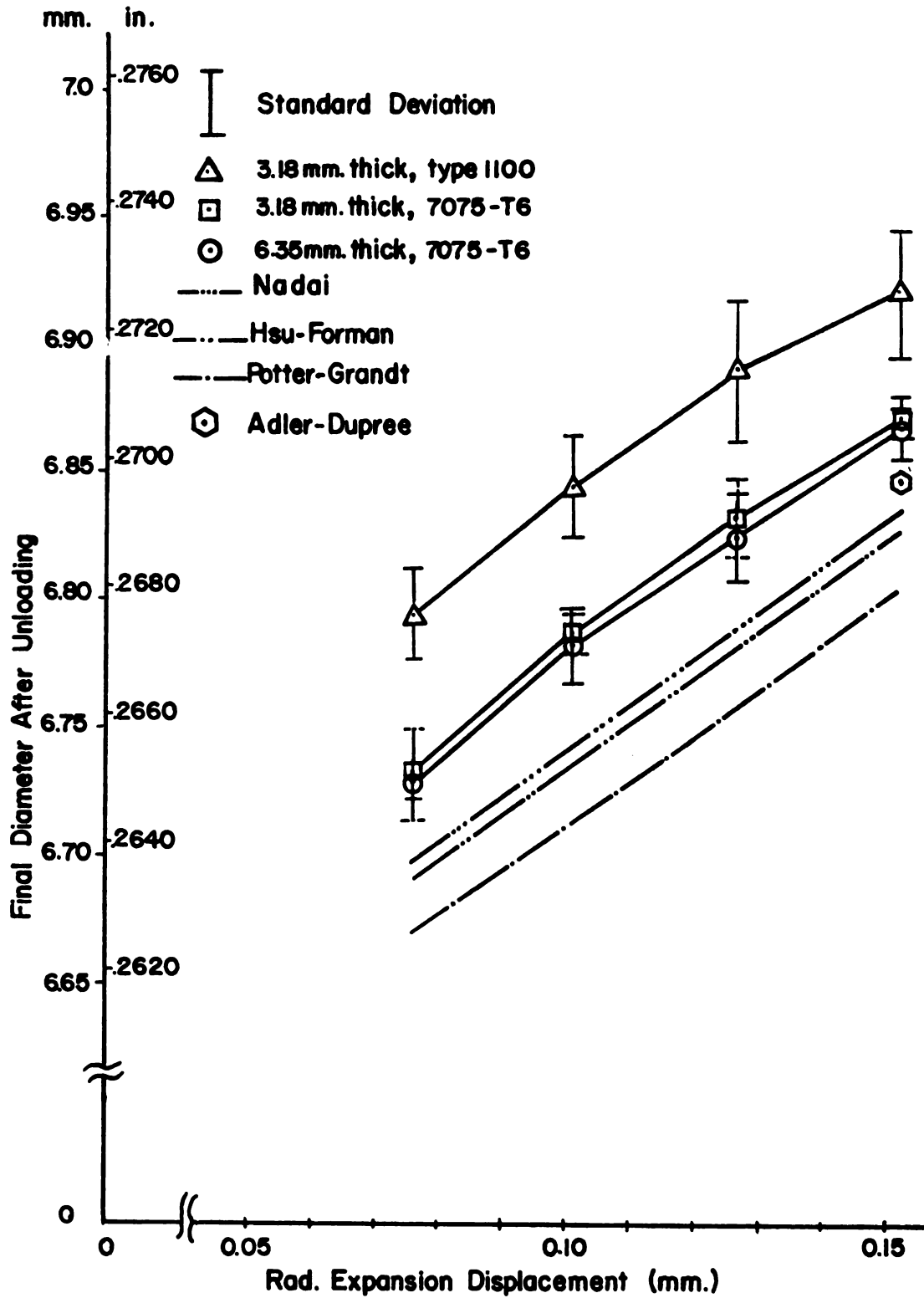


Figure 7.2.--Comparison of the measured final relaxed hole diameters with four theories (Nadai, Hsu-Forman, Potter-Grandt, and Adler-Dupree).

TABLE 7.7.--Comparison of measured final diameters with theories for the 7075-T6 aluminum specimens as four different sizes of the oversize mandrels were pulled through the holes.

Radial Displacement	Thickness	Experiments: larger than (mm.)		
		Nadai	Hsu-Forman	Potter-Grandt
(mm.)	(mm.)			
0.076	6.35 (1/4 in.)	0.044	0.036	0.065
(0.003 in.)	3.18 (1/8 in.)	0.043	0.036	0.063
0.102	6.35	0.051	0.043	0.076
(0.004 in.)	3.18	0.054	0.046	0.076
0.127	6.35	0.048	0.041	0.075
(0.005 in.)	3.18	0.054	0.046	0.077
0.152	6.35	0.047	0.039	0.072
(0.006 in.)	3.18	0.044	0.038	0.067

## CHAPTER 8

### CONCLUSIONS

In this experimental study, three simple techniques were examined for usefulness. Only two techniques (foil strain gage and thickness change measurement) are workable; they gave very close results. With its reasonable accuracy, simplicity, and economy, the thickness change measurement technique may be used for the elastic-plastic boundary measurement around the coldworked hole in the future. The resolution of  $10 \times 10^{-6}$  and  $4 \times 10^{-3}$  in. of the LVDT and the linear potentiometer are high enough to generate an accurate value of the location where the original thickness of the specimen starts to change.

As to comparison with the theories, the results obtained from the thickness change measurement on the coldworked 3.18 mm. (1/8 in.) thick, 7075-T6 aluminum, made by the J. O. King coldworking process, agree quite well with two plane stress theories (Nadai and Hsu-Forman). According to the plane stress assumption of these two theories, it is further indicated that a state of plane stress exists in the plastic region during the coldworking process. In other words, the plane stress assumption appears to be correct for the 3.18 mm. (1/8 in.) thick plate. However, the results of the 6.35 mm. (1/4 in.) thick, 7075-T6 aluminum show a larger  $r_p/a$  than the values predicted by the plane stress assumed theories (except the one by Carter-

Hanagud). Two plane strain assumed theories (the thick-walled tube and Rich-Impellizzeri) agree fairly well with the experiments for the smaller amounts of coldwork. None of the theories agrees with the experiments on the larger amounts of coldwork. The condition of plane stress does not exist in this thicker plate; it tends to be either plane strain or generalized plane strain. It is interesting to point out that as the thickness of the same material is increased (the ratio of a hole-diameter-to-thickness is decreased), the results of the  $r_p/a$  given by the plane stress assumed theories (except the one by Carter-Hanagud) converge to that of the plane strain assumed theories. For the large coldworking levels, the experimental results do not vary greatly with amount of coldwork. Therefore, for a given hole diameter the specimen thickness makes a considerable difference in the location of the elastic-plastic boundary around the hole.

Aluminum type 1100 shows unexpected results due to its softness and very low yield strength, and none of the theories agrees well with the data obtained from the thickness change measurement technique.

The results from the foil strain gage technique show that the industrial coldworking process does not produce the uniform radial expansion of the hole edge that all theories assume. The shearing deformation associated with the pulling of the mandrel is important.

The result for the final diameter of relaxed holes after unloading shows some differences with the calculated values of three theories (Nadai, Hsu-Forman, and Potter-Grandt). The measured diameters are larger than the calculated values, perhaps due to the

difficulty in matching boundary conditions at the experiment hole with theory and to the question of computation of the finite strains near the edge of the hole.

From the conservative design viewpoint, the thickness change measurement technique as developed in this work is quite useful in selecting a theory for a particular use. The results obtained from this technique indicate that some theories can be directly used to evaluate the elastic-plastic boundary around the coldworked hole on two different thicknesses. In the absence of direct measurement, the Hsu-Forman and Nadai theories are the two best adapted for calculating the  $r_p$  of the 3.18 mm. (1/8 in.) thick plate with the required precision. The thick-walled tube and Rich-Impellizzeri theories are optimum for the 6.35 mm. (1/4 in.) thick plate associated with small amounts of coldwork. For larger amounts of coldwork and more precision, it is necessary to make the thickness change measurement. Chang (21) and Rich et al (13) were conservative when they assumed plane strain on the residual stresses computation of the 12.7 mm. (0.5 in.) and 19.05 mm. (0.75 in.) thick plates, respectively. But their radial expansions of 0.18 mm. (0.007 in.) and 0.152 mm. (0.006 in.) were too large to directly evaluate the elastic-plastic boundaries around their coldworked holes from the theories used.

The experimentally measured strains on the upper free surface of the specimen agree quite well with the values predicted by the Hsu-Forman theory. This theory should be the best of all the theories for predicting the elastic-plastic boundary around a coldworked hole of the 3.18 mm. thick plate if uniform deformation is performed,

whereas the Sachs and Rich-Impellizzeri theories should be the best for use with the 6.35 mm. thick plate associated with small amounts of coldwork.

The gap between each level of coldwork considered (0.025 mm. (0.001 in.)) is small enough for one to examine the variation of the elastic-plastic boundary with confidence. However, only one material (7075-T6 aluminum) was studied. In the future, the thickness change measurement technique should be applied to several thicknesses of a variety of other metals for determining the elastic-plastic boundary around coldworked holes.

## REFERENCES

## REFERENCES

1. Timoshenko, S., and J. N. Goodier, Theory of Elasticity (McGraw-Hill, New York, 1951), pp. 80-81.
2. Knott, J. F., Fundamentals of Fracture Mechanics (John Wiley & Sons, New York-Toronto, 1973), pp. 25-45.
3. Allen, M., and J. A. Ellis, "Stress and Strain Distribution in the Vicinity of Interference Fit Fasteners" (Technical Report AFFDL-TR-72-153, Wright-Patterson AFB, Ohio, Jan. 1973).
4. Gran, R. J., et al., "Investigation and Analysis Development of Early Life Aircraft Structural Failures" (Technical Report AFFDL-TR-70-149, Wright-Patterson AFB, Ohio, March 1971).
5. Tiffany, C. F., et al., "Fatigue and Stress-Corrosion Test of Selected Fastener/Hole Process" (Technical Report ASD-TR-111, Wright-Patterson AFB, Ohio, Jan. 1973).
6. Grandt, A. F., and J. P. Gallagher, "Developing an Infinite Life Design Procedure for Fastener Holes Utilizing Fracture Mechanics" (Technical Report AFML/LLP-72-3, Wright-Patterson AFB, Ohio, Sept. 1972).
7. Nadai, A., "Theory of the Expanding of Boiler and Condenser Tube Joints through Rolling" (Trans. ASME 65, Nov. 1943), pp. 865-880.
8. Hsu, Y. C., and R. G. Forman, "Elastic-Plastic Analysis of an Infinite Sheet Having a Circular Hole under Pressure" (J. Appl. Mech. 42:2, 1975), pp. 347-352.
9. Potter, R. M., and A. F. Grandt, Jr., "An Analysis of Residual Stresses and Displacement due to Radial Expansion of Fastener Holes" (preliminary draft, 1976).
10. Sharpe, W.N., Jr., "Measurement of Residual Strains around Coldworked Fastener Holes" (Scientific Report, AFOSR-77-002, April 1976).
11. Adler, W. F., and D. M. Dupree, "Stress Analysis of Coldworked Fastener Holes" (AFML-TR-74-44, Air Force Materials Laboratory, Wright-Patterson AFB, Ohio, 1974).

12. Hoffman, O., and G. Sachs, Introduction to the Theory of Plasticity for Engineers (McGraw-Hill, New York, 1953), pp. 80-95.
13. Rich, D. L., and L. F. Impellizzeri, "Fatigue Analysis of Coldworked and Interference Fit Fastener Holes" (Scientific Report, preliminary draft, 1976).
14. Alexander, J. M., and H. Ford, "On Expanding a Hole from Zero Radius in a Thin Infinite Plate" (Proc. Royal Soc., Series A, 226, 1954), pp. 543-561.
15. Little, R. Wm., Elasticity (Prentice-Hall, Inc., Englewood Cliffs, N. J., 1973), pp. 156-159.
16. Swainger, K. H., "Compatibility of Stress and Strain in Yield Metals" (Phil. Mag., Series 7, 36, 1945), pp. 443-473.
17. Taylor, G. I., "The Formation and Enlargement of a Circular Hole in a Thin Plastic Sheet" (Quar. J. Mech. and Appl. Math., Series 7, 1, 1947), pp. 103-124.
18. Mangasarian, O. L., "Stress in the Plastic Range around a Normally Loaded Circular Hole in an Infinite Sheet" (J. Appl. Mech. 27, 1960), pp. 65-73.
19. Carter, A. E., and S. Hanagud, "Stress Corrosion Susceptibility of Stress-Coined Fastener Holes in Aircraft Structures" (AIAA Journal 13:7, 1975), pp. 858-863.
20. Potter, R. M., and T. W. Ting, "The Problem of Forced Fittings" (Arc. Rational Mech. and Anal. 58:1, 1975), pp. 77-94.
21. Chang, J. B., "Analytical Prediction of Fatigue Crack Growth at Coldworked Fastener Holes" (AIAA Paper, No. 75-805, May 1975).
22. Mendelson, A., Plasticity: Theory and Application (The Macmillan Co., New York, 1968), pp. 80-94.
23. Carey, R. P., "Experimental Determinations of Strain Fields Resulting from Interference Fit Tapered Pins" (ARL/SM 377, Aeronautical Research Laboratories, Melbourne, Australia, June 1972).
24. Ford, S. C., et al., "Interference-Fit Fastener Investigation" (AFFDL-TR-75-93, Air Force Flight Dynamics, Wright-Patterson AFB, Sept. 1975).
25. Durelli, A. J., V. J. Parks, and A. Mulzet, "On the Determination of the Sum of the Principal Stresses in Two-Dimension Problems" (Exp. Mech., Sept. 1966), pp. 19A-27A.

26. Coleman, C. E., and M. J. Ward, "The Measurement of Specimen Profiles after Mechanical Testing" (J. Sci. Instrum. 2, 1961), pp. 283-284.
27. Post, D., and F. Zandman, "Accuracy of Birefringent-Coating Method for Coatings of Arbitrary Thickness" (Exp. Mech., Jan. 1961), pp. 21-32.
28. Lee, T. C., C. Mylonas, and J. Duffy, "Thickness Effects in Birefringent Coatings with the Radial Symmetry" (Exp. Mech., Oct. 1961), pp. 134-142.
29. Zandman, F., S. S. Redner, and E. I. Reigner, "Reinforcing Effect of Birefringent Coatings" (Exp. Mech., Jan. 1962), pp. 55-64.
30. Duffy, J., and C. Mylonas, "An Experimental Study on the Effects of the Thickness of Birefringent Coatings" (in Proc. Intl. Symp. Photoelasticity, edited by M. M. Frocht, Pergamon Press, New York, 1963), pp. 27-42.
31. Dixon, J. R., and W. Visser, "An Investigation of the Elastic-Plastic Strain Distribution Around Cracks in Various Sheet Materials" (in Photoelasticity, Proc. Intl. Symp. Chicago, Ill., 1961, edited by M. M. Frocht, The Macmillan Co., New York, 1963), pp. 231-250.
32. Calcote, L. R., and C. E. Bowman, "Experimental Determination of the Elastic-Plastic Boundary" (Exp. Mech., Aug. 1965), pp. 262-266.
33. Phillips, J. L., "Sleeve Coldworking Fastener Holes" (AFML-TR-74-10, Vol. 1, Air Force Material Laboratory, Wright-Patterson AFB, 1974).
34. Bevington, P. R., Data Reduction and Error Analysis for the Physical Sciences (McGraw-Hill, New York, 1969), pp. 17-23.
35. Fung, Y. C., Foundations of Solid Mechanics (Prentice-Hill, Inc., Englewood Cliffs, N. J., 1965), pp. 144-149.
36. Wang, C. T., Applied Elasticity (McGraw-Hill, New York, 1953), pp. 50-76.
37. Ramberg, W., and W. R. Osgood, "Description of Stress-Strain Curves by Three Parameters" (NACA TN 902, 1943).
38. Budiansky, B., "An Exact Solution to an Elastic-Plastic Stress Concentration Problem" (App. Math. and Mech., Vol. 35, No. 1, 1971), pp. 18-25.

39. Dally, J. W., and W. F. Riley, Experimental Stress Analysis (McGraw-Hill, New York, 1965), pp. 366-474.
40. Dove, R. C., and P. C. Adams, Experimental Stress Analysis and Motion Measurement (Charles E. Merrill Publishing Co., Columbus, Ohio, 1964), pp. 50-124.
41. Drucker, D. C., Introduction to Mechanics of Deformable Solids (McGraw-Hill, New York, 1967).
42. Madayag, A. F., Metal Fatigue Theory and Design (John Wiley & Sons, Inc., New York, 1969).
43. Herceg, E. E., Handbook of Measurement and Control (Schawitz Engineering, HB-72, 1972).
44. Story, R. W., and E. J. Keyes, "Profile Measurement of Coated Abrasive Surface" (J. Eng. Ind., Trans. ASME 91, 1969), pp. 781-786.
45. Sim, P. J., and R. J. Taylor, "High-Sensitivity, Pneumatic, Thickness-Measuring Device for Soft-Metal Strip," (J. Sci. Instrum. 42, 1965), pp. 495-496.
46. Stolow, N., "The Measurement of Film Thickness with a Pneumatic Hydraulic Needle Mechanism" (J. Sci. Instrum. 33, 1956), pp. 333-337.
47. Sachs, G., and J. D. Lubahn, "The Strength of Cylindrical Dies" (J. Appl. Mech., Vol. 10, 1943), pp. A147-A155.
48. Zandman, F., S. Redner, and J. W. Dally, Photoelastic Coating (The Iowa State University Press, Ames, Iowa, SESA, Westport, Conn., 1977).
49. Technical Literature on Seamless Coldworking Method, J. O. King Inc., Atlanta, Georgia 30318.
50. Perry, C. C., and H. R. Lissner, The Strain Gage Primer (McGraw-Hill, New York, 1955).
51. Neubert, H. K. P., Instrument Transducers: An Introduction to Their Performance and Design (Oxford University Press, 1963).

MICHIGAN STATE UNIVERSITY LIBRARIES



3 1293 02965 4740